UNIVERSITY OF TRENTO - Italy

International PhD Program in Biomolecular Sciences

XXVI Cycle

"Mass Spectrometry Imaging: Looking Fruits at Molecular Level"

Tutors

Dr. Pietro Franceschi - *Fondazione Edmund Mach*

Dr. Fulvio Mattivi - *Fondazione Edmund Mach*

Prof. Graziano Guella - University of Trento

Ph.D. Thesis of

Yonghui Dong

Fondazione Edmund Mach di San Michele all'Adige

University of Trento

Academic Year 2012-2013

Declaration

I (Yonghui Dong) confirm that this is my own work and the use of all material from other sources has been properly and fully acknowledged.

Table of Contents

Abstract

Mass spectrometry imaging (MSI) is a MS-based technique. It provides a way of ascertaining both spatial distribution and relative abundance of a large variety of analytes from various biological sample surfaces. MSI is able to generate distribution maps of multiple analytes simultaneously without any labeling and does not require *a prior* knowledge of the target analytes, thus it has become an attractive molecular histology tool. MSI has been widely used in medicine and pharmaceutical fields, while its application in plants is recent although information regarding the spatial organization of metabolic processes in plants is of great value for understanding biological questions such as plant development, plant environment interactions, gene function and regulatory processes.

The application of MSI to these studies, however, is not straightforward due to the inherent complexity of the technique. In this thesis, the issues of plant sample preparation, surface properties heterogeneity, fast MSI analysis for spatially resolved population studies and data analysis are addressed. More specifically, two MSI approaches, namely matrix assisted laser desorption ionization (MALDI) imaging and desorption electrospray ionization (DESI) imaging, have been evaluated and compared by mapping the localization of a range of secondary and primary metabolites in apple and grapes, respectively. The work based on MALDI has been focused on the optimization of sample preparation for apple tissues to preserve the true quantitative localization of metabolites and on the development of specific data analysis tool to enhance the chemical identification in untargeted MSI (chapter 3). MALDI imaging allows high-spatial localization analysis of metabolites, but it is not suitable for applications where rapid and high throughput analysis is required when the absolute quantitative information is not necessary as in the case of screening a large number of lines in genomic or plant breeding programs. DESI imaging, in contrast, is suitable for high throughput applications with the potential of obtaining statistically robust results. However, DESI is still in its infancy and there are several fundamental aspects which have to be investigated before using it as a reliable technique in extensive imaging applications. With this in mind, we investigated how DESI imaging can be used to map the distribution of the major organic acids in different grapevine tissue parts, aiming at statistically comparing their distribution differences among various grapevine tissues and gaining insights into their metabolic pathways in grapevine. Our study demonstrated that this class of molecules

can be successfully detected in grapevine stem sections, but the surface property differences within the structurally heterogeneous grapevine tissues can strongly affect their semi-quantitative detection in DESI, thereby masking their true distribution. Then we decided to investigate this phenomenon in details, in a series of dedicated imaging studies, and the results have been presented in chapter 4. At the same time, during DESI experiments we have observed the production of the dianions of small dicarboxylates acids. We further studied the mechanism of formation of such species in the ion source proposing the use of doubly charged anions as a possible proxy to visualize the distributions of organic acid salts directly in plant tissues (chapter 5). The structural organization of the PhD thesis is as below:

Chapter one and **Chapter two** describe the general MSI principle, compare the most widely used MSI ion sources, and discuss the current status in MSI data pre-processing and statistical methods. Due to the importance of sample preparation in MSI, sample handling for plant samples is independently reviewed in chapter two, with all the essential steps being fully discussed. The first two chapters describe the comprehensive picture regarding to MSI in plants.

Chapter three presents high spatial and high mass resolution MALDI imaging of flavonols and dihydrochalcones in apple. Besides its importance in plant research, our results demonstrate that how data analysis as such Intensity Correlation Analysis could benefit untargeted MSI analysis.

Chapter four discusses how sample surface property differences in a structurally/biologically heterogeneous sample affect the quantitative mapping of analytes in the DESI imaging of organic acids in grapevine tissue sections.

Chapter five discusses the mechanism of formation of dicarboxylate dianions in DESI and ESI

Chapter six summarizes the work in the thesis and discusses the future perspectives.

Contributions

Those who made significant inputs to my research projects and writing of my PhD thesis are listed below:

Chapter 1: Dong Y. wrote the draft; Pietro Franceschi revised the manuscript; Fulvio Mattivi and Graziano Guella approved the final manuscript.

Chapter 2: Dong Y. wrote the draft; Pietro Franceschi revised and approved the final manuscript.

Chapter 3: Dong Y. conducted part of the experiment, wrote the introduction and materials and methods in the manuscript; Franceschi P. conceived and designed the experiment, conducted part of the experiment, performed the data analysis, wrote the results and discussion in the manuscript, and approved the final manuscript; Strupat K. conducted part of the experiment; Vrhovsek U and Mattivi F approved the final manuscript.

Chapter 4: Dong Y. conceived and designed the experiment, conducted the experiment, performed data analysis and wrote the draft; Guella G. and Mattivi F. designed the experiment and approved the final manuscript; Franceschi P. conceived and designed the experiment, revised and approved the final manuscript.

Chapter 5: Dong Y. conducted the experiment, performed data analysis and wrote the draft; Guella G. designed the experiment, revised and approved the final manuscript; Mattivi F. approved the final manuscript; Franceschi P. conceived and design the experiment, revised and approved the final manuscript.

Acknowledgements

This work would not have been possible without the financial support from Fondazione Edmund Mach and University of Trento.

First of all, I would like to express my greatest gratitude to my supervisor, Dr. Pietro Franceschi, for all his competent guidance, incredible kindness and immense encouragement through all my PhD study. He has been always available whenever I need his help (even on weekends). Likewise, I would like to thank my tutor Dr. Fulvio Mattivi and my supervisor Prof. Graziano Guella for the meaningful discussions, great ideas and guidance.

My visit in Dr. Aleš Svatoš's group in Max Planck Institute for Chemical Ecology was a wonderful experience for me. I am thankful to Dr. Aleš Svatoš, Dr. Filip Kaftan, Sybille Lorenz, Dr. Natalie Wielsch, Amol Fatangare, Mayuri Napagoda, Dr. Marco Kai, Dr. Jerrit Weißflog, Yvonne Hupfer, Tan Wenhua and Jingjing Fang for their help and friendships. I have greatly benefited from the interactions from all of them.

I am so lucky to be a part in biostatistics group, a friendly, collaborative and supportive research group. I would like to thank my group leader Dr. Ron Wehrens for all his kind suggestions and knowledge I have learned during group meetings. I would like to thank all my group members Dr. Matthias Scholz, Dr. Marco Giordan, Nir Shahaf, Nikola Dordevi, Nay Min Min Thaw Saw and Mridula Prasad for your suggestions, time and friendships.

I would like to acknowledge all my lab members for their valuable suggestions and technical contributions. Dr. Fulvio Mattivi's Food Quality research group: Dr. Arapitsas Panagiotis, Dr. Weingart Georg, Dr. Mary Ulaszewska, Dr. Kajetan Trost, Ghaste Manoj Shahaji, Narduzzi Luca, Perenzoni Daniele and Angeli Andrea; Dr. Vrhovsek Urska's Metabolomics research group: Masuero Domenico, Carlin Silvia, Gasperotti Mattia, Dr. Vinay Vishwanath, Dr. Della Corte Anna and Lotti Cesare; Dr. Martens Stefan's Biotechnology of Natural Products research group: Dr. Feller Antje Christin, Dr. Elisabete Carvalho and Lorena Herrera; Prof. Graziano Guella's Bioorganic Chemistry research group: Dr.Andrea Anesi and Yu Yang; Dr. Claudio Varotto's Ecogenomics research group: Dr. Li Minai, Wang bo, Qu Dong and Fu Yuan.

I sincerely thank my sister and brother-in-law for their support that ease the hardship of being away from home for long. I would like to convey my deepest gratitude to my parents for their encouragement and support throughout my life. For that, I dedicate my thesis to them.

Chapter 1

Mass Spectrometry Imaging: Principle, Ion Sources and Data Processing

Notes:

Dong Y. wrote the draft; Pietro Franceschi revised the manuscript; Fulvio Mattivi and Graziano Guella approved the final manuscript.

1.1 Mass spectrometry imaging principle

The basic principle of MSI is simple: the instrument collects a series of mass spectra by 'scanning' an area of a tissue sample according to a predefined x-y coordinate. The distribution images of the analytes over the sample surface are then generated by plotting the intensity of their individual m/z peak in the mass spectra against the x-y coordinate [1]. The core of each MSI experiments is the mass spectrometer, which consists of 3 major parts: ion source, mass analyzer and detector. In ion source, analytes are desorbed and ionized. In the analyzer, they are separated on the basis of their mass to charge ratios (m/z). The separated ions are then detected in the detector. as a final output a mass spectrum is generated by displaying the intensity of the detected ions over a full m/z scale [2] (Fig.1).

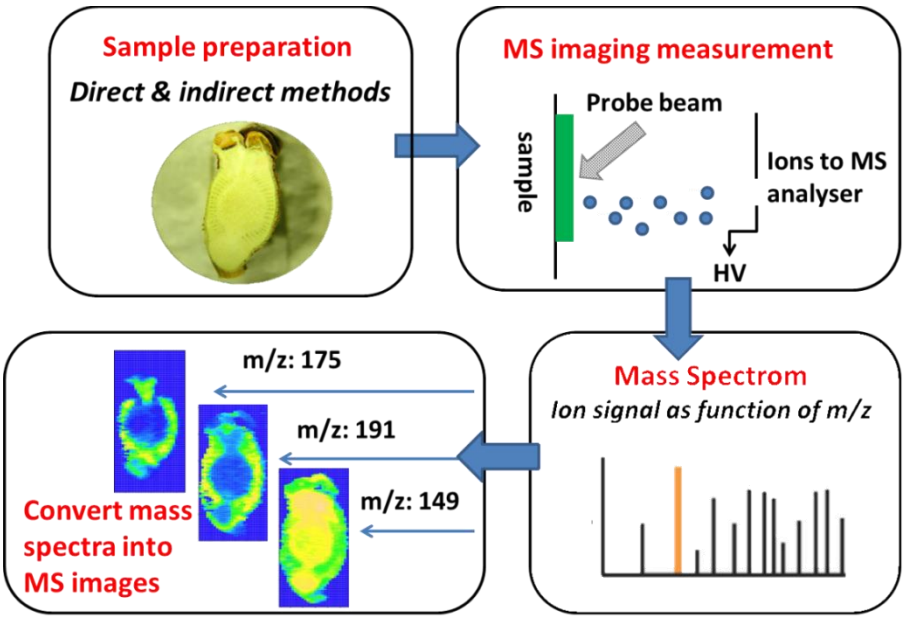

Figure 1. Scheme for mass spectrometry Imaging

1.2. Ionization sources

A large variety of ionization sources are available for MSI (Table 1), among which secondary ion mass spectrometry (SIMS), matrix assisted laser desorption ionization (MALDI) and desorption electrospray ionization (DESI) are the most popular [2-4]. In addition, laser ablation electrospray ionization (LAESI) starts to gain popularity in MSI field. Each of them has their own merits and a brief introduction of the four ionization sources is described below.

Table 1 Common MSI ion sources

Ion source	Matrix & Probe beam	Pressure regime	Spatial resolution	Reference
UV-MALDI	MALDI matrix; UV-laser	Vacuum or Ambient	50-100 µm	[5, 6]
• LDI*	None (only for UV-absorbing metabolites); UV-laser	Vacuum or Ambient	~10 µm by over-sampling	[7]
• GALDI*	Colloidal graphite; UV-laser	Vacuum or Ambient	50-100 µm	[8-10]
IR-MALDI	Native water of the sample; Infrared (IR)-laser	Vacuum or Ambient	~200 µm	[11-13]
DESI	None; High speed gas flow jet	Ambient	~200 µm (can be improved to ~35 µm by optimization of several operational parameters)	[14-16]
SIMS	None; Ion beam	Vacuum	0.1-1 µm	[17-19]
LAESI	Native water of the sample; Sample desorbed by mid infrared (mid-IR) laser	Ambient	100-300 µm (can be improved to single cell level by focusing the laser pulse)	[20-23]

* LDI : laser desorption ionization; GALDI: graphite assisted laser desorption ionization; They are considered as variations of conventional UV-MALDI.

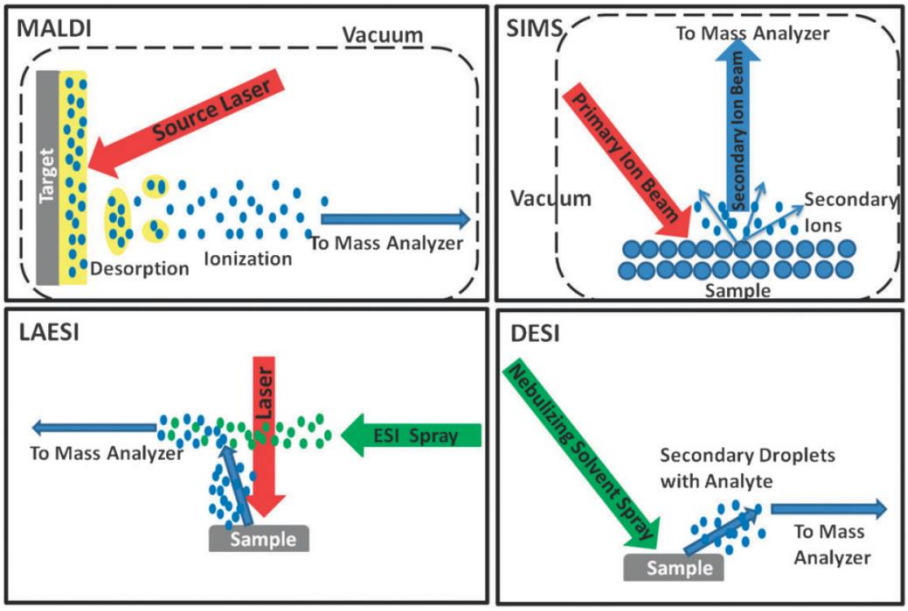

Figure 2. . Simplified mechanistic diagrams for the four most commonly used ionization techniques in mass spectrometry Imaging. Image reproduced by permission from Chemical Communications (Royal Society of Chemistry) of Ref. [24]. It is worth noting that atmospheric pressure MALDI (AP-MALDI) also allows ionization to occur at ambient condition.

1.2.1 Secondary Ion Mass Spectrometry (SIMS)

In SIMS, a focused high energy primary ion beam (e.g. Ar^+, Ga^+, In^+) is used to strike the sample surface. The analyte molecules are released from the surface and ionized upon collision with the primary ions [4]. SIMS is advantageous in its high spatial resolution (~100 nm), enabling MS imaging at subcellular scale. Furthermore, the high energy used in SIMS (typically 5-40 KeV) can sputter individual atoms from the sample surface for elemental analysis [3]. On the other hand, because the elemental distributions cannot be used to address the most relevant biological questions, and the high energy usually causes extensive secondary ion fragmentation (limiting the practical mass range to ~ m/z 1000), SIMS is not widely used for biological applications regardless of its long history [25]. Recently, several strategies aiming at extending the potential of SIMS and to increase the ionization efficiency of large intact biomolecule have been proposed. Among is worth mentioning primary ion beam modifications (i.e. using C_{60}^+) and sample surface treatment (i.e. coating the sample surface with common MALDI matrices and metallization of samples with silver and gold). Both methods modify the way that the energy of the primary ions

is dissipated in the surface so as to increase the survival yield and ionization efficiency of intact biomolecular species [25].

1.*2.2 Matrix Assisted Laser Desorption Ionization (MALDI)*

MALDI can be used for the non-destructive vaporization and ionization of both small and large molecules [26]. In MALDI analysis the deposition of a matrix (usually a UV absorbing weak organic acid) on the sample surface serves several functions: 1). extraction of analytes from the sample surface, 2). co-crystallization of analytes and matrix, and 3). ionization of analytes by absorption of laser energy [27]. The spatial resolution of MALDI imaging is relatively low compared with the one of SIMS (most MALDI imaging is done at 50-100 µm). Several factors are responsible for that but the laser spot size, the matrix crystal size and matrix coverage are worth to be mentioned [28-30]. Oversampling has been used to achieve higher spatial resolution (~ 10 µm), in these applications the laser beam is fired at a fixed position until no more ions are detected, then the laser is moved by a distance smaller than its diameter to a second position; at the second position, ions are only produced from the area which has not yet been exposed to laser irradiation; therefore the effective area is reduced [31]. This higher spatial resolution, however, is obtained at the cost of a slower analysis and of an extensive use of the laser source which can reduce its lifetime.

Due to the high background noise resulting from common MALDI matrices, UV-MALDI is limited in its ability of imaging the distribution of small metabolites (m/z<500). To minimize the high background noises in the low mass region matrix free MALDI laser desorption ionization (LDI) approach has been proposed [7]. As an alternative for non UV-absorbing analytes, new matrices such as colloidal graphite (Graphite assisted laser desorption and ionization, GALDI) [8, 9] and 1,8-bis(dimethylamino) naphthalene (DMAN) [32] have also been developed. Infrared (IR) MALDI uses the water in the sample as matrix, therefore avoiding limitations associated to the use of external matrices. The major drawback of this techniques is that the sample may dry out during IR irritation, and additionally, different locations may give different sensitivities due to inhomogeneous water content [9].

1.2.3 Desorption Electrospray Ionization (DESI)

DESI combines features of ESI with desorption ionization methods. It is mostly used to analyse a large variety of polar compounds such as peptides and proteins, but it can also be used to ionize molecules that are generally not ionized by electrospray, e.g. nonpolar compounds such as cholesterol, carotene, and TNT [14, 33]. In DESI, sample surface is directed with continuous spray of high-speed electrically charged aqueous mist, the initial wetting of the sample surface allows rapid liquid-extraction of analyte molecules, the subsequent splash of the high-speed droplets with the sample surface produces charged secondary micro-droplets with extracted surface molecules. The charged micro-droplets containing the ions of analyte molecules are then released from the surface and transports into an atmospheric inlet of the mass spectrometer [34]. DESI allows rapid ambient surface sampling without sample pretreatment, albeit its spatial resolution is low (typically 200 µm). It has been shown that the spatial resolution can be improved to ~ 35 µm by optimizing several operational parameters, such as spray tip-to-surface distance, solvent flow rate, and spacing of lane scans [15, 16]. Cooks group originally proposed three DESI ionization mechanisms: droplet pick-up, chemical sputtering (based on charge transfer from gas-phase ion to the analyte on surface) and neutral volatilization/desorption (based on volatilization or desorption of neutral species from the surface into the gas phase) [14]. Droplet pickup is now considered as the most common mechanism [33, 35], and at a practical point of view it sufficiently explains why DESI and normal ESI spectra are similar, often identical [36]. Droplet pickup involves extraction of the analyte into the droplet by impacting of electrosprayed droplets onto the surface, followed by dissolution of the analyte from the surface into the droplets. The droplets are again released from the surface and subsequent evaporation of the solvent and Coulomb fission generates ions by processes analogous to conventional ESI [14, 35].

1.2.4 *Laser Ablation Electrospray Ionization (LAESI)*

In LAESI, the sample is kept at atmospheric pressure and a focused mid-IR laser beam (wavelength: 2.940 µm) is used to excite the OH vibrations of native water molecules in the tissue sample. As rapid micro-scale ablation driven by phase explosion sets in, a microscopic volume of the sample in the form of neutral particulates and/or molecules is ejected from the sample (similar as IR-MALDI). The resulting plume is then crossed with charged droplets produced by an electrospray, and a fraction of them is converted into gas-phase ions [21, 37, 38].

The intrinsic spatial resolution of LAESI is low (~ 300 µm), but recently, it has been shown that by focusing the laser pulse through an etched optical fiber, the spatial resolution can be improved to single cell level [20, 22]. A unique feature of LAESI imaging is depth profiling which, in combination with lateral imaging, enables three-dimensional molecular imaging, with lateral and depth resolutions of ~100 µm and ~40 µm, respectively [23]. As IR-MALDI, LAESI is only suitable for biological samples with appreciable water content, sample can then dry out during IR irritation and sensitivities may also get affected by inhomogeneous water content in the sample [9]. Despite being in its infancy, this technique is expected to give interesting results in water rich tissues like the ones commonly found in plants.

1.3 MSI data processing

A large number of powerful, integrated software suites are commercially and freely available for MS image construction and/or statistical analysis (Table 2). The MSI data analysis includes 2 steps: preprocessing and statistical analysis.

Table 2 Commercial and open source MSI software

Software	Company/Authors	Web
ImageQuest	Thermo Scientific	http://www.thermoscientific.com/en/home.html
FlexImaging	Brucker	http://www.bruker.com
HDI	Waters	http://www.waters.com/waters/home.htm?locale=en_US
SCiLS Lab	SciLS	http://scils.de/software
MALDIVision	Premier Biosoft	http://www.premierbiosoft.com
TissueView	AB SCIEX	http://www.absciex.com
Quantinetix	Imabiotech	http://www.imabiotech.com
Biomap	M. Rausch & M. Stoeckli	http://www.maldi-msi.org
Datacube Explorer	AMOLF	www.imzml.org

MSiReader	NC State University, W.M. Keck FT-ICR Mass Spectrometry lab	http://www4.ncsu.edu/~dcmuddim/msireader.html
OpenMSI*	Lawrence Berkeley National Lab	https://openmsi.nersc.gov/openmsi/client/index.html

1.3.1 Pre-processing

The purpose of pre-processing of MSI data is to reduce experimental variance and transform the big amount of raw spectral data into a much cleaner, smaller, and statistically manageable set of peaks. The pre-processing of MSI dataset includes baseline correction, peak picking, normalization, and spectra alignment. It is worth noting that data preprocessing is instrument specific, different instrument may require various data pre-processing methods.

The baseline is a mass-to-charge dependent offset of mass intensities easily visible in ToF spectra, commonly such that it is highest at low m/z values, and shows an exponential decay towards higher masses [39]. Many algorithms have been developed for baseline correction. The simplest one is to identify the lowest point in the spectrum and set it to 0, and meanwhile the base peak is still kept as 100% intensity. As a consequence, the spectrum is stretched along the y-axis. More advanced methods take into account that baseline varies across the spectrum and try to locally fit some functions (e.g. polynomial and spline) to find regions of signal that consist only of the baseline without peaks of real signal [40-42].

The objective of peak picking is to locate peaks within a spectrum. Its purpose is to reduce the number of m/z values by removing those peaks corresponding to noise or non-specific baseline signals [43]. Various approaches have been used in the mass spectrometry community to identify the peaks, some of them look for signals above a certain noise level (signal to noise ratio SNR), others use more advanced mathematical tools like continuous wavelet transform (CWT), or template based peak detection [44]. Peak picking in MSI can be challenging due to the large amount of spectra (i.e. high spatial resolution MALDI imaging). Computationally inefficient methods such as continuous wavelet transformation or ridge lines are therefore less common in MSI. Peak picking methods should be robust to strong noise, those which create too many false

positives such as simple local maxima or signal to noise ratio are less favored [45]. To improve speed, peak picking applied to the dataset mean spectrum has been proposed, in this way, the position of the possible peaks is identified on the base of only one spectrum; however this approach is not sensitive as it does not favor high and relevant peaks presented only in a small part of a sample. For example, if a peak is present only in 1% of spectra, then its contribution to the mean spectrum will be reduced by 100 times as compared to a low peak present in all spectra [43, 45]. To overcome this problem, peak picking is performed pixel-wise and a peak is retained if it is found in at least 1% of the spectra [45]. A possible appealing alternative to the pixel-wise approach is to look for m/z-images exhibiting a spatial structure, regardless of its intensity [46].

Normalization is a process employed to minimize intra-spectrum differences in peak intensities which might derive from sample variability, sample preparation, instrument variation and experimental error [47]. This is often performed by dividing the intensity of each mass spectrum by a normalization factor [43, 48]. The most common method used in MSI is total ion count (TIC) normalization, where all the mass spectra are divided by their TIC value. In certain cases, however, TIC normalization may create misleading results and lead to wrong conclusions. This is typical when signals with very high intensity are solely present in localized tissue areas, as the example present in Figure 3, where the dominant insulin signal causes artificial attenuation of m/z 14,104 signal when vector (Fig 3D) and TIC (Fig 3F) are used. Normalization to the median (Fig 3J) or the noise level (Fig 3L) are suggested as more robust methods (although TIC normalization with the manual exclusion achieves best results (Fig 3H), this approach requires manual intervention) [49]. The use spraying of a section with an internal standard is a very robust strategy, which is commonly applied in targeted MSI by using isotopically labeled standards. In such case, the molecule-specific ion suppression and global effects are also affecting the internal standard which can then be used to extract (semi-)quantitative information [48].

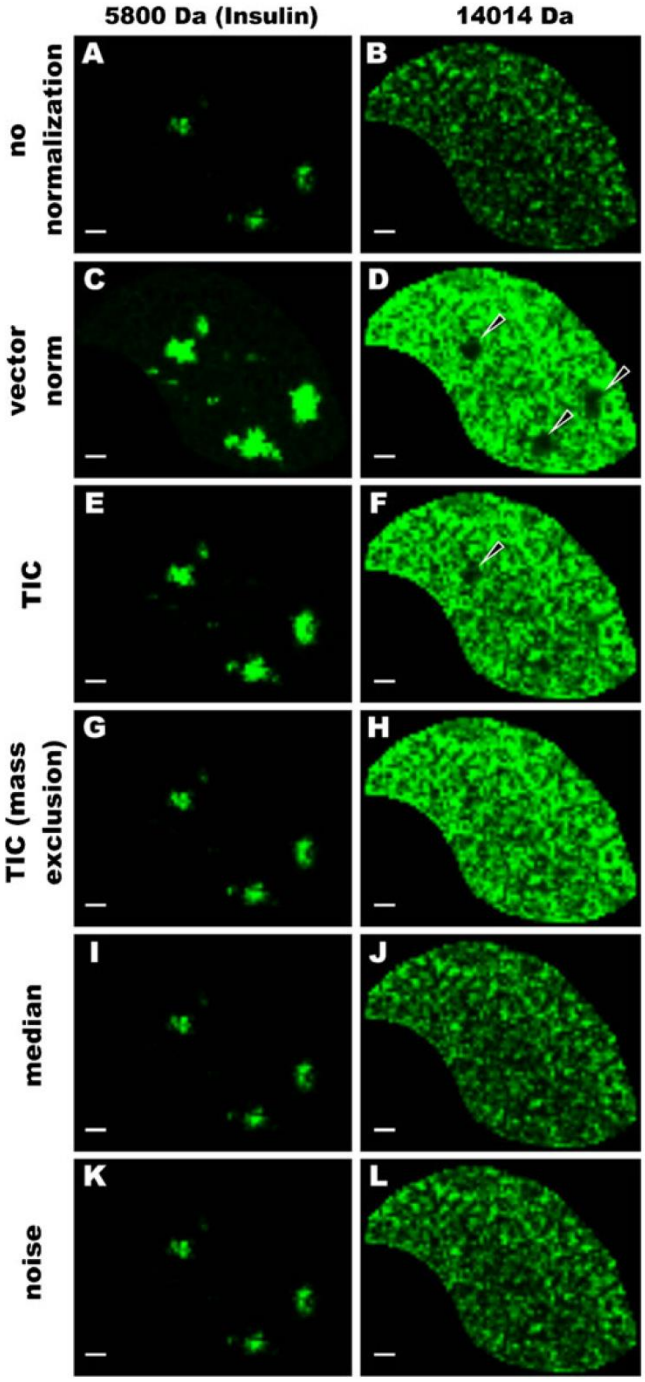

Figure 3. MALDI images of insulin (m/z 5,800) and a ubiquitous signal at m/z 14,014 in the mouse pancreas visualized using several normalization algorithms. The dominant insulin signal causes artificial attenuation of m/z 14,104 signal when vector and TIC normalization methods are used (as indicated by arrows). Image reproduced by permission from Analytical and Bioanalytical Chemistry (Springer) of Ref. [49].

Spectra alignment aims at correcting for possible mass shifts occurring from spectrum to spectrum. In practice this is done by finding, for each spectrum, a warping function in order to match or bin peaks with similarly mass into categories to ensure that we are comparing the intensity of the same ions across multiple spectra [42, 50]. In many cases, the warping function is not simple because mass shift varies with m/z in a nonlinear fashion as a result of experimental and instrumental complexity and data variation [42], so it cannot be found by using a single "lock mass" value This limitation can be overcome by using several internal standards covering the whole span of the entire mass range. Anther similar but internal standards free method is to identify a subset of common peaks present in most of the datasets using the criteria that a peak must be found in more than 90% of the spectra, and then use these peaks as basis for spectra alignment). Typically, 10-20 peaks are selected and it is important to ensure that these peaks span the entire mass range [47, 50]. As before, a simple and fast method for peak alignment is to use the dataset mean spectrum [51].

1.3.2 Statistical analysis

Statistical analysis can be divided into unsupervised and supervised methods. Unsupervised methods do not rely on a prior knowledge. They can be applied for preliminary data examination, and aim at revealing general data structure [43], while supervised methods are used for biomarker discovery. They require specifying at least 2 groups of spectra, and aims at identifying discriminative m/z values [43, 47].

1.3.2.1 Unsupervised methods

In unsupervised methods, MSI dataset is decomposed into a series of components, score images and loadings plots are then created for each component. In the majority of cases, each pixel of the image is projected in the space of the mass spectra and the organization of the point is analyzed by multivariate methods [52]. Various unsupervised approaches have been used for MSI data representation such as Principle Component Analysis (PCA) [53, 54], Independent Component Analysis (ICA) [55], Probabilistic Latent Semantic Analysis (PLSA) [56] and K-Means Clustering [57, 58]. A comprehensive comparison of the different methods can be found in [52, 56].

(1) Principal Component Analysis: Performs linear orthogonal transformation of the data to maximize variance, resulting in a set of orthogonal principal components that describe the largest variance in the dataset (PC1), the next largest variance (PC2), and so on [52].

(2) Independent Component Analysis: separates a multivariate signal into additive sub-components by assuming that the characteristic component spectra are statistically independent with a non-Gaussian distribution [56].

(3) Probabilistic Latent Semantic Analysis: Each single tissue type is characterized by a distinct distribution and each acquired spectrum is regarded as a specific mixture of these structures. It provides physical interpretability and allows identification of the discriminating peaks for a specific tissue type within a spectrum [56].

(4) K-Means Clustering: Assigns each pixel to a predefined number of classes using the squared Euclidean distance between spectra [52].

1.3.2.2 Supervised methods

Supervised method in MSI is mainly used to identify profiles or specific bio-molecular ions to discriminate samples from different groups, e.g. a tumor from benign tissue. If information is known about patient outcome or response-to-treatment, the supervised analysis of the tumor specific profiles is then used to search for candidate bio-markers. These candidates are then tested in a larger sample set to test their ability to distinguish samples from different groups. This step usually yields only several candidate bio-markers, which can be then finally validated by using well established assays [48, 59]. To find candidate biomarkers, the pixels belonging to different areas of the tissues (e.g. tumor/benign) are compared, another time in the multivariate space of the m/zs, to find which variables are more important to distinguish one area from the other. Currently the widely used supervised classification methods include Partial Least Squares Discriminant Analysis (PLS-DA) [60, 61], Support Vector Machine (SVM) [62, 63] and Artificial Neural Network (ANN) [64, 65]. The foremost advantage of supervised methods is that the output manipulated by the algorithm is meaningful and can be easily used for discriminative pattern classification, but there are several disadvantages, such as 1) over-training of some

patterns while other patterns are left untrained or under-trained and 2) training data can be time-consuming and costly.

(1) Partial Least Squares Discriminant Analysis: Calculates scores and loadings like PCA from the training spectra groups and a discrimination line is created to represent the area of maximum separation between training spectra. The new spectra are then projected onto the training spectra for discrimination [60].

(2) Support Vector Machine: finds a hyper-plane that separates one or more classes. A peak ranking is derived from the hyper-plane. The best number of peaks is determined by a clustering in the subspace taken from the k best peaks, and the (best) solution is stored as the final model. The generated models are then used to classify each spectrum of the sample [66].

(3) Artificial Neural Network (back-propagation): feeds the information forward through the ANN layers, compares with outcome result with the known value, and then propagate the error backwards through the network. During the sequence of forward and backward cycles, the error is minimized by adjusting the weights that are applied to the interconnection between the input and hidden nodes, and hidden and output nodes. The training is terminated when the error reaches an acceptable threshold, The trained model is then used to classify each spectrum [67].

1.4 Conclusion

Most current data processing methods (both pre-processing and statistical analysis) follow algorithms designed for metabolomics. Those methods, unfortunately, cannot always be directly applied for MSI. Additionally, considering the large dataset produced in MSI, more time and memory efficient methods are required. These methods should also be instrument (both ion source and mass analyzer) specific. For example, base line correction could be easily done by smoothing for MSI data generated by high resolution Orbitrap, while it is not the case at all for those produced by TOF-MS. Although several ion sources have been widely used in MSI community, the data analysis is still focused on MALDI imaging, thus ion source-specific data processing methods are expected in the near future.

References

1. Goodwin, R.J., S.R. Pennington, and A.R. Pitt, *Protein and peptides in pictures: imaging with MALDI mass spectrometry.* Proteomics, 2008. **8**(18): p. 3785-3800.
2. Svatos, A., *Mass spectrometric imaging of small molecules.* Trends Biotechnol, 2010. **28**(8): p. 425-434.
3. Lee, Y.J., et al., *Use of mass spectrometry for imaging metabolites in plants.* The Plant Journal, 2012. **70**(1): p. 81-95.
4. Amstalden van Hove, E.R., D.F. Smith, and R.M. Heeren, *A concise review of mass spectrometry imaging.* J Chromatogr A, 2010. **1217**(25): p. 3946-3954.
5. Franceschi, P., et al., *Combining intensity correlation analysis and MALDI imaging to study the distribution of flavonols and dihydrochalcones in Golden Delicious apples.* J Exp Bot, 2012. **63**(3): p. 1123-1133.
6. Peukert, M., et al., *Spatially resolved analysis of small molecules by matrix-assisted laser desorption/ionization mass spectrometric imaging (MALDI-MSI).* New Phytol, 2012. **193**(3): p. 806-815.
7. Holscher, D., et al., *Matrix-free UV-laser desorption/ionization (LDI) mass spectrometric imaging at the single-cell level: distribution of secondary metabolites of Arabidopsis thaliana and Hypericum species.* Plant Journal, 2009. **60**(5): p. 907-918.
8. Cha, S., et al., *Direct profiling and imaging of plant metabolites in intact tissues by using colloidal graphite-assisted laser desorption ionization mass spectrometry.* Plant J, 2008. **55**(2): p. 348-360.
9. Zhang, H., S. Cha, and E.S. Yeung, *Colloidal graphite-assisted laser desorption/ionization MS and MS(n) of small molecules. 2. Direct profiling and MS imaging of small metabolites from fruits.* Analytical chemistry, 2007. **79**(17): p. 6575-6584.
10. Cha, S. and E.S. Yeung, *Colloidal graphite-assisted laser desorption/ionization mass spectrometry and MSn of small molecules. 1. Imaging of cerebrosides directly from rat brain tissue.* Anal Chem, 2007. **79**(6): p. 2373-2385.
11. Shrestha, B., Y. Li, and A. Vertes, *Rapid analysis of pharmaceuticals and excreted xenobiotic and endogenous metabolites with atmospheric pressure infrared MALDI mass spectrometry.* Metabolomics, 2008. **4**(4): p. 297-311.
12. Li, Y., B. Shrestha, and A. Vertes, *Atmospheric pressure molecular imaging by infrared MALDI mass spectrometry.* Anal Chem, 2007. **79**(2): p. 523-532.
13. Li, Y., B. Shrestha, and A. Vertes, *Atmospheric pressure infrared MALDI imaging mass spectrometry for plant metabolomics.* Anal Chem, 2008. **80**(2): p. 407-420.
14. Takats, Z., et al., *Mass spectrometry sampling under ambient conditions with desorption electrospray ionization.* Science, 2004. **306**(5695): p. 471-473.
15. Kertesz, V. and G.J. Van Berkel, *Improved imaging resolution in desorption electrospray ionization mass spectrometry.* Rapid Commun Mass Spectrom, 2008. **22**(17): p. 2639-2644.
16. Campbell, D.I., et al., *Improved spatial resolution in the imaging of biological tissue using desorption electrospray ionization.* Anal Bioanal Chem, 2012. **404**(2): p. 389-398.
17. Metzner, R., et al., *Imaging nutrient distributions in plant tissue using time-of-flight secondary ion mass spectrometry and scanning electron microscopy.* Plant Physiol, 2008. **147**(4): p. 1774-1787.
18. Smart, K.E., et al., *High-resolution elemental localization in vacuolate plant cells by nanoscale secondary ion mass spectrometry.* Plant J, 2010. **63**(5): p. 870-879.
19. Saito, K., et al., *Direct mapping of morphological distribution of syringyl and guaiacyl lignin in the xylem of maple by time-of-flight secondary ion mass spectrometry.* Plant J, 2012. **69**(3): p. 542-552.
20. Shrestha, B., J.M. Patt, and A. Vertes, *In situ cell-by-cell imaging and analysis of small cell populations by mass spectrometry.* Anal Chem, 2011. **83**(8): p. 2947-2955.

21. Nemes, P., A.A. Barton, and A. Vertes, *Three-dimensional imaging of metabolites in tissues under ambient conditions by laser ablation electrospray ionization mass spectrometry.* Anal Chem, 2009. **81**(16): p. 6668-6675.
22. Shrestha, B. and A. Vertes, *In situ metabolic profiling of single cells by laser ablation electrospray ionization mass spectrometry.* Anal Chem, 2009. **81**(20): p. 8265-8271.
23. Nemes, P. and A. Vertes, *Atmospheric-pressure molecular imaging of biological tissues and biofilms by LAESI mass spectrometry.* J Vis Exp, 2010(43).
24. Dill, A.L., et al., *Perspectives in imaging using mass spectrometry.* Chem Commun (Camb), 2011. **47**(10): p. 2741-2746.
25. Heeren, R.M.A., et al., *Why don't biologists use SIMS? A critical evaluation of imaging MS.* Applied Surface Science, 2006. **252**(19): p. 6827-6835.
26. Jessome, L., et al., *Matrix-assisted laser desorption/ionization mechanism study with dihydroxybenzoic acid isomers as matrices.* Rapid Communications in Mass Spectrometry, 2008. **22**(2): p. 130-134.
27. Lewis, J.K., J. Wei, and G. Siuzdak, *Matrix‐Assisted Laser Desorption/Ionization Mass Spectrometry in Peptide and Protein Analysis.* Encyclopedia of Analytical Chemistry, 2000.
28. Boggio, K.J., et al., *Recent advances in single-cell MALDI mass spectrometry imaging and potential clinical impact.* Expert Rev Proteomics, 2011. **8**(5): p. 591-604.
29. Anderson, D.M., et al., *High-resolution matrix-assisted laser desorption ionization-imaging mass spectrometry of lipids in rodent optic nerve tissue.* Mol Vis, 2013. **19**: p. 581-592.
30. Puolitaival, S.M., et al., *Solvent-free matrix dry-coating for MALDI imaging of phospholipids.* J Am Soc Mass Spectrom, 2008. **19**(6): p. 882-886.
31. Snel, M.F. and M. Fuller, *High-Spatial Resolution Matrix-Assisted Laser Desorption Ionization Imaging Analysis of Glucosylceramide in Spleen Sections from a Mouse Model of Gaucher Disease.* Analytical chemistry, 2010. **82**(9): p. 3664-3670.
32. Shroff, R., et al., *Acid-base-driven matrix-assisted mass spectrometry for targeted metabolomics.* Proc Natl Acad Sci U S A, 2009. **106**(25): p. 10092-10096.
33. Takats, Z., J.M. Wiseman, and R.G. Cooks, *Ambient mass spectrometry using desorption electrospray ionization (DESI): instrumentation, mechanisms and applications in forensics, chemistry, and biology.* Journal of Mass Spectrometry, 2005. **40**(10): p. 1261-1275.
34. Ifa, D.R., et al., *Desorption electrospray ionization and other ambient ionization methods: current progress and preview.* Analyst, 2010. **135**(4): p. 669-681.
35. Nefliu, M., et al., *Internal energy distributions in desorption electrospray ionization (DESI).* J Am Soc Mass Spectrom, 2008. **19**(3): p. 420-427.
36. Kaftan, F., et al., *Scanning electron microscopic imaging of surface effects in desorption and nano-desorption electrospray ionization.* Journal of Mass Spectrometry, 2011. **46**(3): p. 256-261.
37. Nemes, P., A.S. Woods, and A. Vertes, *Simultaneous Imaging of Small Metabolites and Lipids in Rat Brain Tissues at Atmospheric Pressure by Laser Ablation Electrospray Ionization Mass Spectrometry.* Analytical chemistry, 2010. **82**(3): p. 982-988.
38. Nemes, P. and A. Vertes, *Laser ablation electrospray ionization for atmospheric pressure, in vivo, and imaging mass spectrometry.* Analytical chemistry, 2007. **79**(21): p. 8098-8106.
39. Williams, B., et al., *An algorithm for baseline correction of MALDI mass spectra*, in *Proceedings of the 43rd annual Southeast regional conference - Volume 1*2005, ACM: Kennesaw, Georgia. p. 137-142.
40. Yu, W.C., et al., *Detecting and aligning peaks in mass spectrometry data with applications to MALDI.* Computational Biology and Chemistry, 2006. **30**(1): p. 27-38.
41. Eidhammer, I., et al., *Computational methods for mass spectrometry proteomics*. 2008: John Wiley & Sons.

42. Antoniadis, A., J. Bigot, and S. Lambert-Lacroix, *Peaks detection and alignment for mass spectrometry data.* Journal de la Société Française de Statistique, 2010. **151**(1): p. 17-37.
43. Alexandrov, T., *MALDI imaging mass spectrometry: statistical data analysis and current computational challenges.* BMC Bioinformatics, 2012. **13 Suppl 16**: p. S11.
44. Bauer, C., R. Cramer, and J. Schuchhardt, *Evaluation of peak-picking algorithms for protein mass spectrometry.* Methods Mol Biol, 2011. **696**: p. 341-352.
45. Alexandrov, T., et al., *Spatial segmentation of imaging mass spectrometry data with edge-preserving image denoising and clustering.* J Proteome Res, 2010. **9**(12): p. 6535-6546.
46. Alexandrov, T. and A. Bartels, *Testing for presence of known and unknown molecules in imaging mass spectrometry.* Bioinformatics, 2013. **29**(18): p. 2335-2342.
47. Nimesh, S., et al., *Current status and future perspectives of mass spectrometry imaging.* Int J Mol Sci, 2013. **14**(6): p. 11277-11301.
48. Jones, E.A., et al., *Imaging mass spectrometry statistical analysis.* J Proteomics, 2012. **75**(16): p. 4962-4989.
49. Deininger, S.O., et al., *Normalization in MALDI-TOF imaging datasets of proteins: practical considerations.* Anal Bioanal Chem, 2011. **401**(1): p. 167-181.
50. Norris, J.L., et al., *Processing MALDI Mass Spectra to Improve Mass Spectral Direct Tissue Analysis.* International Journal of Mass Spectrometry, 2007. **260**(2-3): p. 212-221.
51. Alexandrov, T. and J.H. Kobarg, *Efficient spatial segmentation of large imaging mass spectrometry datasets with spatially aware clustering.* Bioinformatics, 2011. **27**(13): p. i230-238.
52. Jones, E.A., et al., *Multiple statistical analysis techniques corroborate intratumor heterogeneity in imaging mass spectrometry datasets of myxofibrosarcoma.* PLoS One, 2011. **6**(9): p. e24913.
53. Race, A.M., et al., *Memory efficient principal component analysis for the dimensionality reduction of large mass spectrometry imaging data sets.* Anal Chem, 2013. **85**(6): p. 3071-3078.
54. Yao, I., et al., *In situ proteomics with imaging mass spectrometry and principal component analysis in the Scrapper-knockout mouse brain.* Proteomics, 2008. **8**(18): p. 3692-3701.
55. Siy, P.W., et al., *Matrix Factorization Techniques for Analysis of Imaging Mass Spectrometry Data.* 8th Ieee International Conference on Bioinformatics and Bioengineering, Vols 1 and 2, 2008: p. 875-880.
56. Hanselmann, M., et al., *Concise representation of mass spectrometry images by probabilistic latent semantic analysis.* Anal Chem, 2008. **80**(24): p. 9649-9658.
57. Louie, K.B., et al., *Mass spectrometry imaging for in situ kinetic histochemistry.* Scientific reports, 2013. **3**.
58. Konicek, A.R., J. Lefman, and C. Szakal, *Automated correlation and classification of secondary ion mass spectrometry images using a k-means cluster method.* Analyst, 2012. **137**(15): p. 3479-3487.
59. Schwamborn, K., *Imaging mass spectrometry in biomarker discovery and validation.* J Proteomics, 2012. **75**(16): p. 4990-4998.
60. Barnes, C.A., et al., *Identifying individual cell types in heterogeneous cultures using secondary Ion mass spectrometry imaging with C60 etching and multivariate analysis.* Analytical chemistry, 2012. **84**(2): p. 893-900.
61. Ferguson, L.S., et al., *Direct detection of peptides and small proteins in fingermarks and determination of sex by MALDI mass spectrometry profiling.* Analyst, 2012. **137**(20): p. 4686-4692.
62. Gormanns, P., et al., *Segmentation of multi-isotope imaging mass spectrometry data for semi-automatic detection of regions of interest.* PLoS One, 2012. **7**(2): p. e30576.
63. Casadonte, R., et al., *Imaging mass spectrometry (IMS) to discriminate breast from pancreatic cancer metastasis in FFPE tissues.* Proteomics, 2014.

399 64. Xiong, X.C., et al., *Artificial Neural Networks for Classification and Identification of Data of*
400 *Biological Tissue Obtained by Mass-Spectrometry Imaging.* Chinese Journal of Analytical
401 Chemistry, 2012. **40**(1): p. 43-49.
402 65. Rauser, S., et al., *Classification of HER2 receptor status in breast cancer tissues by MALDI*
403 *imaging mass spectrometry.* J Proteome Res, 2010. **9**(4): p. 1854-1863.
404 66. Schwamborn, K., et al., *Identifying prostate carcinoma by MALDI-Imaging.* Int J Mol Med, 2007.
405 **20**(2): p. 155-159.
406 67. Wilkins, C.L. and J.O. Lay, *Identification of microorganisms by mass spectrometry*. Vol. 169. 2005:
407 John Wiley & Sons.

408

Chapter 2

Mass Spectrometry Imaging in Plants: Sample Preparation and Application

Yonghui Dong, Pietro Franceschi

Notes:

This Chapter has been prepared for submission. Dong Y. wrote the draft; Pietro Franceschi revised and approved the final manuscript.

2.1 Introduction

Sample handling is one of the most crucial steps in MSI. Appropriate sample preparation method ensures high-quality signals, sufficient spatial resolution, and maintains the origin distribution and abundance of the molecules in biological samples [1-3]. Although sample preparation for proteins and peptides has been somewhat standardized [4, 5], it is still a major challenge for metabolites, largely because metabolites can be easily metabolically modified, diffuse from the sample, or be removed during sample preparation [5]. Figure 1 presents an example showing how small variations in sample handling (use ascorbic acid to prevent oxidation) can greatly influence the quantitative mapping of metabolites in MSI by comparing three ion images at two different areas in the same apple section. Enzymatic oxidation is effectively prevented in the area where ascorbic acid solution is sprayed, and quercetin and phloretin are solely detected in the sepal bundle. While in the ascorbic acid-free area, quercetin is found to diffuse out of the sepal bundle and phloretin is completely undetectable. Alongside, a marker of m/z 490.948 is identified in the enzymatic browning area. Everyone agrees on the fact that sample preparation is important to ensure true and accurate mapping of molecules with a reproducible manner, but it is common to think that sample preparation is appropriate if there are not visible alternations in tissue. This is in general true, but cannot be generalized to all cases. Sample preparation method is MSI instrument, sample tissue and target analyte molecules dependent, and therefore should be carefully optimized accordingly.

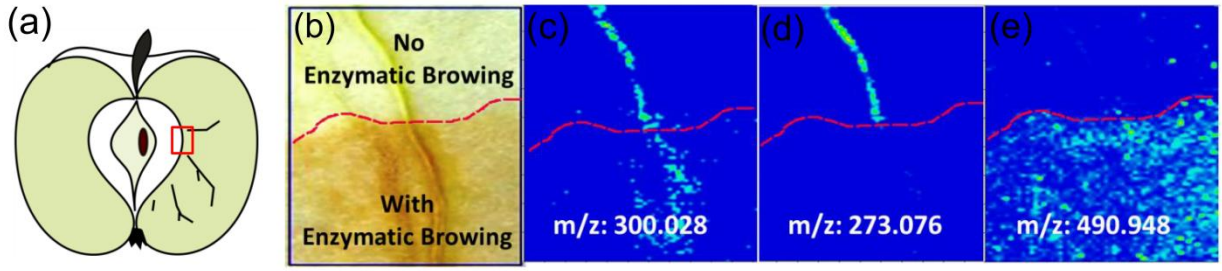

Figure 1. Effects of sample preparation on quantitative mapping of flavonols in apple by using MALDI imaging. Apple section was manual sliced using a razor blade. After mounted on a glass slide, the upper part of the section was immediately sprayed with 10 mM/L ascorbic acid to prevent the enzymatic oxidation, while the lower part remained untreated. After vacuum dehydration (~4h), the section was uniformly sprayed coated with 7 g/L CHCA using an

ImagePrep station and analyzed by MALDI Orbitrap at negative mode. (a) An apple sketch illustrating the origin of apple tissue sample. (b) The optical image of apple section prior to matrix coating, showing difference between ascorbic acid treated (upper) and untreated (lower) parts following vacuum dehydration. (c) Delocalization: quercetin (m/z 300.028) detected in sepal bundle in both upper and lower apple section, but it was diffused from the sepal bundle in lower part. (d) False negative: phloretin (m/z 273.076) only present in the sepal bundle in upper part. (e) False positive: marker (m/z 490.948) only present in the lower part as a result of enzymatic browning.

A comprehensive overview of different aspects of MSI sample preparation for mammalian tissues has been recently published [6]. MSI sample preparation for plants, however, is more challenging as plant surfaces are hydrophobic, making ionization more difficult. In addition, plant surface are often covered with cuticles, direct MSI of molecules under the cuticle layer become difficult by using soft ionization methods like MALDI and DESI; therefore it is necessary to efficiently remove the cuticle barriers while preserving the analytes original localization. Furthermore, application of MSI in plants is recent, and there is a necessity to adapt the current sample preparation protocols for plant tissues [1]. This review will thereby focus on MSI sample preparation methods for plants. In particular, the optimal sample preparation strategy for different classes of metabolites in plants will be discussed on the bases of the most recent publications.

2.2 Sample Preparation

The sample preparation protocol consists of several steps: tissue storage, sectioning, mounting and ionization aiding treatment [6, 7]. The steps vary in methods and sequences depending on MSI instrument, nature of sample tissues and analytes to be imaged. Therefore each step need to be carefully designed and optimized accordingly.

2.2.1 sample storage

Most MSI in plants are done on freshly prepared samples, MSI on long-term-stored plant samples are seldom reported. When necessary, plant samples can be stored as section slides. In our lab, apple sections are vacuum dried (~50 Torr, 4 h), mounted onto the glass slide, and

placed into a 50 ml centrafigation tube with several small holes (~ 2mm) drilled on its cap (i.e. corning® 50 mL PP centrifuge tubes, Sigma Aldrich). The tubes are then vacuum sealed in a vacuum bag, and stored at -80 ^{o}C. Vacuum sealing prevents the sample from contacting with air and water, while placing the section slide into the tube avoids the deformation of section during vacuum sealing, and avoids direct contact with the bag during storage. When ready for MSI, the sections can be recovered for 2 h under vacuuum (~50 Torr). Our MALDI imaging of flavonoids suggests that there are no significant quantitative detection differences between long-term-stored (9 months) and fresh-prepared apple sections for the target analytes. A possible alternative is to store plant samples as imprints, although the effect of storage on the quantitative detection in MSI still needs to be evaluated (details about Impring are discusses in the following section). When samples are small, they can also be stored as intact tissues, but freezing and thawing are a critical process that has an effect on the tissue architecture.

2.2.2 Sectioning

Plant cells have rigid cell walls and large intercellular spaces, embedding materials are often used to maintain the tissue morphology and to ensure precise sample sectioning in conventional histology practice. Unfortunately, many of these commonly used embedding mediums are incompatible with MSI, for example, optimum temperature cutting (OTC) compounds can diffuse easily into sample tissues and act as significant ion suppressors (as they have a high ionization efficiency) in MALDI-MSI [8]. Carboxymethyl cellulose (CMC) [9], gelatin [10], ice [11] or their combinations [12] have been successfully employed for embedding mammalian tissues. While for plant tissues in the specific case of rice seed, Zaima and coworkers found that the rice section quality is rather poor when using 2% CMC alone as embedding medium; with the assistance of adhesive film, CMC embedding offers good performance for both sectioning and MALDI imaging of rice metabolites [13, 14] because the presence of adhesive film largely reduces section distortion and dislocation, facilitating the transfer and attachment of sections to slides [15].

Cryosectioning is the most commonly used method to prepare plant sample sections. Frozen samples are prepared by using freezer (mostly -80 ^{o}C), powdered dry ice, liquid nitrogen or liquid nitrogen-chilled isopentane [8]. Liquid nitrogen frozen usually makes plant sections brittle,

and can result in ice crystal formation, thus rapid plunging of the tissue into the liquid nitrogen is not recommended. Floating tissues in aluminum foil in liquid nitrogen [16, 17] or freezing plant tissues on dry ice-chilled steel plate is more favoured. Besides, plant sample sections can be prepared using microtome sectioning [18] and hand-cutting [19, 20] at room temperature.

Sample thickness is another important parameter to consider as it can affect peak numbers and peak intensity in some MSI instruments. For mammalian tissues, section thickness between 5-20 µm is recommended for analysis of low molecular weight molecules, and < 5 µm thickness for high molecular weight proteins (m/z>9000) [21]. In contrast, relationship between tissue thickness and spectrum quality is seldom studied in MSI of plant sections. As a general rule it is difficult to cut tiny slices from the water rich tissues commonly found in plants, so tissue thickness of most plant sections in current MSI studies is around 50 µm, which provides a good compromise between optimum MSI performance and practicality, especially when a large number of samples has to be prepared [1]. Thicker sections, however, usually cause poor molecule ionization, which is probably due to electrical non-conductivity (especially in ToF-MS), high impurities in thick tissues [21], tissue distortion and matrix absorption (in MALDI MSI) [1]. In particular, matrix absorption is often observed in spongy tissue sections, and this causes a strong signal loss. This phenomenon has been observed in the pith region of a tobacco root section when the tissue thickness is over 45 µm [1].

2.2.3 Mounting

The simplest mounting method is to place the tissue slices directly onto the target plate, however, target plate must be thoroughly cleaned after each measurement [17]. A more common method involves attaching the sample slices onto a glass slide. It is worth noting that indium tin oxide coated (ITO) conductive glass slide is not a must, it is only needed when good electric conductivity is essential, i.e. non-orthogonal TOF-MS. In contrast, since DESI involves landing and releasing of charged particles in the surface, such conductive materials should not be used to avoid neutralization on the surface [22].

Three approaches are commonly used to mount plant sections to the glass slide, the use of double sided tapes, epoxy glue and thaw mounting. Using double sided tape is fast and easy, but it should be careful not to contaminate the sample. Epoxy glue is suitable for delicate samples and

it does not produce extra mass signals. Thaw mounting is usually used to attach plant samples sectioned which are acquired by cryosectioning. It minimizes the risk of sample contamination, while relocation of water soluble analytes due to water condensation during thaw mounting of frozen sections is a major concern [23]. Thaw mounting also limits the downstream sample processing steps, as the tissue risks being washed off the sample plate by any vigorous solution-based treatments (i.e. the washing steps in MSI of proteins for the purpose of removing salts) [4]. To avoid this problem, thaw mounted samples are usually freeze dried on the sample plate to improve the mounting efficiency.

2.2.4 Ionization aiding treatments

Most widly used matrices in MALDI MSI are α-cyano-4-hydroxycinnamic acid (CHCA) and 2,5-dihydroxybenzoic acid (DHB). However, there is a valid concern that imaging of small molecules, especially those with molecule weights in the matrix region, is affected by interference with matrix [24]. For these reasons, alternative metrics are designed to limit these artifacts, such as porphyrins [25], inorganic materials [23, 26, 27], porous silicon [28], and 1,8-bis(dimethylamino) naphthalene (DMAN) [29].

Four matrix application methods are generally used:

- The first is spray based method, including manual spraying (i.e. with an airbrush) and automatic spraying (i.e. using ImagePrep (Brucker) or M-Sprayer™ (HTXImaging)). Manual spray requires high skills as inhomogeneous matrix application and analyte delocalization can easily occur, while with automatic spraying sample surface could be homogeneously covered with matrices easily.
- The second method is spotting based (matrix is delivered by microspotting to a specific sample surface location), such as using CHIP-1000 chemical printer (Shimadzu) or Portrait® 630 Spotter (Labcyte). The spotting method allows accurate matrix depositition onto tissue sections, which thus ensures a good quantitative MS signal generation in MSI [30].
- The thrid method is sublimation, where matrix can be homogeneouly applied to sample surface under reduced pressure and elevated temperature in a fast manner. This method requires no solvent; therefore diffusion of the analyte molecules during matrix

application is eliminated. Other advantages include high reproducibility, increased matrix purity and formation of fine matrix crystals [31].

- The matrix can be dry coated by filtering through a sieve (i.e. 20 µm) directly onto the tissue sections without any solvent. This method is simple, fast and meanwhile it avoids analyte delocalization [32],], even though it can reduce the extraction of the metabolites from the tissues.

In DESI, matrix coating on sample surface is not necessary because analyte molecules are ionized by a high-speed, charged liquid jet stream. In this case, however, the spray solvent composition is the critical element. It should be optimized according to the metabolites under investigation, but also taking into account specific characteristics of the samples like surface wettability [33, 34]. In general, an higher fraction of water is used for long lasting signal, while an higher proportion of methanol is used when higher spatial resolution is required [35] .

2.2.5 Other considerations for plant samples

2.2.5.1 Fresh sample versus dry sample

Fresh plant tissues are ideal for MSI studies since they are chemically unmodified and treatment-free, which largely keep the origin and integrity of molecules spatial arrangement and avoid the chemical contamination during sample handling. One obvious problem is that the fresh plant samples may shrink significantly during MSI analysis even when they are firmly attached on the sample plate. This is particularly true when the experiments are performed under vacuum like in the case of UV-MALDI or SIMS. The shrinkage would result in mismatch between MS image and optical image [23], which makes biological interpretation difficult. Alongside, the shrinkage during MSI analysis may bring in large mass shift under ToF-MS analyzer, and molecule identification and reproducibility of MS images are thus limited. Another concern is that the biological processes are still active inside the fresh samples and they may cause degradation and/or chemical modification during MS imaging. In the case of (IR)-MALDI and LAESI, native water in the plant samples are employed as matrix, so the sample tissues should be fresh or at least not totally dried out [36-38].

Most plant tissue samples are usually vacuum or freeze dried prior to MSI. Vacuum desiccation is generally applied at room temperature to thin plant organs without sectioning, such as plant leaves and flowers [23, 39-41], or to plant samples sectioned with a microtome or a razor blade, such as apple [20]. Vacuum pressure and drying time should be carefully optimized, according to the nature of sample and analytes of interest. Sample surface regulation after drying is usually necessary to reduce the distortion of plant tissues. It is likely that some volatiles would be removed from plant sections upon vacuum desiccation, while the majority of molecules are expected to be unaffected due to their low vapor pressure [20]. This has been confirmed by comparing MS profiles of target metabolites between fresh and dried *Arabidopsis* samples before MSI studies [23].

2.2.5.2 Removal of plant cuticle

Land plant body, such as leaves and flowers, is usually covered with cuticles (0.1-10 µm thick). Soft ionization techniques such as MALDI and DESI are unable to penetrate through the plant cuticle, causing signal intensity insufficient and instability during MSI of analyte molecules below the cuticle layer. There are several ways to deal with the plant cuticle barrier. Direct methods include physical and chemical treatments. Sample cuticles can be either physically removed or chemically washed off. For example, after peeling off the epidermis, distribution of hydroxynitrile glucosides was successfully mapped in barley leaves [40]; Kaempferol and kaempferol rhamnoside were mostly detected in *Arabidopsis* leaf area where it was pre-treated with chloroform for 60 s [39]. However those ‘stress methods’ may delocalize and/or wash away the target compounds, and not all plant epidermis can be easily removed physically.

Alternatively, an indirect method is the use of blotting or imprinting. Plant tissues are pressed onto porous Teflon [40, 42, 43], porous polytetrafluoroethylene (PTFE) [44] or print paper surfaces [45] by applying a moderate pressure over the plant tissues, thereby transferring the plant molecules onto flat hard surfaces while keeping their spatial distribution. A recent publication demonstrates that the transfer efficiency could be improved with the assistance of solvent extraction and/or heating during imprinting [46]. Imprinting is simple, fast and robust, and MSI results are quite reproducible. However, this method is restricted to relatively ‘juicy’ plant tissues. Spatial resolution is also limited since analytes can be smeared during imprinting

[5]. The loss of compartmentalization of enzymes during imprinting may also trigger the reaction of the enzymes with their metabolites, causing the degradation or inter-conversion of the metabolites.

2.2.5.3 Tissue sample surface effect

The multicellular nature of higher plants presents many challenges for mapping the distribution of analyte molecules [5]. It is well known that that sample surface properties affect the ionization processes in MSI, while it is often ignored that the differences of sample surface properties in a structurally/biologically heterogeneous sample can largely affect the quantitative detection of analytes, causing the MS images misrepresenting their true distribution. This phenomenon has been observed in MALDI [1], SIMS [47] and DESI (chapter 4). In MALDI imaging, spraying the surface with large amounts of matrix can to some degree minimize the surface effect differences [5], while it is more difficult for SIMS and DESI imaging. Complementary quantification methods such as LC-MS or GC-MS, novel sample handling methods (see details in chapter 4) are thus suggested to validate the MSI results.

2.3 Application of MSI in plants

MSI studies in plants are still focused on method development and technological applications and this type of studies has been mainly performed by mapping distribution of readily accessible metabolites [48], only recently has MSI started to be applied to the solution of biologically relevant questions [5], including: 1) plant-environment interaction [49-51], 2) new compound identification [52], and 3) functional genomics [41].

In the following section, we will summarize the recent studies of MSI in plants according to different classes of primary and secondary metabolites. More specifically, the choice of matrix/spray solvent is also a crucial factor contributing to MSI quality, i.e., spatial resolution, peak resolution, sensitivity, intensity, noise. Thereby the use of different matrices/spray solvents to specifically map various classes of molecules will be also discussed.

Table 1 A summarize of current MSI of different classes of plant metabolites.

Chemical class	MSI Source (Ion mode)	Matrix or Spray solvent	Sample	Analyte	Sample preparation	Ref.
Carbohydrates	UV-MALDI (+)	CHCA (in MeOH:H_2O, 1:1, + 0.1% FA)	Wheat stem *(Triticum aestivum)*	oligosaccharides	• cryosecting (-20°C, 50 µm) & hand sectioning • matrix applied with airbrush • doubly sided tape mounting	[19]
	UV-MALDI (+)	DHB, CHCA, SA 20mg/ml (ACN:H_2O, 1:1, +0.1% TFA)	Poplar stem	Cellulose	• cryosecting (-8°C, 50 µm) • matrix applied with oscillating capillary nebulizer • doubly sided tape mounting	[53]
	UV-MALDI (+)	DHB, 25mg/ml (in 0.05 mM aqueous sodium acetate)	Poplar stem	cellulose hemicellulose	• microtome sectioning (room temperature, 50 µm) • matrix applied with Meinhard nebulizer • cryoJane tape mounting	[18]
	IR-MALDI (+)	Native water in the samples	Strawberry	fructose/glucose sucrose	• hand cutting (room temperature, 0.2-0.5 mm) • fresh sample	[36]
	DESI (+)	MeOH:H_2O,1:1 +1%FA	Datura stramonium	hexose sucrose	• imprinting on porous Teflon	[42]
Organic acids	GALDI (-)	Colloidal graphite (in 2-propanol)	Apple Strawberry	malic acid ascorbic acid citric acid quinic acid	• cryosecting (liquid nitrogen pre-treated) • colloidal graphite applied by air spray • doubly sided tape mounting	[26]
	DESI (-)	ACN:H_2O,4:1	Grape leaf, stem	malic acid tartaric acid citric acid	• hand cutting (room temperature, 0.3mm) & imprinting • doubly sided tape mounting	unpublished

Lipids & Fatty acids	MALDI (+/-)	DHB, 50mg/ml (in MeOH:H_2O, 7:3)	Black rice seed (*Oryza sativa L.*)	lysophosphatidylcholine, phosphatidylcholine, Phytic acid gamma-Oryzanol ahpha-Tocopherol	• cryosecting (-80°C frozen section & freeze imbedded section with 2% CMC at -80°C, 8 µm) • matrix applied with airbrush • doubly sided tape mounting	[13]
	MALDI (+)	DHB	Cotton seed *(Gossypium hirsutum)*	phosphatidylcholines, triacylglycerols, phospholipids	• cryosecting (unfixed & paraformaldehyde fixed sections, -20°C, 30 µm) • matrix applied via sublimation	[54]
	LDI (+)	Colloidal silver	A. thaliana leaf & flower	epicuticular wax metaboliyes	• vacuum dried (~50 Torr, 30-60 min) • MicroFlow PFA-ST Nebulizer • doubly sided tape mounting	[39]
	MALDI (+)	Lithium-DHB, 20mg/ml (in acetone: dichloromethane, 9:1)	A. thaliana leaf Date palm tree leaf (Phoenix sp.)	Wax esters	• desiccator dried samples • matrix applied with airbrush •	[55]
Proteins & Peptides	MALDI (?)	Sinapinic acid	soybean cotyledon	Proteins	• cryosectioning (10-15 µm)	[2]
	MALDI (?)	?	Barley grain	Proteins	?	[3]

Terpenoids	LDI (-)		Hypericum leaf, placenta, stamen and stylus	Naphthodianthrones	• cryosecting of placenta (60 µm)	[56]
	DESI (-)	MeOH:H_2O, 1:1, +1% ammonium	*Hypericum perforatum*	Hyperforin Hypericin	• imprinting on porous Teflon	[42]
	DESI (-)	100 uM NH4Cl in MeOH		Bromophycolide A and B	• preserved with 10% formalin in seawater and kept moist with seawater	[50]
Alkaloids	MALDI (+)	Saturated HCCA (in methanol)	Capsicum fruit	Capsaicin	• cryosectioning (-20°C, 70 µm) • matrix applied with airbrush • thaw-mounted	[57]
	DESI (-)	MeOH:H_2O, 9:1	*Myristica malabarica* seed	Malabaricone C	• imprinting on printer paper	[45]
	MALDI (+)	DHB, 30mg/ml (in MeOH:H_2O, 1:1+1%TFA)	Fruiting bodies of *M. metata**	6-Hydroxymetatacarboline D	• freeze-dried • matrix applied with ImagePrep • double sided tape mounting	[52]
Phenolics	GALDI (-)	Colloidal graphite (in 2-propanol)	A. thaliana leaf , flower and stem	Favonoids	• vacuum dried (for leaf and flower, ~50 Torr, 30 min) & cryosectioning (for stem)	[23, 41]
	MALDI (+)	DHB, 50 mg/mL (in MeOH:H_2O, 7:3)	Black rice seed (*Oryza sativa L.*)	Anthocyanins	• cryosectioning (freeze-embedded with 2% CMC at -80°C, 10 µm) • matrix applied with airbrush • doubly sided tape mounting	[14]

	MALDI (+)	DHB, 50 mg/mL (in MeOH:H_2O, 7:3)	Rabbiteye blueberry (*Vaccinium ashei*)	Anthocyanins	• cryosectioning (50 µm) • matrix applied with airbrush • thaw-mounted and air dried	[58]

CHCA: α-Cyano-4-hydroxycinnamic acid; DHB: 2,5-dihydroxybenzoic acid; SA: sinapinic acid; ACN: acetonitrile; FA: formic acid; TFA: Trifluoroacetic acid

**M. metata* is not classified as plant

2.3.1 Primary metabolites

2.3.1.1 Carbohydrates

Distribution of carbohydrates has been mapped by UV-MALDI imaging in several plant systems [18, 19, 53], in which DHB and CHCA are the common matrices for most types of carbohydrates, and DHB is proved slightly better than CHCA in detecting the small oligosaccharides such as glucose and sucrose [26]. Colloidal graphite is proposed as an alternative matrix for imaging the small oligosaccharides as it largely reduced the matrix interference in small mass region (m/z < 500). Besides, IR-MALDI is also used for imaging carbohydrates in different plants, such as strawberry [36] and lily flower [37]. Carbohydrates are mostly detected in MALDI imaging under positive mode.

Only one case on DESI imaging of carbohydrates in plants has reported [42], partially because of its low selectivity and sensitivity for carbohydrates. Yet 3-nitrophenylboronic acid and N-methyl-4-pyridineboronic have been suggested as effective reagents added in DESI spray solvent for *in-situ* derivatization of sugars (reactive-DESI), which therefore largely improves both selectivity and sensitivity of intact sugars in complicated biological matrices [59].

2.3.1.2 Lipids and Fatty Acids

Localization of various unsaturated lipids have been mapped in rice [13] and cotton seeds by MALDI MSI [54]. In these tissues, they are readily detected as multiple adducted ions (primarily H^+, Na^+ and K^+) under positive ion mode by using DHB as matrix. MALDI imaging of saturated hydrocarbons (Hcs) is more challenging as they do not contain any polar groups neither susceptible to protonation nor to which a cation or an anion can be easily attached [60].

Monovalent cations of transition metals (e.g. Fe, Mn, Cu), when co-deposited on the MALDI target with Hcs, can give cationized species which can be detected in a mass spectrometer. Due to the high reactivity of transition metals, Hcs are highly fragmented during analysis, and molecule identification is thus limited [60]. The reactivity of silver with Hcs is lower than that of any other transition metals and it usually generates intact silver adduct ions. MALDI imaging of epicuticular wax in *Arabidopsis* has been successfully reported by using silver colloid as matrix, in which 14 cuticular wax compounds are identified in *Arabidopsis* wild-type (Ler) and CS8 mutant leaves [39]. The pitfall is that silver is present with similar abundance of the two stable isotope. Each molecule produces a group of silver adduct ion peaks including two major ions [monoisotopic mass of the metabolite + ^{107}Ag or ^{109} Ag]$^{+}$, making compound identification and quantification difficult [39, 60]. Another report on MALDI imaging of saturated wax esters in *Arabidopsis* and date palm leaves by using LiDHB suggests that LiDHB is the most versatile matrix for detection of a majority of neutral lipids and it can potentially replace currently used silver salts [55].

DESI imaging of lipids is the most frequent application of DESI MSI in mammalian tissues, while DESI imaging of lipids in plants has not yet been reported. Since lipids are more readily ionized by DESI, DESI will be a complimentary to MALDI for imaging lipids in plants where high spatial resolution is not required. In mammalian tissues, mixtures of water and methanol acetonitrile, with or without an acidic modifier are the most commonly used spray solvents DESI imaging of lipids [61].

2.3.1.3 Proteins and Peptides

Only few MSI of proteins and peptides have been reported in plants ad this is probably due to several concurring reasons.

- Difficulties in plant protein identification: protein identification relays heavily on the complete protein databases but to date only few plant genomes are fully sequenced [3];
- Challenges in sample preparations: sample preparation for proteins is more sophisticated than for other molecules. Several additional washing steps are required to remove the contaminate salts and sugars, to ensure tissue dehydration and fixation, and to prevent

proteolysis [17]. The wash procedure varies in solvent composition, temperature and duration among different tissues, which needs to be optimized accordingly.

- Detection limit: Proteins larger than 25KD are not routinely detectable by MALDI MSI, as they are not efficiently stabilized in the matrix solution and are not extractable from the tissue [62]. On-tissue digestion of large proteins enables their detection and identification in MSI while the treatment with proteolytic enzymes will enhance analyte diffusion and thus reduce the spatial resolution [3]. The application of MSI of proteins in plants has, however, been illustrated by two examples. MALDI imaging of proteins in developing barley grain [3] and in soybean cotyledon [2], where tissue-specific and color-specific protein expression patterns have been revealed. A detailed protocol is also attached in the latter example, in which sinapinic acid (SA) is suggested as matrix for MALDI imaging of proteins (>3000 Da), and CHCA and DHB for Peptides (< 3000 Da).

2.3.2 Secondary metabolites

2.3.2.1 The terpenoids

Distribution of terpenoids in *Hypericum perforatum* have been studied by LDI imaging on fresh tissues [56] and DESI imaging on tissue imprints [42], respectively. Results of those two studies from different MSI ion sources are in complete agreement that hyperforin and adhyperforin are found in translucent glands, and hypericin, pseudohypericin, protopseudohypericin, and protohypericin are exclusively located in dark glands in leaves. In particular, since they are highly UV absorbing compounds, application of a matrix is not necessary thus LDI removes the barriers of matrix for spatial resolution, and a 10 um resolution is achieved under the 10 x 10 um laser focus setting. Understanding the true biological function of a natural product requires direct fine-scale evaluation in the producing organism's tissues [63]. MSI provides a definitive measurement of the physical location of natural products with semi-quantitative information, which would facilitate our understanding in chemically-mediated biological processes. One example is the DESI imaging of a tropical red alga tissue surface, where bromophycolide A and B are found exclusively distributed in association with distinct surface patches at concentrations sufficient to inhibit the detrimental Lindra thalassiae fungus [50]. Notice that all those terpenoids in the above examples are imaged under negative ion mode.

2.3.2.2 The Alkaloids

Alkaloids are often highly present in particular medicinal plant organs, namely 'medicinal part' [64]. Knowing their localization is valuable not only to understand their metabolic origins, but also for the optimization of isolation process since the extraction can be focused on compound containing parts. Rapid profiling of alkaloids have been studied in several plants by DESI and MALDI, such as DESI profiling of alkaloids in *Conium maculatum*, *Datura stramonium* and *Atropa belladonna* [65], and MALDI profiling of alkaloids in several medicinal herbs, including *Radix Aconiti Lateralis Preparata*, *Rhizoma Coptidis and Strychnos nux-vomica L.* [66]. This type of studies provides potential protocols for the application of MSI of alkaloids in plants. Distribution of alkaloids has been mapped for several purposes. For example, MALDI imaging of capsaicin in capsicum fruits [57] and DESI imaging of malabaricone C. in Myristica malabarica seed [45] to study their metabolic origin; MALDI imaging of fruiting bodies of a mushroom to screen for new metabolites [52]. All the above studies are performed under positive mode in DESI and MALDI, and alkaloids are detected mainly as $[M+H]^+$, and some salt adducts, such as $[M+K]^+$.

2.3.2.3 The Phenolics

Distribution of phenolics have been mapped in several plants including strawberry [26], apple [20, 26], *Arabidopsis* [23, 56], rice [14] and blueberry [58] by using MALDI, GALDI and LDI imaging. Flavonols are mainly detected as $[M-H]^-$ at negative mode, while anthocyanins are primarily identified under positive mode as $[M]^+$. Both CHCA and DHB are common matrices in MALDI imaging of phenolics in plants. DESI imaging is recently applied to localize flavonols in gingo leaves under negative mode, and anthocyanins in strawberry under positive mode [46]. MSI also can be utilized to understand the gene expression pattern. One good example is the LDI imaging of flavonoids on the wild-type and mutant (tt7) *Arabidopsis* flowers. *Arabidopsis* TT7 mutant effectively blocks the production of quercetin and isorhamnetin and their glycoside derivatives, but leads to the accumulation of kaempferol and its glycoside glycosides. By comparing distribution of various flavonoids on the flower of the wild-type and mutant (tt7) *Arabidopsis*, results strongly suggests that the expression of the TT7 gene is localized on the

proximal part of the petal while the other genes in the upper stream pathway are evenly expressed throughout the petal [41].

References

1. Peukert, M., et al., *Spatially resolved analysis of small molecules by matrix-assisted laser desorption/ionization mass spectrometric imaging (MALDI-MSI).* New Phytol, 2012. **193**(3): p. 806-815.
2. Grassl, J., N.L. Taylor, and A.H. Millar, *Matrix-assisted laser desorption/ionisation mass spectrometry imaging and its development for plant protein imaging.* Plant Methods, 2011. **7**(1): p. 21.
3. Kaspar, S., et al., *MALDI-imaging mass spectrometry - An emerging technique in plant biology.* Proteomics, 2011. **11**(9): p. 1840-1850.
4. Goodwin, R.J., S.R. Pennington, and A.R. Pitt, *Protein and peptides in pictures: imaging with MALDI mass spectrometry.* Proteomics, 2008. **8**(18): p. 3785-3800.
5. Lee, Y.J., et al., *Use of mass spectrometry for imaging metabolites in plants.* The Plant Journal, 2012. **70**(1): p. 81-95.
6. Goodwin, R.J., *Sample preparation for mass spectrometry imaging: small mistakes can lead to big consequences.* J Proteomics, 2012. **75**(16): p. 4893-4911.
7. Pol, J., et al., *Molecular mass spectrometry imaging in biomedical and life science research.* Histochem Cell Biol, 2010. **134**(5): p. 423-443.
8. Zaima, N., et al., *Matrix-assisted laser desorption/ionization imaging mass spectrometry.* Int J Mol Sci, 2010. **11**(12): p. 5040-5055.
9. Goto-Inoue, N., et al., *Imaging mass spectrometry visualizes ceramides and the pathogenesis of dorfman-chanarin syndrome due to ceramide metabolic abnormality in the skin.* PLoS One, 2012. **7**(11): p. e49519.
10. Chen, R.B., et al., *Three Dimensional Mapping of Neuropeptides and Lipids in Crustacean Brain by Mass Spectral Imaging.* J Am Soc Mass Spectrom, 2009. **20**(6): p. 1068-1077.
11. Khatib-Shahidi, S., et al., *Direct molecular analysis of whole-body animal tissue sections by imaging MALDI mass spectrometry.* Anal Chem, 2006. **78**(18): p. 6448-6456.
12. Nelson, K.A., et al., *Optimization of whole-body zebrafish sectioning methods for mass spectrometry imaging.* J Biomol Tech, 2013. **24**(3): p. 119-127.
13. Zaima, N., et al., *Application of imaging mass spectrometry for the analysis of Oryza sativa rice.* Rapid Commun Mass Spectrom, 2010. **24**(18): p. 2723-2729.
14. Yoshimura, Y., et al., *Different localization patterns of anthocyanin species in the pericarp of black rice revealed by imaging mass spectrometry.* PLoS One, 2012. **7**(2): p. e31285.
15. Kawamoto, T., *Use of a new adhesive film for the preparation of multi-purpose fresh-frozen sections from hard tissues, whole-animals, insects and plants.* Archives of Histology and Cytology, 2003. **66**(2): p. 123-143.
16. Nimesh, S., et al., *Current status and future perspectives of mass spectrometry imaging.* Int J Mol Sci, 2013. **14**(6): p. 11277-11301.
17. Schwartz, S.A., M.L. Reyzer, and R.M. Caprioli, *Direct tissue analysis using matrix-assisted laser desorption/ionization mass spectrometry: practical aspects of sample preparation.* Journal of Mass Spectrometry, 2003. **38**(7): p. 699-708.
18. Lunsford, K.A., G.F. Peter, and R.A. Yost, *Direct matrix-assisted laser desorption/ionization mass spectrometric imaging of cellulose and hemicellulose in Populus tissue.* Anal Chem, 2011. **83**(17): p. 6722-6730.

19. Robinson, S., et al., *Localization of water-soluble carbohydrates in wheat stems using imaging matrix-assisted laser desorption ionization mass spectrometry.* The New phytologist, 2007. **173**(2): p. 438-444.
20. Franceschi, P., et al., *Combining intensity correlation analysis and MALDI imaging to study the distribution of flavonols and dihydrochalcones in Golden Delicious apples.* J Exp Bot, 2012. **63**(3): p. 1123-1133.
21. Sugiura, Y., S. Shimma, and M. Setou, *Thin Sectioning Improves the Peak Intensity and Signal-to-Noise Ratio in Direct Tissue Mass Spectrometry.* Journal of the Mass Spectrometry Society of Japan, 2006. **54**(2).
22. Takats, Z., J.M. Wiseman, and R.G. Cooks, *Ambient mass spectrometry using desorption electrospray ionization (DESI): instrumentation, mechanisms and applications in forensics, chemistry, and biology.* Journal of Mass Spectrometry, 2005. **40**(10): p. 1261-1275.
23. Cha, S., et al., *Direct profiling and imaging of plant metabolites in intact tissues by using colloidal graphite-assisted laser desorption ionization mass spectrometry.* Plant J, 2008. **55**(2): p. 348-360.
24. Jun, J.H., et al., *High-spatial and high-mass resolution imaging of surface metabolites of Arabidopsis thaliana by laser desorption-ionization mass spectrometry using colloidal silver.* Anal Chem, 2010. **82**(8): p. 3255-3265.
25. Ayorinde, F.O., K. Garvin, and K. Saeed, *Determination of the fatty acid composition of saponified vegetable oils using matrix-assisted laser desorption/ionization time-of-flight mass spectrometry.* Rapid Communications in Mass Spectrometry, 2000. **14**(7): p. 608-615.
26. Zhang, H., S. Cha, and E.S. Yeung, *Colloidal graphite-assisted laser desorption/ionization MS and MS(n) of small molecules. 2. Direct profiling and MS imaging of small metabolites from fruits.* Analytical chemistry, 2007. **79**(17): p. 6575-6584.
27. Cha, S. and E.S. Yeung, *Colloidal graphite-assisted laser desorption/ionization mass spectrometry and MSn of small molecules. 1. Imaging of cerebrosides directly from rat brain tissue.* Anal Chem, 2007. **79**(6): p. 2373-2385.
28. Ronci, M., et al., *Mass spectrometry imaging on porous silicon: investigating the distribution of bioactives in marine mollusc tissues.* Anal Chem, 2012. **84**(21): p. 8996-9001.
29. Shroff, R., et al., *Acid-base-driven matrix-assisted mass spectrometry for targeted metabolomics.* Proc Natl Acad Sci U S A, 2009. **106**(25): p. 10092-10096.
30. Vegvari, A., et al., *Essential tactics of tissue preparation and matrix nano-spotting for successful compound imaging mass spectrometry.* J Proteomics, 2010. **73**(6): p. 1270-1278.
31. Hankin, J.A., R.M. Barkley, and R.C. Murphy, *Sublimation as a method of matrix application for mass spectrometric imaging.* J Am Soc Mass Spectrom, 2007. **18**(9): p. 1646-1652.
32. Puolitaival, S.M., et al., *Solvent-free matrix dry-coating for MALDI imaging of phospholipids.* J Am Soc Mass Spectrom, 2008. **19**(6): p. 882-886.
33. Badu-Tawiah, A., et al., *Non-Aqueous Spray Solvents and Solubility Effects in Desorption Electrospray Ionization.* J Am Soc Mass Spectrom, 2010. **21**(4): p. 572-579.
34. Green, F.M., et al., *The effect of electrospray solvent composition on desorption electrospray ionisation (DESI) efficiency and spatial resolution.* Analyst, 2010. **135**(4): p. 731-737.
35. Manicke, N.E., et al., *Desorption electrospray ionization (DESI) mass spectrometry and tandem mass spectrometry (MS/MS) of phospholipids and sphingolipids: ionization, adduct formation, and fragmentation.* J Am Soc Mass Spectrom, 2008. **19**(4): p. 531-543.
36. Li, Y., B. Shrestha, and A. Vertes, *Atmospheric pressure molecular imaging by infrared MALDI mass spectrometry.* Anal Chem, 2007. **79**(2): p. 523-532.
37. Li, Y., B. Shrestha, and A. Vertes, *Atmospheric pressure infrared MALDI imaging mass spectrometry for plant metabolomics.* Anal Chem, 2008. **80**(2): p. 407-420.

431 38. Shrestha, B., J.M. Patt, and A. Vertes, *In situ cell-by-cell imaging and analysis of small cell*
432 *populations by mass spectrometry.* Anal Chem, 2011. **83**(8): p. 2947-2955.
433 39. Cha, S., et al., *Direct profiling and imaging of epicuticular waxes on Arabidopsis thaliana by laser*
434 *desorption/ionization mass spectrometry using silver colloid as a matrix.* Anal Chem, 2009. **81**(8):
435 p. 2991-3000.
436 40. Li, B., et al., *Characterization of barley leaf tissue using direct and indirect desorption*
437 *electrospray ionization imaging mass spectrometry.* Journal of Mass Spectrometry, 2011. **46**(12):
438 p. 1241-1246.
439 41. Korte, A.R., et al., *Mass spectrometric imaging as a high-spatial resolution tool for functional*
440 *genomics: Tissue-specific gene expression of TT7 inferred from heterogeneous distribution of*
441 *metabolites in Arabidopsis flowers.* Analytical Methods, 2012. **4**(2): p. 474-481.
442 42. Thunig, J., S.H. Hansen, and C. Janfelt, *Analysis of secondary plant metabolites by indirect*
443 *desorption electrospray ionization imaging mass spectrometry.* Anal Chem, 2011. **83**(9): p. 3256-
444 3259.
445 43. Li, B., et al., *Visualizing metabolite distribution and enzymatic conversion in plant tissues by*
446 *desorption electrospray ionization mass spectrometry imaging.* Plant J, 2013.
447 44. Muller, T., et al., *Direct plant tissue analysis and imprint imaging by desorption electrospray*
448 *ionization mass spectrometry.* Anal Chem, 2011. **83**(14): p. 5754-5761.
449 45. Ifa, D.R., et al., *Tissue imprint imaging by desorption electrospray ionization mass spectrometry.*
450 Analytical Methods, 2011. **3**(8): p. 1910-1912.
451 46. Cabral, E.C., et al., *Blotting Assisted by Heating and Solvent Extraction for DESI-MS Imaging.* J Am
452 Soc Mass Spectrom, 2013.
453 47. Jones, E.A., N.P. Lockyer, and J.C. Vickerman, *Mass spectral analysis and imaging of tissue by*
454 *ToF-SIMS—The role of buckminsterfullerene, C_{60}^{+}, primary ions.* International Journal of Mass
455 Spectrometry, 2007. **260**(2): p. 146-157.
456 48. Matros, A. and H.P. Mock, *Mass spectrometry based imaging techniques for spatially resolved*
457 *analysis of molecules.* Front Plant Sci, 2013. **4**: p. 89.
458 49. Hamm, G., et al., *Determination and imaging of metabolites from Vitis vinifera leaves by laser*
459 *desorption/ionisation time‐of‐flight mass spectrometry.* Rapid Communications in Mass
460 Spectrometry, 2010. **24**(3): p. 335-342.
461 50. Lane, A.L., et al., *Desorption electrospray ionization mass spectrometry reveals surface-mediated*
462 *antifungal chemical defense of a tropical seaweed.* Proc Natl Acad Sci U S A, 2009. **106**(18): p.
463 7314-7319.
464 51. Shroff, R., et al., *Nonuniform distribution of glucosinolates in Arabidopsis thaliana leaves has*
465 *important consequences for plant defense.* Proc Natl Acad Sci U S A, 2008. **105**(16): p. 6196-6201.
466 52. Jaeger, R.J., et al., *HR-MALDI-MS Imaging Assisted Screening of beta-Carboline Alkaloids*
467 *Discovered from Mycena metata.* J Nat Prod, 2013.
468 53. Jung, S., et al., *Direct analysis of cellulose in poplar stem by matrix-assisted laser*
469 *desorption/ionization imaging mass spectrometry.* Rapid Commun Mass Spectrom, 2010. **24**(22):
470 p. 3230-3236.
471 54. Horn, P.J., et al., *Spatial Mapping of Lipids at Cellular Resolution in Embryos of Cotton.* Plant Cell,
472 2012. **24**(2): p. 622-636.
473 55. Vrkoslav, V., et al., *MALDI imaging of neutral cuticular lipids in insects and plants.* J Am Soc Mass
474 Spectrom, 2010. **21**(2): p. 220-231.
475 56. Holscher, D., et al., *Matrix-free UV-laser desorption/ionization (LDI) mass spectrometric imaging*
476 *at the single-cell level: distribution of secondary metabolites of Arabidopsis thaliana and*
477 *Hypericum species.* Plant Journal, 2009. **60**(5): p. 907-918.

57. Shu Taira* , Shuichi Shimma 2 , Issey Osaka 3 , Daisaku Kaneko 1 , Yuko Ichiyanagi 4,5 , Ryuzo Ikeda 1 , Yasuko Konishi-Kawamura 6 , Shu Zhu 7 , Koichi Tsuneyama 8 and Katsuko Komatsu 7, *Mass Spectrometry Imaging of the Capsaicin Localization in the Capsicum Fruits* 2012.
58. Yoshimura, Y., et al., *Visualization of anthocyanin species in rabbiteye blueberry Vaccinium ashei by matrix-assisted laser desorption/ionization imaging mass spectrometry.* Anal Bioanal Chem, 2012. **403**(7): p. 1885-1895.
59. Zhang, Y. and H. Chen, *Detection of saccharides by reactive desorption electrospray ionization (DESI) using modified phenylboronic acids.* International Journal of Mass Spectrometry, 2010. **289**(2-3): p. 98-107.
60. Cvacka, J. and A. Svatos, *Matrix-assisted laser desorption/ionization analysis of lipids and high molecular weight hydrocarbons with lithium 2,5-dihydroxybenzoate matrix.* Rapid Commun Mass Spectrom, 2003. **17**(19): p. 2203-2207.
61. Eberlin, L.S., et al., *Desorption electrospray ionization mass spectrometry for lipid characterization and biological tissue imaging.* Biochim Biophys Acta, 2011. **1811**(11): p. 946-960.
62. Franck, J., et al., *MALDI mass spectrometry imaging of proteins exceeding 30,000 daltons.* Med Sci Monit, 2010. **16**(9): p. BR293-299.
63. Esquenazi, E., P.C. Dorrestein, and W.H. Gerwick, *Probing marine natural product defenses with DESI-imaging mass spectrometry.* Proc Natl Acad Sci U S A, 2009. **106**(18): p. 7269-7270.
64. Shitan, N. and K. Yazaki, *Accumulation and membrane transport of plant alkaloids.* Curr Pharm Biotechnol, 2007. **8**(4): p. 244-252.
65. Talaty, N., Z. Takats, and R.G. Cooks, *Rapid in situ detection of alkaloids in plant tissue under ambient conditions using desorption electrospray ionization.* Analyst, 2005. **130**(12): p. 1624-1633.
66. Lu, L., et al., *Rapid Profiling of Alkaloids in Several Medicinal Herbs by Matrix-assisted Laser Desorption/Ionization Mass Spectrometry.* Chemical Research in Chinese Universities, 2010. **26**(1): p. 11-16.

Chapter 3

Combining intensity correlation analysis and MALDI imaging to study the distribution of flavonols and dihydrochalcones in Golden Delicious apples

Pietro Franceschi[1], Yonghui Dong[1], Kerstin Strupat[2], Urska Vrhovsek[1] and Fulvio Mattivi[1]

[1]Fondazione E. Mach–Research and Innovation Centre, Via Edmund Mach 1, 38010 San Michele all'Adige (TN), Italy

[2]Thermo Fisher Scientific (Bremen) GmbH, Hanna-Kunath-Str. 11, D-28199 Bremen, Germany

Notes:

This chapter is adapted from the manuscript entitled 'Combining intensity correlation analysis and MALDI imaging to study the distribution of flavonols and dihydrochalcones in Golden Delicious apples', which has been published in Journal of Experimental botany. Dong Y. conducted part of the experiment, wrote the introduction and materials and methods in the manuscript; Franceschi P. conceived and designed the experiment, conducted part of the experiment, performed the data analysis, wrote the results and discussion in the manuscript, and approved the final manuscript; Strupat K. conducted part of the experiment; Vrhovsek U and Mattivi F approved the final manuscript.

3.1 Introduction

Assessment of the spatial and temporal distribution of metabolites in tissues is important for rationalizing many biological processes occurring in plants. Qualitative or semi-quantitative imaging techniques are thus ideal for complementing the expanding field of metabolomics, when studying the tissue specific distribution of metabolic biomarkers.

Of the various imaging techniques, mass spectrometry (MS) based technologies would seem to be particularly promising, due to their sensitivity, broad response and speed. Matrix Assisted Laser Desorption Ionization Imaging (MALDI-MSI) [1] in particular has become one of the most important molecular histology methods for understanding the spatial complexity of biological samples, and has been demonstrated to be applicable to different kinds of animal and plant tissues [2].

As far as the imaging of small molecules is concerned, the performance of MALDI is hindered by the presence of ions resulting from matrix ionization at the lower end of the mass spectrum [3]. There are different approaches to dealing with the matrix background produced by MALDI or related techniques, mainly relying on specific laser absorbing media (such as graphite or colloidal silver) [4-7] or on matrix-free approaches [8]. However, due to the robustness and widespread use of conventional MALDI protocols, there is definitive interest in developing tools to use them in metabolic imaging applications.

In these MS based technologies the unique chemical identification of the ions is a major challenge, in absence of separative techniques applied to neutral molecules (e.g. Liquid Chromatography). The use of high resolution spectrometers is of great help to reduce the set of possible molecular formulas [2], but more detailed structural information has to be obtained from fragmentation experiments [5, 6].

In fragmentation experiments, however, primary ions have to be selected according to their mass-to-charge ratio, so acquisition time, isolation width and progressive matrix depletion represent a limit to the information yield of MS/MS which can be performed on a specific tissue section. Of these factors, analysis time is particularly relevant, considering that a MALDI imaging run composed of a full scan spectrum and a few fragmentation experiments can easily last 20 to 30 hours.

In conclusion, although full scan MALDI would be suitable for untargeted profiling, in practice it is often necessary to make an a priori choice of the molecules of interest, thus reducing the profiling potential of the technique.

Due to the dynamics of the MALDI process, however, in-source fragmentation is ubiquitous and fragmentation information is already embedded in a full scan spectrum. The development of tools optimized for its extraction would then represent a key step for the full exploitation of MALDI profiling. To take advantage of such information it is necessary to develop and validate a framework to compare the "localization" of primary and fragment ions. A visual approach, indeed, is not optimal because its results are likely to depend very much on the experimenter and manual inspection cannot be applied over an extensive database of biomarkers as should be required in untargeted experiments. All these considerations, push towards the development of bioinformatic tools to treat MALDI-MSI datasets, but the topic is particularly challenging, considering the size and the complexity of the data files. To date, bioinformatic algorithms have been developed to perform reduction and image segmentation for biomarker discovery [9] and to measure the correlation of different ion images [10].

In this chapter we propose an approach for applying conventional untargeted MALDI profiling and advanced data analysis to perform imaging of metabolites in apple tissues, developing an unique framework taking advantage of the in-source fragmentation information to increase the chemical selectivity of the technique. With the proposed pipeline, co-localization between parent and fragment ions is assessed, validated and exploited to reconstruct compound-specific images which can be used for interpretation purposes.

In our experiment, MALDI-MSI data were acquired using a high resolution mass spectrometer. An algorithm based on Intensity Correlation Analysis (ICA) was developed to study the co-localization between parent and fragment ions, thus visualizing the distribution of specific metabolites in tissues.

To perform our experiment, we set up a simple sample preparation protocol to optimize the sectioning of the apple tissues, while minimizing the negative effects of oxidation of the molecules concerned.

The proposed approach was applied to study the distribution of some relevant glycosylated flavonols and dihydrochalcones in apple sections. This latter class of molecules is challenging from the spectrometric point of view. Indeed, polyphenol glycosides easily fragment in nearly

all ionization sources losing primarily their sugar subunits. Furthermore, they show relevant UV absorption in the wavelength region typical of nitrogen lasers and for this reason, they have been proposed as MALDI matrices [11], and have been analyzed in imaging applications in matrix-free conditions [8]. In this class of molecules, then, ionization and fragmentation happen at the same time in the laser desorption process, making them suitable for the application of the proposed bioinformatic approach.

The distribution this particular class of metabolites in plant tissues can be also visualized by optical/UV microscopy, possibly in combination with histological staining [12, 13]. Several families of phenolic compounds like hydroxycinnamic acids, coumarins, stilbenes, and styryl pyrones, for example, are, strongly autofluorescent when irradiated with UV or blue light [13], while non-fluorescent phenolyc compound can be stained with chromogenic reagents, like in the case of proanthocyanidins with dimethylamino-cinnamaldehyde [14] or vanillin-HCl [15]. In terms of spatial resolution, however, these methods show a definitive advantage over MS-based approaches. In fact, with optimized sample preparation protocols, it is possible to achieve subcellular resolution [12], still beyond the capabilities of the majority of MS-based imaging platforms.

In terms of generality and selectivity, however, MS show some relevant advantages. Metabolites are identified on the bases of their mass spectra, often allowing the reconstruction of molecule-specific pictures. In addition, these techniques can be applied to the analysis of many different classes of metabolites, permitting a more comprehensive profiling of the tissue sections.

From a biological point of view, this particular class of molecules is known to have important and diverse key functions in plant growth, development and protection, while antioxidant activity is relevant to food and nutrition [16]. The tissue-specific synthesis of glycosylated polyphenols in apples has already been proposed on the basis of High Performance Liquid Chromatography Diode Array Detection (HPLC-DAD) studies and has been suggested by a Graphite assisted Laser Desorption Ionization study [5]. The availability of this background knowledge is of fundamental importance for the overall validation of the proposed methodology.

3.2 Material and Methods

3.2.1 Reagents

α-cyano-4-hydroxycinnamic acid (CHCA) and 2,5-dihydrobenzoic acid (DHB) were purchased from Sigma-Aldrich (Steinheim, Germany), L(+)-ascorbic acid from VWR international (Geldenaaksebaan, Leuven, Belgium), while acetonitrile was of LC-MS Chromasolv grade (Sigma-Aldrich, Steinheim, Germany).

3.2.2 Preparation of apple sections

Apples (Golden Delicious) were purchased locally. Metabolite localization was tested in three types of sections; their position within the fruit is presented in Figure 1, with a schematic view of the anatomy of the fruit [17, 18]. The central part of a longitudinal section of the fruit was used to investigate the pericarp (20 mm x 20 mm), while two other different types of cross sections were selected to study the transition region between the skin and the hypanthium (aroud 6.6 x 6.6 mm). In relation to the skin, sectioning was performed orthogonally and obliquely (Figure 1). In this second type of sectioning, cell layers just below the skin were cut with a favourable projection, enhancing the histological resolution of the MSI images.

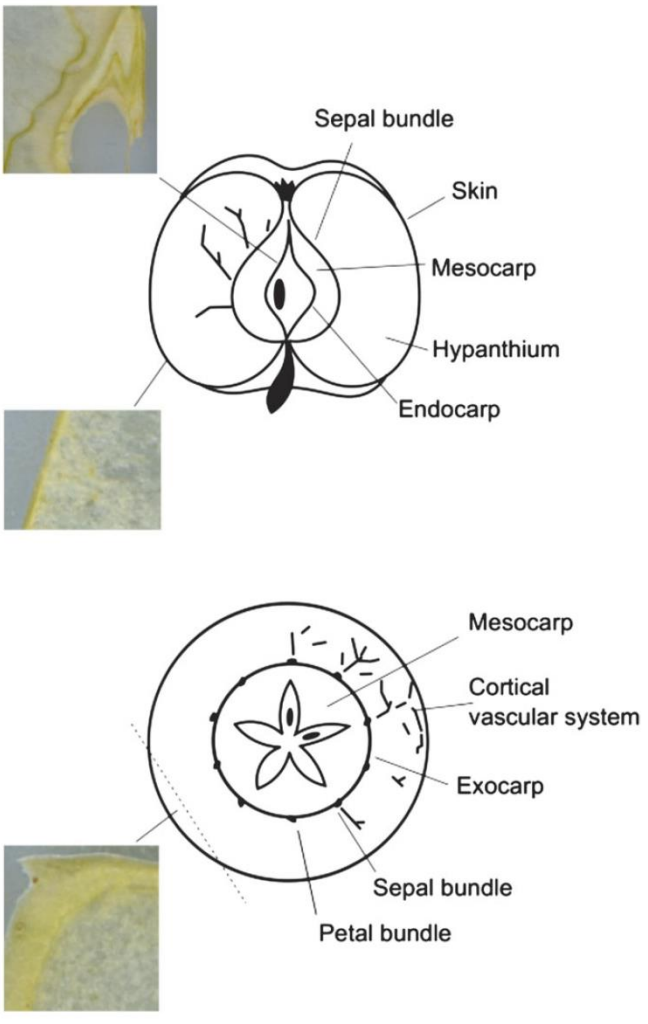

Figure 1. Graphic representation of the different sections considered in the study. The schematic view of the apple anatomy is reconstructed from Trentham (2008) and Tukey and Young (1942). The pericarp is the fruit wall developed from the ovary; it can be subdivided in endocarp, mesocarp and exocarp.

Apple sections for MALDI-MSI were obtained by manual cutting of slices (around 0.5 mm thick) using a razor blade. The sections were mounted on a glass slide and immediately sprayed with ascorbic acid (10 $mmolL^{-1}$) to prevent oxidation during handling and dehydration. After vacuum drying (12 h), the sections were regularized using a razor blade. Regularization was necessary due to shrinkage differences within the tissue during drying.

Vacuum drying was necessary considering the high water content of the sections; during this stage volatile molecules are likely to be removed from the section, but the same would happen inside the low vacuum MALDI interface. However, the majority of metabolites are not expected to be affected by the same phenomenon due to its low vapour pressure. This observation is also confirmed by the consistency MALD-MSI results of experiments performed in a wide range of drying conditions and MALDI acquisition times.

Optical images of apple sections were obtained using a photo scanner (HP Scanjet G4050) at 600 dpi. High resolution scans were acquired using the optical scanner embedded in the MS Instrument via the xy stage, holding the MALDI MSI sample and the camera to examine the sample optically.

3.2.3 MALDI Imaging

MALDI spectra were acquired by using α-cyano-4-hydroxycinnamic acid (CHCA) as the UV-absorbing matrix. Standard MALDI conditions were preferred over matrix free solutions for two reasons: a) to avoid an almost complete fragmentation of the UV-absorbing metabolites; b) to increase the profiling efficiency of the acquisition, by increasing the efficency towards non UV-absorbing metabolites. According to the ImagePrep protocols, both CHCA and 2,5-dihydrobenzoic acid (DHB) were tested as possible MALDI matrices. The former was selected since its regular crystallization produces higher quality images. Matrix solution (7 g/L CHCA in 50 % acetonitrile) was sprayed uniformly over the sections using an ImagePrep station (Bruker Daltonics, Germany) adopting the following program: 22 spray cycles, 75 % sprayer power, 0 % modulation, 1s spray, 2s incubation, and 70s dry time. The matrix deposition program was optimized to minimize the wetting of the samples, because this would

result in metabolite delocalization and possibly in the reactivation of oxidative degradation. The ImagePrep station performs the entire spraying process under nitrogen flux, which prevents oxidation of the sections during matrix deposition.

MALDI-MSI analysis was performed using a MALDI LTQ Orbitrap XL mass spectrometer (Thermo Fisher Scientific (Bremen), GmbH, Germany) with a resolution of 60,000 (at m/z 400, FWHM). Positive and negative ion modes were evaluated. The latter was preferred because, in negative mode, the ions resulting from the ionization of the matrix were less in quantity and intensity.

FTMS full scans from m/z 120 to m/z 1000 were acquired using the Instrument Control Software (LTQ Tune Plus 2.5.5 SP1) and Xcalibur 2.1. The same software was used to automatically raster the laser beam across the sectioned surface in x and y dimensions. The Automatic Gain Control mode of the spectrometer was used to optimize the number of laser shots for every pixel. Typical values were varying from 10 to 80 laser shots depending on the ion yield. In the case of the skin sections, each spectrum were obtained by averaging two full scan spectra, while only one spectrum was acquired for the pericarp section presented in this chapter. Due to this setting, the acquisition time is different for every pixel, while the scan time for the spectrometer is determined by the resolution at around 0.7 s.

The laser step size between adjacent x/y positions was set at 150, 100 and 75 µm. The pericarp section presented in this chapter was analyzed with a step of 150 µm, leading to an image of 125 X 136 pixels (17000 steps). In the case of the skin region the two sections were acquired with a step of 100 and 75 µm resulting in images with 90 x 69 (6210 steps) and 67 x 68 (4556) pixels. Total acquisition times for the images were 9 h for the pericarp section and 6 and 7 hours for the skin sections, respectively.

The Orbitrap was calibrated prior to mass analysis by external calibration using standard peptide mixtures (ProteoMass MALDI calibration kit for LTQ XL and LTQ hybrids, Sigma-Aldrich) for the normal mass range. To increase the accuracy of the acquisition, the spectra were internally calibrated at m/z 333.088, the matrix dimer having undergone a loss of CO_2 ($[2CHCA - CO_2 - H]^-$]).

3.2.4 Data Analysis

Data files were converted into open-source CDF format using Xcalibur Software. The analysis and visualization pipeline was developed in Python version 2.5 (http://www.python.org/). To correct any uneven responses in the sample, the total ion current of each pixel was normalized to one. Extracted ion chromatograms (XICs) were extracted from the full scan data with different levels of tolerance depending on the mass range. Mass selected images were reconstructed from these traces. Plots were produced by using the interactive Ipython shell (http://ipython.scipy.org) with Scipy (http://www.scipy.org/) and Matplot (http://matplotlib.sourceforge.net/) libraries.

Intensity Correlation Analysis (ICA) – originally developed to assist the analysis and interpretation of immunohystochemical images [19] – was selected as a strategy to compare the co-distribution of ions in the image. The starting point of ICA is comparison of the intensities of two ions within the same pixel. For each pixel i in the image, the Intensity Correlation Factor (ICi) between two ions at m/z a and b is calculated according to the following relation.

$$IC_i = \left(Ia_i - \overline{Ia_i}\right) \cdot \left(Ib_i - \overline{Ib_i}\right)$$

Here ion of m/z ratio *a* has an intensity Ia_i at position pixel i and ion of m/z ratio *b* has an intensity Ib_i at pixel i, while $\overline{Ia_i}$ and $\overline{Ib_i}$ are the averages of the intensities of ions *a* and *b* over the whole rastered area.

The rationale behind this approach is that IC_i is positive for a given pixel i, if both intensities are on the same side of their respective mean values on the image. If the ions at m/z a and m/z b are correlated – as in the case of a fragmentation occurring during ionization – their intensities should vary “in tune” almost in every pixel resulting in a set of positive IC factors.

The intensity correlation framework was adapted to the specific characteristics of MS images acquired using a FTMS instrument. First of all, the intensity range of ion signals spanned several orders of magnitude (up to 4 or 5) so logarithmic scaling of the normalized intensities was performed. This type of scaling also had the positive effect of making the distribution of the intensities less skewed. Co-localization is only meaningful when both species are present, so ICA analysis was only performed on pixels where the intensities of m/z a and m/z b were different from zero.

A strategy to validate the results of ICA analysis was also developed to evaluate the probability of obtaining only by chance a given set of IC factors. If one considers how IC factors are calculated, their distribution for two uncorrelated species should be symmetric around zero. Any asymmetry in the distribution towards positive values is therefore an indication of intensity correlation between the two ion traces, which indicates the presence of significant co-localization. To validate the asymmetry in ICs it is then possible to consider the distance between the medians of the distributions of positive and negative IC values ((med+)-(med-)). The significance of this parameter was tested by checking its variability in a series of random permutations of pixel intensities for either m/z *a* or m/z *b*. In this way it was possible to probe the intrinsic variability of IC factors distribution, calculating the likelihood of obtaining the actual asymmetry by chance. This validation strategy also had the advantage of being non-parametric, not requiring any a priori hypotheses regarding the distribution of IC factors.

If ICA analysis is performed on two ion traces which can be the result of an in-source fragmentation process – such as glycoside and its corresponding aglycone –, the presence of significant intensity correlation confirms the chemical identification of the parent ion. On the other hand, the presence of correlation between ions relative to two different metabolites suggests that the two species could be biologically related, since, on average, they show the same trend in relation to their means.

The results of the IC analysis were used to reconstruct maps showing the spatial distribution of highly correlated pixels. These images were then used for interpretation purposes.

3.3 Results and Discussion

In this section the results of applying the proposed framework to the MALDI MSI of Golden Delicious apple are presented. In the first paragraph, the effectiveness of the sample preparation protocol and high resolution MS analysis is assessed by studying the distribution of some metabolites known to be present in apple. Subsequently, IC analysis will be applied to study the distribution of flavonoid glycosides in apples, focusing on the pericarp and on the skin.

3.3.1 Imaging of test metabolites

The reconstructed images for malic acid ($C_4H_6O_5$), detected as $C_4H_5O_5$ ($(M-H)^-$ ions at m/z = 133.014) are shown in Figure 2(B).

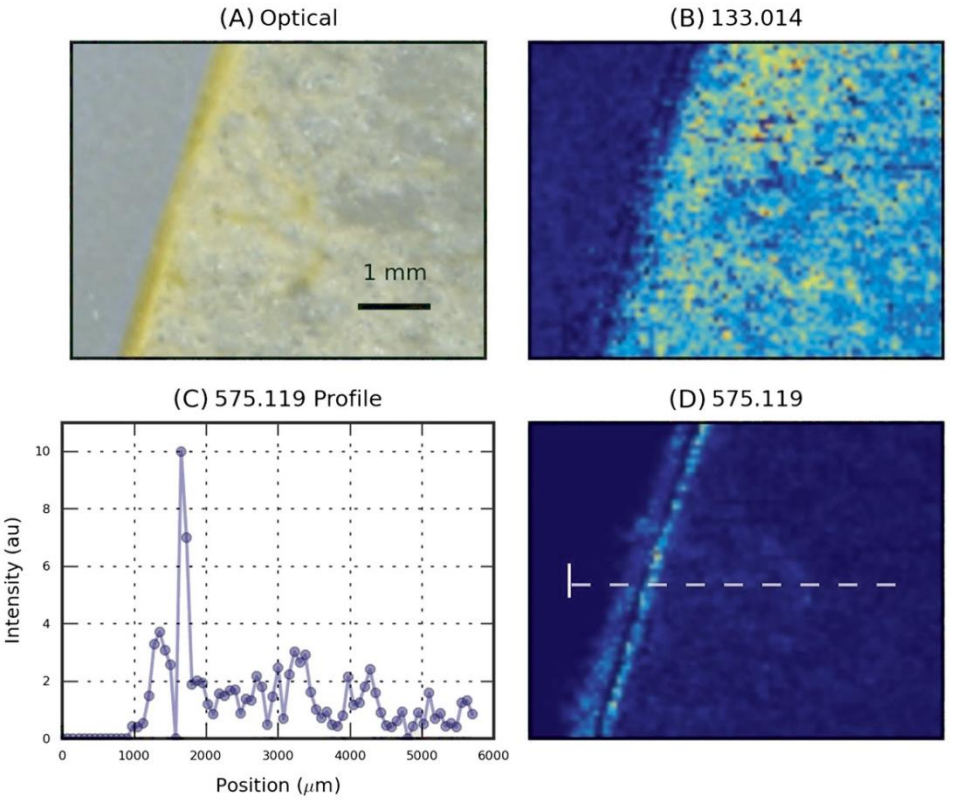

Figure 2. Spatial distribution of some metabolites known to be present in apples. The color scale goes from blue to red (linear scaled plots). MS images have been acquired with a raster step of 100 µm. (A) Optical Image. (B) Image reconstructed from XIC at m/z 133.014, identified as malic acid. (C) Intensity profile of m/z 575.119 along the dotted line. (D) Image reconstructed from XIC at m/z 575.119, identified as a procyanidin-related ion.

Malic acid was detected inside apple hypanthium with an almost constant concentration. Malic acid, as its name suggests, accounts for 90 % of total organic acids in apple (Ackermann et al., 1992). Figure 2(D) shows the same graphic representation for an ion detected at m/z = 575.119. Among the possible molecular formulas for this ion, $C_{30}H_{23}O_{12}$ can be related to procyanidin B ($C_{30}H_{26}O_{12}$ detected as $(M-H^2-H)^-$). The observed ion is compatible either with the direct ionization of procyanidin B or with UV induced fragmentation of higher order procyanidins. Procyanidins – polymeric flavonoids made up of catechin/epicatechin units – are known to be abundant in apples, where they can account for a significant fraction of overall phenolic content [2]. The ion image presented in Figure 2(D) is reconstructed from a trace extracted with a 10 ppm window, corresponding to 0.005 mDa.

Figure 2(C) displays the intensity profile of the signal along a line crossing the skin. The images indicate that the metabolite was more concentrated in the cell layers just below the cuticle and that its concentration decreased inside the fruit. This trend agrees with the relatively high content of procyanidin B2 in Golden Delicious hypanthium reported in a previous HPLC-DAD study [20] where a 1-2 mm thick "peel" fraction was analyzed. The intensity of the 575.119 ion decreased by approximately a factor of five moving from the external hypanthium cells towards the inner hypanthium (Figure 2(C)). This particular localization could explain the much lower content of procyanidin B2 in "pulp" reported by Chinnici et al. [21], since in this experiment a 5 mm thick "peel" fraction was sampled, which was also including the procyanidin/rich cells present below the skin. This example demonstrates the capability of MS-imaging to provide semiquantitative information, complementary to those obtained from the analysis of extracts or homogenates.

3.3.2 Imaging of selected polyphenol glycosides

The polyphenol glycosides detected in different apple sections are listed in Table 1. The table displays also the molecular formulas and their main ions observed in the spectra. In all tested sections, diglycosides were not detected or were close to the detection limit, so they were not taken into account.

Table 1. Polyphenol glycosides considered in our investigation, with their respective aglycones. 6S stands for 6 carbon sugars, excluding rhamnose. Likewise, 5S stands for all the 5 carbon sugars.

Name	Molecular Formula	Ion observed	Theoretical m/z
Quercetin	$C_{15}H_{10}O_7$	$[M-2H]^{-\bullet}$	300.028
Kaempferol	$C_{15}H_{10}O_6$	$[M-H]^-$	285.040
Phloretin	$C_{15}H_{14}O_5$	$[M-H]^-$	273.076
quercetin-hexoside [querc-6S]	$C_{21}H_{20}O_{12}$	$[M-H]^-$	463.088
quercetin-rhamnoside [querc-rham]	$C_{21}H_{20}O_{11}$	$[M-H]^-$	447.093
kaempferol-hexoside [kaemp-6S]	$C_{21}H_{20}O_{11}$	$[M-H]^-$	447.093

phloretin-hexoside [phlor-6S]	$C_{21}H_{24}O_{10}$	$[M-H]^-$	435.129
quercetin-pentoside [querc-5S]	$C_{20}H_{18}O_{11}$	$[M-H]^-$	433.077
kaempferol-pentoside [kaemp-5S]	$C_{20}H_{18}O_{10}$	$[M-H]^-$	417.082

Most of the molecules concerned were detected as $[M-H]^-$ ions, while quercetin was mainly detected as $[M-2H]^{-\bullet}$ radical anion. The production of such an anion in the ionization was checked in the MALDI analysis of a standard. The formation of radical anions in the fragmentation of flavonoid glycosides has already been reported [22]. Even though the two experiments cannot be directly compared due to the different ionization interfaces, the ESI experiments suggest that the collision induced fragmentation of the flavonoid glycoside parent ions can produce radical anions. These phenomenons can also occur during the extraction of the ions within the MALDI source.

Table 1 shows the expected m/z value for the metabolites of interest. These values have been used to extract the XICs necessary for ICA analysis (10 ppm tolerance). The experimentally measured m/z values for the metabolites identified in each tissue section are presented in the Appendix one (Table S1). The values obtained in the different sections are slightly different as can be expected for acquisitions running over several days; however measured values are always very close to the theoretical ones.

As discussed in the introduction the presence of the mass in Table 1 in the spectra is not sufficient to assess the distribution of the corresponding metabolite in the tissue. To increase the chemical selectivity of the analysis it is necessary to run a co-localization analysis between the ions in Table 1 and a characteristic fragment.

It has already been pointed out that this class of molecules undergoes fragmentation during ionization so aglycones show generally high intensity profiles, and were therefore selected as characteristic fragments for the running of the ICA analysis. The aglycons of dihydrochalcons (i.e. phloretin) are absent in apple tissues and only traces of those of flavonols are present [23], thus supporting this specific choice. In Table 1 the abbreviation 6S refers to the six carbon sugars, excluding rhamnose, which is not isobaric as it is a deoxy-hexose, while 5S indicates all the pentoses attached to the specific polyphenols. Isomeric forms are indeed difficult to distinguish by mass spectrometry. Full scan information alone cannot help, but MS/MS or

higher order MS studies possibly could provide structural and linkage information helping to differentiate isoforms. The only phloretin hexoside in apples is the phloretin-2-glucoside (phloridzin), while the main known quercetin-hexosides in Golden Delicious apples are (in decreasing order) quercetin 3-galactoside and quercetin 3-glucoside. The quercetin-pentosides are quercetin 3-arabinoside and quercetin 3-xyloside [23]. Kaempferol is not usually reported in apples. It was recently reported as 3-glucoside [24] or as aglycon.

3.3.2.1 Apple pericarp

The distribution of masses corresponding to flavonoid hexosides in the apple pericarp is presented in Figure 3.

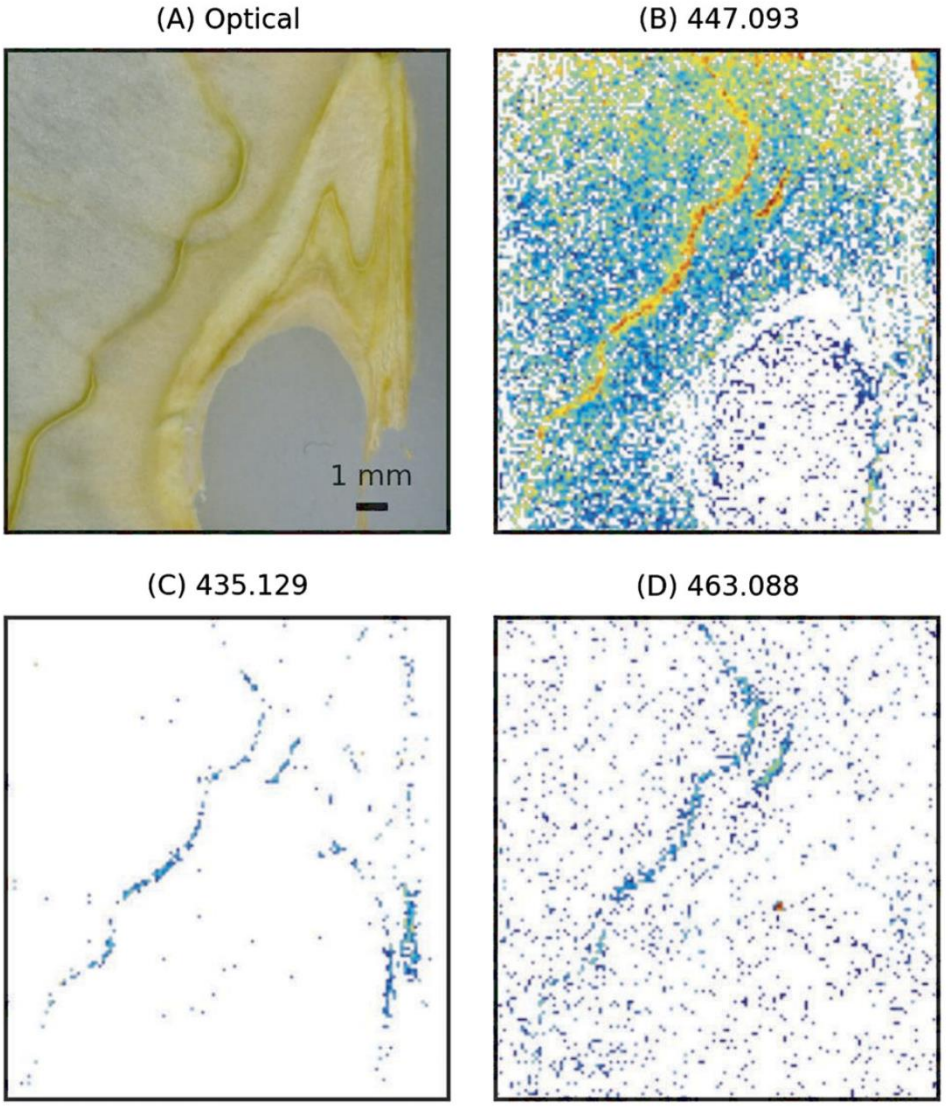

Figure 3: Spatial distribution of flavonoid glycosides (Table 1) in apple pericarp. The intensities were calculated as the logarithm of the normalized ion trace. The color scale ranges

from blue (low) to red (high). MS images have been acquired with a raster step of 150 µm. (A) Optical image. (B) Image reconstructed from XIC at m/z 447.093. This mass can be assigned either to quercetin-rhamnoside or kaempferol-6S. (C) Image reconstructed from XIC at 435.129 (phloretin-6S). (D) Image reconstructed from XIC at 463.088 (quercetin-6S).

The experimental results indicated that the ion at m/z 447.093 was distributed over the tissue with a maximal intensity on the sepal bundle. The ion at m/z 435.129, was detected at both locations, the sepal bundle and the rims of the endocarp. The yield of the ion at m/z 463.088 was low, showing a slight increase towards the sepal bundle. Table1 indicates that the ion at m/z 447.093 can be related to the presence of both quercetin-rhamnoside and kaempferol-6S, while the ions at m/z 435.129 and m/z 463.088 can be assigned to phloretin-6S and quercetin-6S, respectively. To discriminate between the two contributions in the ion trace of m/z 447.093 and to confirm the chemical origin of the ions, ICA analysis of these ions and the relative aglycones was performed. The results of this analysis for m/z ratios 447.093, 300.028 and 285.040 are summarized in Figure 4. The results of ICA analysis are presented in the two plots on the left (A,B): each point in the plot represents a pixel of the image in which two masses were related, m/z 447.093 and m/z 300.028 in the case of (A). IC factors are displayed on the horizontal coordinate, while the mean centered value of the ion intensity is used as vertical coordinate[19]. In this representation, pixels showing positive intensity correlation show up in the right hand plane, with the high intensity pixels occupying the top right quadrant. A significant skew in the distribution of the IC factors towards the right therefore indicates that the two m/z traces are positively intensity-correlated, and this allows to conclude that the two ions are significantly co-localized. This is clearly visible on the first scatter plot (A), in which the high correlation tail is clearly directed towards the top right. Validation was performed with the permutation test discussed in the previous section and the results are summarized in Figure 4(C). The two histograms show the variability of the (med+)-(med-) parameter over 1000 permutations, while the vertical lines indicate the values obtained from the measured values. For both IC analyses, validation indicated that the null hypothesis should be discarded at a 0.001 level of confidence, indicating significant co-localization of the two ion traces.

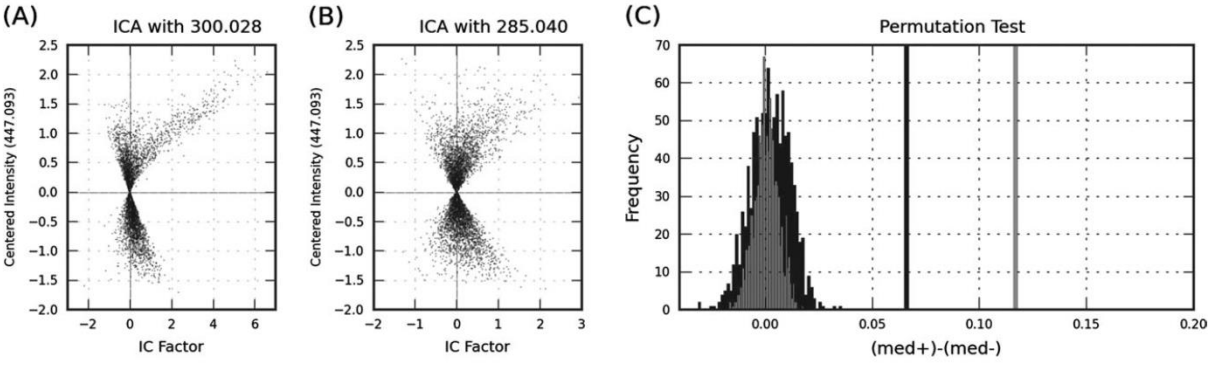

Figure 4. Graphic representation of the ICA for m/z 447.093/300.028 and m/z 447.093/285.040. (A,B) Position of each pixel in the IC/intensity plane. The intensity of mass 447.093 was mean centered. (C) Validation of the ICA between m/z 447.093/300.028 (gray) and m/z 447.093/285.040 (black). The histograms show the variability of the ((med+)-(med-)) parameter with 1000 permutations of the intensities. Vertical lines indicate the measured values.

For interpretative purposes, it is helpful to reconstruct the spatial distribution of the pixels showing positive IC. This image is also included in Figure 5(C,D), where positive IC pixels are displayed with colors ranging from gray to red depending on the IC value. The image shows that, for pixels where m/z 447.093 was present, a part – mainly distributed in the central part of the endocarp – could not be co-localized neither to m/z 300.028 nor to m/z 285.040, thus suggesting that, in this region, the signal at m/z 447.093 was likely to come from a neutral molecule not listed in Table 1. Of the other pixels, maximal co-localization – in correspondence of the pixels with the highest IC factors –, was found almost exclusively along the sepal bundle. This was mainly true for m/z 300.028, while correlation with the ion at m/z 285.040 was less strong. Due to the choice of ions – glycoside and aglycones here – the presence of high intensity correlation confirmed the chemical assignment of the ion at m/z 447.093, while the spatial distribution of the high IC pixels showed highly localized presence of both metabolites in the tissue.

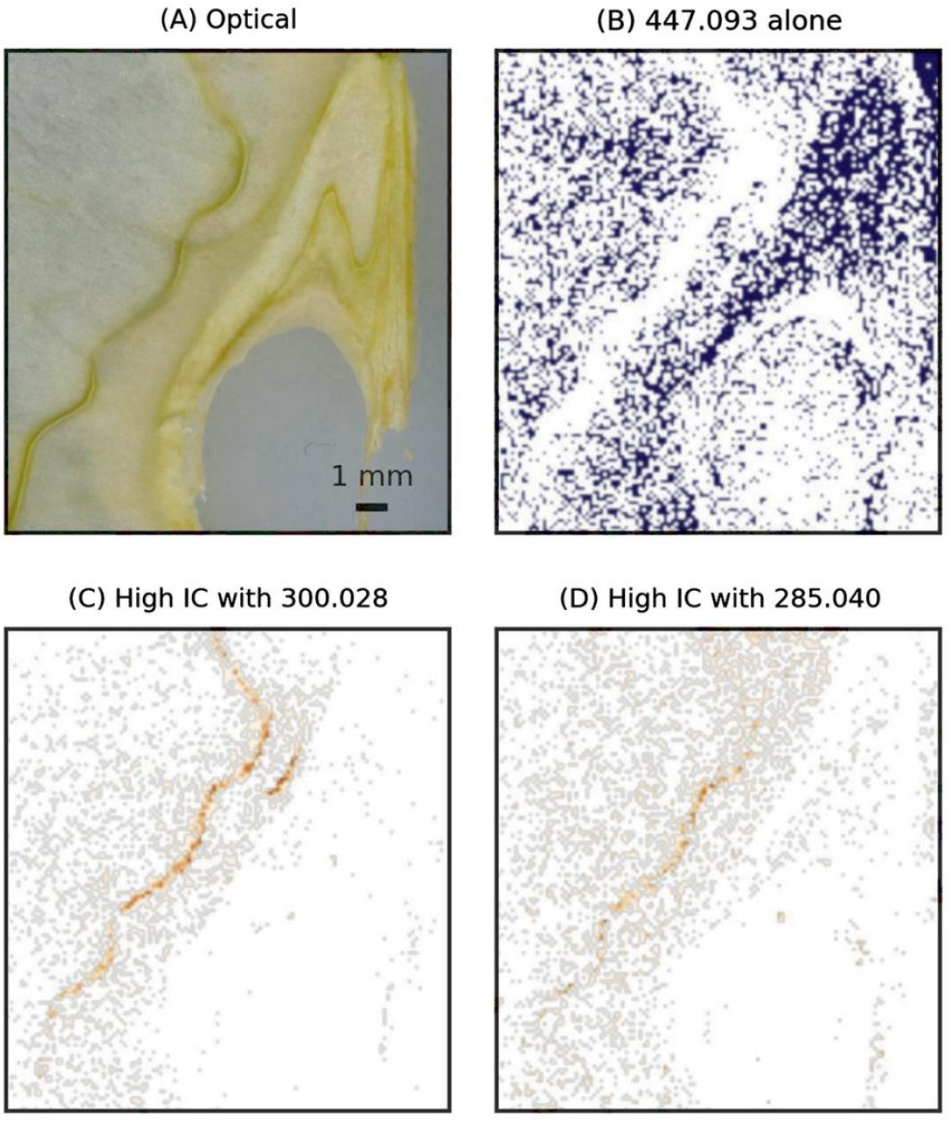

Figure 5. Results of the ICA on the ion at m/z 447.093. (A) Optical image. MS images have been acquired with a raster step of 150 µm. (B) Mask showing the distribution of the ion at m/z 447.093 not correlated with m/z 300.028 or m/z 285.040. (C,D) Images reconstructed from the pixels showing positive IC factors between m/z 447.093/300.028 (C) and m/z 447.093/300.028 (D). Color scale ranges from gray (low) to red (high).

The same pipeline was applied to analyze the couple of masses at m/z 435.129 and 273.076, which correspond to phloretin-6S and phloretin, respectively. The results are presented in Appendix one (Figure S1). Here, the distribution of intensity correlation factors peaks noticeably towards the right side of the plot, indicating that the intensities of these two masses were correlated almost everywhere, speaking of an almost perfect co-localization. This result would be expected if the smaller m/z ion is produced in the fragmentation of the larger one, so

it is substantially confirming that the trace of the ion at m/z 435.129 shows the distribution of phloretin-6S.

The results of the correlation analysis for the masses corresponding to pentosides (m/z 417.082 with m/z 285.040 and m/z 433.077 with m/z 300.028) are also included in the Appendix one (Figure S1). Distribution of IC factors for the couple m/z 417.082/285.040 shows a significant asymmetry in the permutation test, but lacks a clear tail with higher IC. Furthermore, the higher IC pixels do not show a definite spatial pattern. Thus the assignment of m/z 417.082 to kaempferol-5S is not conclusive on this basis. On the other hand, quercetin-5S (m/z 433.077/300.028 couple) shows a markedly asymmetric IC distribution, with higher IC factors (meaning higher correlation) being observed towards the sepal bundle.

On the basis of the chemical assignment obtained from ICA analysis, the spatial distribution of flavonoid glycosides in the tissue section was assessed. Quercetin-6S (m/z 463.088 co-localized with m/z 300.028) was not abundant in the apple pericarp only showing up with a low intensity on the sepal bundle. Quercetin-Rhamnoside (m/z 447.093 co-localized with m/z 300.028) was instead present, mainly within this bundle. Kaempferol-6S (m/z 447.093 co-localized with m/z 285.040) was probably also present in the same position, albeit at low concentration. In the pericarp, phloretin-6S (m/z 435.129 co-localized with m/z 273.076) was mainly present in the sepal bundle, but was also detectable on the papery rim of the endocarp near the seed locules. Finally, quercetin-5S (m/z 433.077 co-localized with m/z 300.028) was present mainly on the sepal bundle.

3.3.3.2 Skin region

The skin is the outher part of the apple and it is composed of cuticle, epidermis and hypodermal layer [17, 18]. The skin is known to be rich in secondary metabolites. In particular, flavonoid glycoside accumulation in this area guarantees the protection of the fruit from UV radiation [16]. In keeping with the analysis pipeline applied for the core data, MS images for the ions at m/z 447.093 and m/z 463.088 are shown in Figure 6, with the distribution of pixels with high IC between m/z 463.088 and m/z 300.028. The results indicate that m/z 447.093 was present in low concentration in the tissue sections of the skin region. On the contrary, the signal at m/z 463.088 was intense, showing a decrease towards the hypanthium. Intensity correlation with m/z 300.028 was higher in the region just below the

cuticle, with an increase in correspondence with one of the bundles of the cortical vascular system, visible as a high intensity spot within the apple flesh.

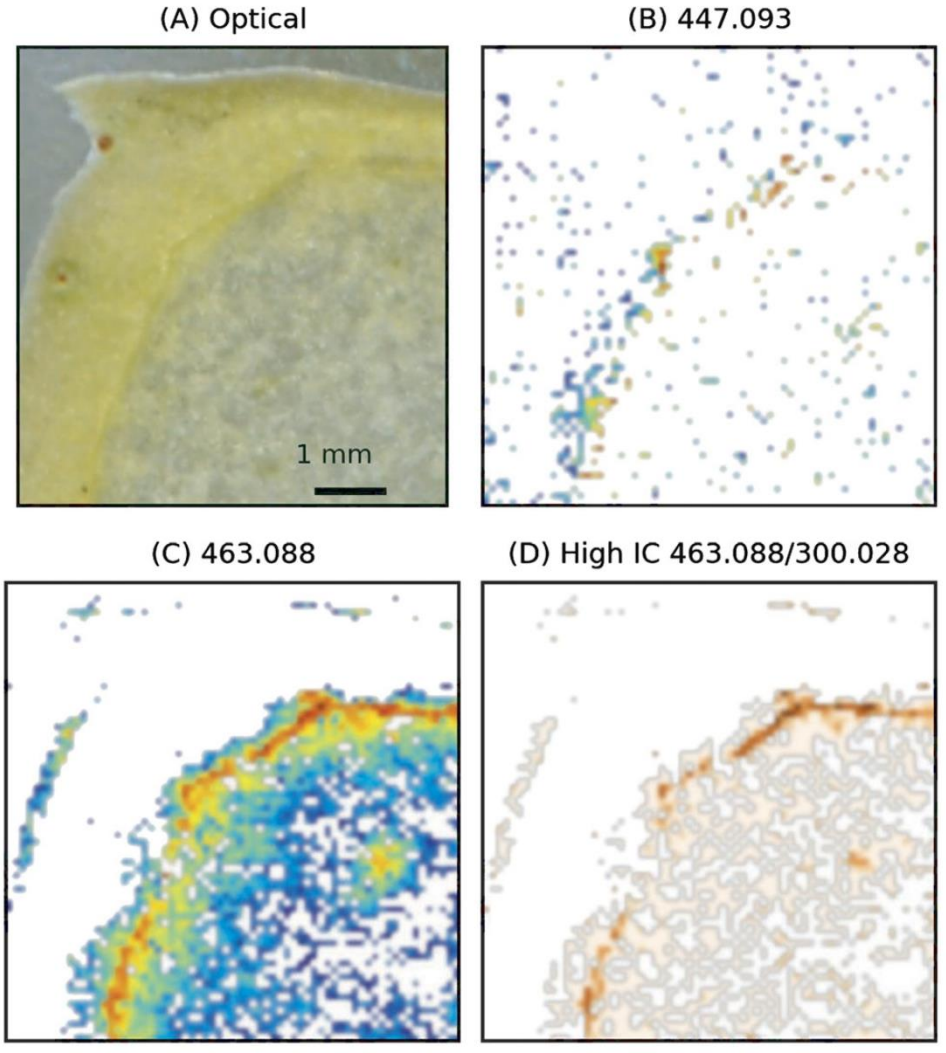

Figure 6. MS Imaging of the oblique section of the skin region. MS images have been acquired with a raster step of 75 µm. (A) Optical Image. (B,C) Images reconstructed from XIC at m/z 447.093 (assigned to quercetin-rhamnoside) and m/z 463.088 (assigned to quercetin-6S). Logaritmic scaling. The color scale ranges from blue to red. (D) Images reconstructed from the pixels showing positive intensity correlation between m/z 463.088 and m/z 300.028. Color scale from gray (low) to red (high).

In this area of the apple, the ion at mass m/z 435.129 was not detected, while the intensity of the ion at m/z 273,076 was low, showing a decreasing profile towards the hypanthium (see Figure S2 in Appendix one). As far as the m/z 433.077/300.028 couple is concerned, ICA analysis identified the co-localization region right below the skin. As before, the situation for

the pair at m/z 417.082/285.040 was not clear cut and ICA analysis resulted in a relatively symmetric distribution. Pixels showing higher correlation were located in the skin region but, interestingly, they were not found where the intensities of the ions at m/z 417.082 and m/z 285.040 were higher. In this specific case the results of ICA analysis were not conclusive for assignment of the ion at m/z 417.082 to kaempferol-5S, in agreement with the fact that its presence in the apple has never been reported to date.

The same analysis pipeline was applied to the orthogonal section: results for masses at m/z 447.093 and m/z 463.088 are presented in the Appendix one (Figure S3). In this case, MS images show a picture consistent with the one just discussed. The same consideration applies to the ions at m/z 273.076, 417.082 and 433.077 observed by MALDI MSI of the orthogonal section.

The experiments performed to characterize the apple skin region indicate that quercetin-6S (m/z 463.088 co-localized with m/z 300.028) was strongly concentrated in the region just below the cuticle. With a rastering step of 75 μm, the width of the high concentration region can be estimated to be around 150 μm. This evidence is supported by previous HPLC analysis which indicated quercetin-galactoside as the main glucoside present in the skin [21]. In contrast to the pericarp, quercetin-rhamnoside was less abundant. In none of the skin sections a clear signature of phloretin-glycosides was detected, though a weak phloretin signal was detectable. Considering that the signals of aglycone fragment ions are more intense than the corresponding glycosides, this observation did not rule out the presence of a low concentration of phloretin-glycosides below the cuticle. This hypothesis is supported by the observation that the phloretin signal, decreased in the hypanthium: in accordance to what was observed for phloridzin in HPLC-DAD measurements [21].

As far as pentosides were concerned, the results of ICA analysis made it possible to conclude that quercetin-5S was present in higher concentrations just below the cuticle, dropping rapidly in the hypanthium. Interestingly, flavonoid glycosides also showed a higher concentration in correspondence of the cortical vascular system.

3.4 Conclusions

In a biological context, our study supports the idea of tissue-specific biosynthesis of flavonoid glycosides in the apple, in agreement with what has already been proved in Arabidopsis at the genetic expression level [25]. Major differences were found in the distributions of quercetin-

6S – present mainly below the cuticle – and quercetin-rhamnoside and phloretin-6S, detected in the pericarp.

In the skin region, glycosides were more concentrated in the cell layers lying just below the cuticle – the thickness of the polyphenol-rich layer was about 150 μm –, while in the pericarp they were located mainly in correspondence with the vascular system.

As a general rule, the distribution of glycosides was very much localized. This makes the study of their spatial tissue-specific biosynthesis a challenge using more conventional analytical methods. In particular, great care must be taken in studies involving the analysis of peel and pulp after mechanical separation, in the light of the critical concentration of some important metabolites in tissues close to the cuticle. This specific observation also has important practical implications, in view of the industrial production of foods with an increased content of beneficial compounds.

The experimental results discussed so far indicate that the proposed pipeline based on the application of ICA to study co-localization in high resolution MALDI spectra is effective for studying the distribution of polyphenol glycosides in apples. Substantial agreement with previous HPLC studies validated this approach, which showed a higher potential for ascertaining detailed metabolite localization. Intensity Correlation Analysis proved to be of great help in assessing co-localization and extracting and interpreting fragmentation profiles from un-targeted MALDI profiles, by increasing the selectivity of high resolution spectra.

References

1. Caprioli, R.M., T.B. Farmer, and J. Gile, *Molecular imaging of biological samples: Localization of peptides and proteins using MALDI-TOF MS.* Analytical chemistry, 1997. **69**(23): p. 4751-4760.
2. Vrkoslav, V., et al., *MALDI imaging of neutral cuticular lipids in insects and plants.* J Am Soc Mass Spectrom, 2010. **21**(2): p. 220-231.
3. Krutchinsky, A.N. and B.T. Chait, *On the nature of the chemical noise in MALDI mass spectra.* J Am Soc Mass Spectrom, 2002. **13**(2): p. 129-134.
4. Jun, J.H., et al., *High-spatial and high-mass resolution imaging of surface metabolites of Arabidopsis thaliana by laser desorption-ionization mass spectrometry using colloidal silver.* Anal Chem, 2010. **82**(8): p. 3255-3265.
5. Zhang, H., S. Cha, and E.S. Yeung, *Colloidal graphite-assisted laser desorption/ionization MS and MS(n) of small molecules. 2. Direct profiling and MS imaging of small metabolites from fruits.* Analytical chemistry, 2007. **79**(17): p. 6575-6584.

6. Cha, S., et al., *Direct profiling and imaging of plant metabolites in intact tissues by using colloidal graphite-assisted laser desorption ionization mass spectrometry.* Plant J, 2008. **55**(2): p. 348-360.
7. Cha, S., et al., *Direct profiling and imaging of epicuticular waxes on Arabidopsis thaliana by laser desorption/ionization mass spectrometry using silver colloid as a matrix.* Anal Chem, 2009. **81**(8): p. 2991-3000.
8. Holscher, D., et al., *Matrix-free UV-laser desorption/ionization (LDI) mass spectrometric imaging at the single-cell level: distribution of secondary metabolites of Arabidopsis thaliana and Hypericum species.* Plant Journal, 2009. **60**(5): p. 907-918.
9. McCombie, G., et al., *Spatial and spectral correlations in MALDI mass spectrometry images by clustering and multivariate analysis.* Analytical chemistry, 2005. **77**(19): p. 6118-6124.
10. McDonnell, L.A., et al., *Mass spectrometry image correlation: Quantifying colocalization.* J Proteome Res, 2008. **7**(8): p. 3619-3627.
11. Petkovic, M., et al., *Flavonoids as matrices for MALDI-TOF mass spectrometric analysis of transition metal complexes.* International Journal of Mass Spectrometry, 2010. **290**(1): p. 39-46.
12. Abeynayake, S.W., et al., *A high-resolution method for the localization of proanthocyanidins in plant tissues.* Plant Methods, 2011. **7**.
13. Hutzler, P., et al., *Tissue localization of phenolic compounds in plants by confocal laser scanning microscopy.* J Exp Bot, 1998. **49**(323): p. 953-965.
14. Feucht, W., D. Treutter, and E. Christ, *The Precise Localization of Catechins and Proanthocyanidins in Protective Layers around Fungal-Infections.* Zeitschrift Fur Pflanzenkrankheiten Und Pflanzenschutz-Journal of Plant Diseases and Protection, 1992. **99**(4): p. 404-413.
15. Liu, Y., et al., *Investigation of the Site-Specific Accumulation of Catechins in the Tea Plant (Camellia sinensis (L.) O. Kuntze) via Vanillin− HCl Staining.* J Agric Food Chem, 2009. **57**(21): p. 10371-10376.
16. Andersen, O.M. and K.R. Markham, *Flavonoids: chemistry, biochemistry and applications*. 2010: CRC Press.
17. Trentham, W.R., C.E. Sams, and W.S. Conway, *Histological effects of calcium chloride in stored apples.* Journal of the American Society for Horticultural Science, 2008. **133**(4): p. 487-491.
18. Tukey, H. and J.O. Young, *Gross morphology and histology of developing fruit of the apple.* Botanical Gazette, 1942: p. 3-25.
19. Li, Q., et al., *A syntaxin 1, Gαo, and N-type calcium channel complex at a presynaptic nerve terminal: analysis by quantitative immunocolocalization.* The Journal of neuroscience, 2004. **24**(16): p. 4070-4081.
20. Tsao, R., et al., *Polyphenolic profiles in eight apple cultivars using high-performance liquid chromatography (HPLC).* J Agric Food Chem, 2003. **51**(21): p. 6347-6353.
21. Chinnici, F., et al., *Radical scavenging activities of peels and pulps from cv. Golden Delicious apples as related to their phenolic composition.* J Agric Food Chem, 2004. **52**(15): p. 4684-4689.
22. Hvattum, E. and D. Ekeberg, *Study of the collision‐induced radical cleavage of flavonoid glycosides using negative electrospray ionization tandem quadrupole mass spectrometry.* Journal of Mass Spectrometry, 2003. **38**(1): p. 43-49.
23. Vrhovsek, U., et al., *Quantitation of polyphenols in different apple varieties.* J Agric Food Chem, 2004. **52**(21): p. 6532-6538.
24. Feliciano, R.P., et al., *Characterization of traditional and exotic apple varieties from Portugal. Part 1–Nutritional, phytochemical and sensory evaluation.* Journal of Functional Foods, 2010. **2**(1): p. 35-45.

542 25. Pourcel, L., et al., *TRANSPARENT TESTA10 encodes a laccase-like enzyme involved in oxidative*
543 *polymerization of flavonoids in Arabidopsis seed coat.* The Plant Cell Online, 2005. **17**(11): p.
544 2966-2980.

545

Chapter 4

Tissue surface properties jeopardize quantitative detection of metabolites in DESI imaging

Yonghui Dong, Graziano Guella, Fulvio Mattivi, Pietro Franceschi

Notes:

This chapter has been prepared for submission. Dong Y. conceived and designed the experiment, conducted the experiment, performed data analysis and wrote the draft; Guella G. and Mattivi F. designed the experiment and approved the final manuscript; Franceschi P. conceived and designed the experiment, revised and approved the final manuscript.

4.1 Introduction

Mass spectrometry imaging (MSI) enables direct analyses to be made of both the distribution and abundance of metabolites on the surfaces of a large variety of samples. The most widely used MSI ionization sources for biological applications are secondary ion mass spectrometry (SIMS), matrix-assisted laser desorption ionization (MALDI), and desorption electrospray ionization (DESI) [1, 2]. Although spatial resolution is still low (~ 200 µm), DESI can be performed under ambient conditions with minimal or no sample preparation [3]，making it a fast analytical tool for investigating the anisotropic distribution of metabolites in biological matrices with enormous potential in high throughput applications. DESI imaging has gained popularity in mapping drugs and metabolites in animal tissues [4, 5], but has only very recently been applied in plant sciences. Several studies have demonstrated that the chemical properties and texture of the surface can have a strong effect on the desorption process in DESI [6-9], although the impact of these phenomena on imaging applications has not yet been investigated. When imaging heterogeneous tissues, such as those commonly found in plants, differences in surface effects could mask the real distribution of metabolites, potentially undermining the biological significance of DESI measurements.

In this chapter we present the results of an extensive study on the impact of surface effects on DESI imaging of small organic acids in tissues of *Vitis vinifera*. Organic acids are an important class of metabolites playing a fundamental role in plant biology and wine production [10-13]. Previous work on grapevine has shown that there are spatial gradients of organic acids in grape berry [14], suggesting anisotropic distribution of metabolites within and across different grapevine tissues.

In the first part of the chapter the results of DESI imaging experiments on several endogenous organic acids in grapevine stem are critically assessed by comparing them with the results of

spatially resolved ion chromatography (IC) analysis. The effects of sample surface are further investigated by imaging grapevine stem sections enriched in exogenous organic acids. Possible strategies for minimizing surface effects are critically evaluated.

The second part of the chapter investigates the effects of surface textures on DESI detection of organic acids by means of a series of MS measurements performed on Teflon (PTFE) surfaces of varying porosities.

4.2 Experimental

4.2.1 Chemicals and Reagents

Acetonitrile (LC-MS grade) was purchased from Sigma-Aldrich (Italy), water was purified using a Milli-Q water purification system (Sartorius Stedim Biotech Gmbh, Germany). Succinic (>99.5%), malic (99%) and tartaric acids (>99.7%) were purchased from Sigma-Aldrich (Italy), adipic (>99.5%) and glutaric (>99.0%) acids from Fluka AG (Germany). Three types of PTFE sheet, flat PTFE, porous PTFE1 (pore size 1-3 μm, porosity 25-30%) and PTFE14 (pore size 7-14 μm, porosity 45-50%) were obtained from the Porex Corporation (Germany). One-year-old grapevine stems were obtained (at post-veraison in 2 growing seasons) from Cabernet Sauvignon vines (*Vitis vinifera* L.) planted in the vineyard of the Fondazione Edmund Mach, San Michele all'Adige, Italy (Coordinates: 46° 11' 42" N, 11° 8' 15" E; Elevation: 250 m).

Instrumentation

Mass spectra were collected with a Thermo-Fisher Scientific LTQ Orbitrap XL mass spectrometer (Bremen, Germany) equipped with an OmniSpray™ 2D ion source from Prosolia Inc. (Indianapolis, IN). Optimized instrumental parameters were: -100 V tube lens voltage, -10 V capillary voltage, 3 kV spray voltage, 200 ^{o}C capillary temperature, 2 micro scans, 200 ms MS injection time, AGC mode off. Mass spectra were acquired in full scan at negative mode over an

m/z range of 50-200. DESI source parameters were: 55 degree spray angle, 1-1.5 mm tip-to-surface distance, 4 mm tip-to-inlet distance, 10° collection angle, 8 bar nitrogen carrier gas pressure. A mixture of Milli-Q water and acetonitrile (1:4, vol/vol) was used as spray solvent and was delivered at a flow rate of 3 μl/min. Unless otherwise stated, the instrumental and ion source parameters were constant for all the experiments in this study.

4.2.2 DESI imaging and profiling

Four imaging experiments were performed: (a) DESI imaging of endogenous organic acids (malic, tartaric and citric acids) in grapevine stems, both fresh and vacuum dried (1h at 50 torr); as no significant differences in the quantitative distribution of the three targeted organic acids were observed, vacuum dried grapevine stems were preferred in order to avoid sample shrinkage during the imaging process. (b) DESI imaging of exogenous organic acids (glutaric and adipic acids) in grapevine stem. Fresh grapevine stem sections were dipped into an adipic and glutaric acid aqueous solution (2.5 mM, 1h, 50 torr) then dried under the same vacuum conditions for 1 h. The uppermost layer of the grapevine stem was cut away with a razor blade to remove any inhomogeneous glutaric and adipic acid crystallization following vacuum dehydration. (c) DESI imaging experiment in which glutaric and adipic acids were added to the spray solvent to a final concentration of 0.5 mM. DESI imaging was then performed on vacuum dried grapevine stems to see whether surface characteristics affect detection of glutaric and adipic acids. (d) Indirect DESI imaging of endogenous organic acids (malic, tartaric and citric) in grapevine leaf. Leaf blade was imprinted on a porous PTFE sheet (pore size 7-14 μm, porosity 45-50%) following a previously described protocol [15]. The imprints were made by pressing a sandwich consisting of a porous PTFE sheet, the plant material with its abaxial surface facing the PTFE surface, and a few layers of filter paper. A 10 mL round-bottomed flask was used as a plunger to imprint the

leaf sap onto the porous PTFE surface. After a few minutes of vacuum desiccation, the imprints were ready to use. For DESI Imaging, the sample was scanned at a velocity of 200 μm/s in *x* direction and 200 μm step size in *y* direction until the entire sample was analyzed. The thickness of grapevine stem sections was ~200 μm.

For the DESI profiling experiments, an organic acid solution containing equimolar amounts of the 5 organic acid standards (2.5 mM), namely malic, tartaric, citric, glutaric and adipic acids, was prepared by dissolving them in a 1:4 (v/v) water/acetonitrile mixture. Three microliters of this solution was spotted onto the three PTFE surfaces. The deposits were air dried before analysis. Each analysis was repeated 10 times with an acquisition time of 1 min.

4.2.3 Quantification of organic acids

Endogenous organic acids (malic, tartaric and citric acids) were quantified in the pith and outer pith regions of grapevine stem, and in leaf lamina and leaf vein of grapevine leaf blade by IC following the method recommended by Thermo Scientific [16]. Detailed sample preparation and analytical methods are described in the Appendix 2. Exogenous organic acids (glutaric and adipic acids) were quantified by direct infusion ESI-MS in the pith and outer pith region. Detailed sample preparation and analytical methods are described in the Appendix 2.

4.2.4 Data processing and data analysis

The mass spectra files (.raw) were converted into common data format (CDF) by Xcalibur™ 2.1 (Thermo Fisher Scientific). The CDF files were then analyzed and converted into 2-D ion maps using an in-house R package [17]. Each pixel was normalized over the total ion count (TIC), and visualization was improved with 2-D median smoothing over each ion map. Figures were produced with R package ggplot2 [18] and lattice [19].

4.3 Results and Discussion

4.3.1 DESI Imaging of Vitis vinifera tissues

DESI imaging revealed uneven distribution of organic acids in grapevine stem

In total, eight organic acids were detected in the different grapevine tissues using negative ion mode ESI. Identification was confirmed by high resolution mass measurements carried out on the corresponding $[M-H]^-$ parent ions and by comparing their MS/MS spectra with those of the corresponding pure standards (table S1). We focused our attention on the results obtained for the 3 major endogenous organic acids (malic, tartaric and citric) on grapevine stem to investigate surface effects on parent ion detection and to establish a rough quantitative estimate. Grapevine stem was selected as reference because it is structurally highly heterogeneous and gives reproducible DESI imaging results (the imaging experiments were repeated on 10 stem sections, each from 1 of 10 different plants). From a histological point of view, one-year-old grapevine stem is mainly composed of pith, xylem, phloem and cortex [20] and its structural heterogeneity can be readily discerned, for example, the pith is a brown, sponge-like area in the middle of a transverse grapevine stem section, while xylem is distinguished by its xylem vessels (black pores) and rays (Fig 1).

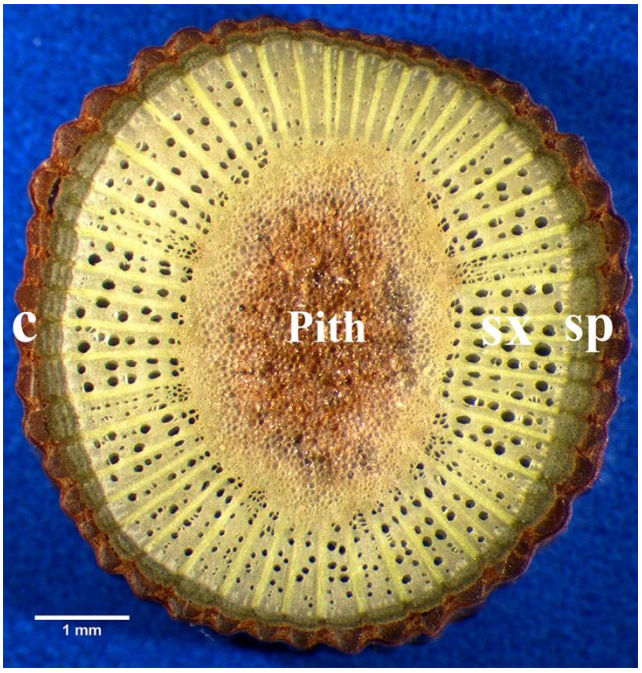

Fig 1 Microscope image of a cross section of a one-year-old grapevine stem clearly showing its structural heterogeneity. Pith, containing large parenchyma cells and brown in color, is located at the center of the stem; secondary xylem (SX) is distinguished by its xylem vessels (black pores) and rays; surrounding the secondary xylem is the secondary phloem (SP), a dark green ring; cortex (C) is the outmost brown layer.

Typical results of the imaging experiments are shown in figure 2a. Malic and citric acids were detected in the outer pith region with a rather homogeneous distribution; in contrast, tartaric acid was distributed over the entire grapevine stem but with a higher concentration in the pith. It is noteworthy that no traces of any of the organic acids investigated could be found in the xylem, phloem and cortex. We were able to perform a semi-quantitative comparison of the concentrations of the three organic acids in the different grapevine tissues [4, 21] from the reconstructed ion images.

In order to validate the semi-quantitative potential of DESI, the outer parts of the grapevine stem (xylem + phloem + cortex), termed the outer pith region, were separated from the pith, and the

quantities of malic, tartaric and citric acids in the two sample types were measured by IC. The results are shown in Figure 2b. A Wilcoxon signed-rank test ($p<0.01$) clearly show that malic acid is present in comparable concentrations in the pith and outer pith region, while citric acid and tartaric acid are present in significantly different concentrations (citric acid is more abundant in the outer pith region and tartaric acid is present in greater concentrations in the pith (Fig 2b)). The IC results are therefore in agreement with DESI for tartaric and citric acid, but they do not confirm the quantitative distribution of malic acid. DESI is a surface analysis technique, while IC measures averaged concentrations ('bulk' mainly) of the same metabolites, so it could be argued that comparison of the two methods is unfair. We therefore designed an imaging experiment in which the grapevine stem tissue sections were uniformly enriched in two xenobiotic compounds (adipic and glutaric acids) with physico-chemical properties quite similar to the endogenous acids under investigation (see Materials and Methods).

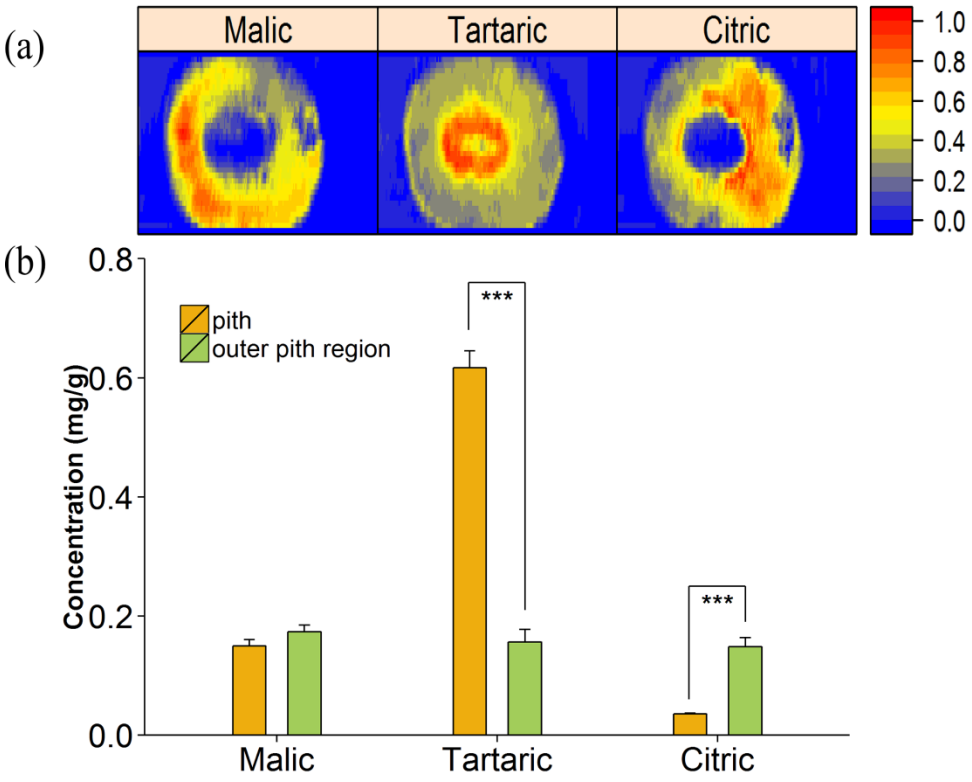

Fig 2 Quantitative mapping of three major organic acids, malic, tartaric and citric acids, in one-year-old grapevine stem. **(a)** DESI imaging of the three organic acids at negative ion mode. The color bar represents TIC normalized ion intensity from 0 (blue) to 1 (red). **(b)** IC quantification of the three organic acids in the pith and outer pith region of one-year-old grapevine stem. Values represent mean+SD (n=3). Statistical differences were calculated using a Wilcoxon signed-rank test. Asterisks denote significant differences ($P<0.01$) in the organic acids between the pith and outer pith region.

Before proceeding to the DESI imaging, uniformity of enrichment of the stem sections was checked by ESI-MS. The pith and outer pith region of several stems were manually separated and the relative concentrations of glutaric and adipic acids in the extracts were measured by Direct Infusion ESI-MS (see Appendix 2). The results, shown in Figure 3b, show that there are no statistically significant differences between the quantities of the two xenobiotics in the different parts of the grapevine stem, confirming that the samples were uniformly enriched in adipic and glutaric acids.

The enriched stem sections were then imaged by DESI. The results, shown in Figure 3a, revealed that glutaric and adipic acids were detected to a lesser extent in the pith region compared with the remaining part of the stem. As discussed in 'Materials and Methods', the different DESI imaging scans were normalized to the corresponding Total Ion Current (TIC) to account for local changes in overall ionization efficiency. These results show that in DESI imaging measurements, the matrix effect due to the different physico-chemical properties of the tissue surface has a strong impact on the desorption response factors of the metabolites and hence on their semi-quantitative detection.

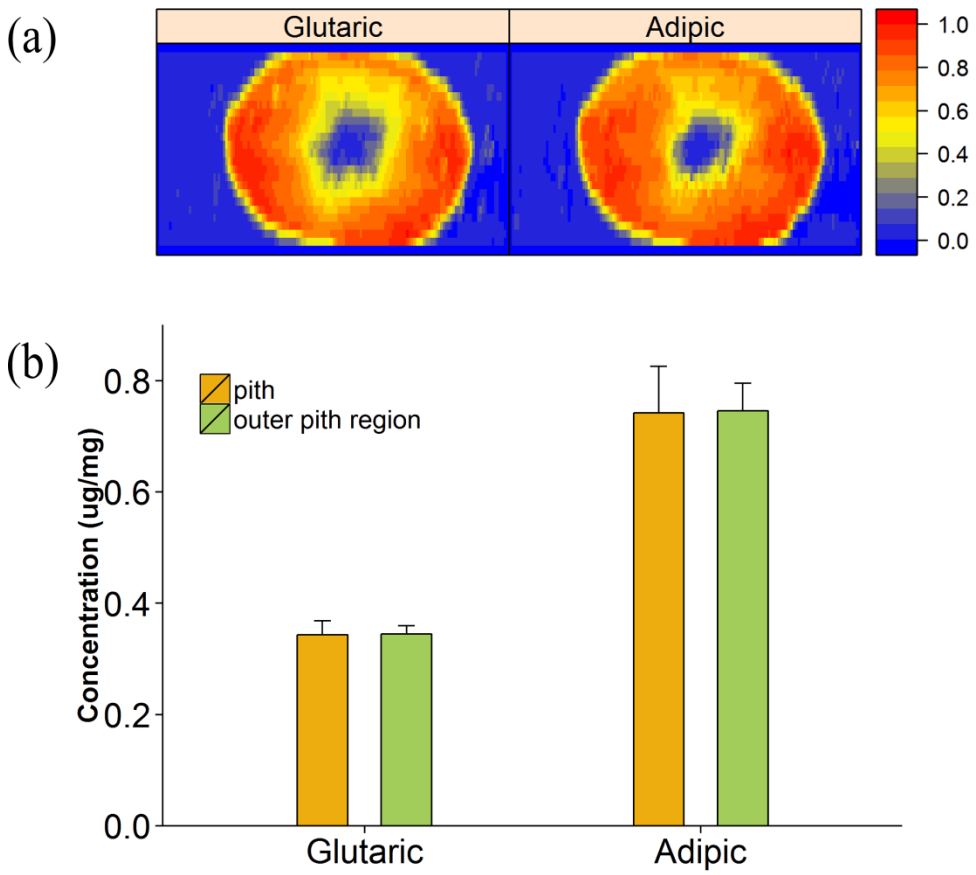

Fig 3 Quantitative mapping of exogenous glutaric and adipic acids in one-year-old grapevine stem. **(a)** DESI imaging of the two organic acids at negative ion mode in one-year-old grapevine stem enriched in glutaric and adipic acids. The color bar represents TIC normalized ion intensity from 0 (blue) to 1 (red). **(b)** Quantification through direct infusion ESI-MS of the two organic acids in the pith and outer pith region of one-year-old stem enriched in glutaric and adipic acids. Values represent mean+SD (n=3). No statistical differences were found between pith and outer pith region ($P<0.01$) for both organic acids according to a Wilcoxon signed-rank test.

Strategies to correct for surface effects

Going one step further, we investigated how these surface effects could be minimized. Since, as already discussed, TIC normalization is not a suitable solution to this problem, the addition of

internal standards was considered. When making DESI measurements, internal standards can be added to the DESI spray solvent, an approach already reported in the literature to improve quantification accuracy [9]. We tested this approach in imaging applications by adding glutaric and adipic acids (0.5 mM) to the solvent spray. For this to be a useful tool for avoiding and/or measuring surface effects, the signal of these standards should change during acquisition depending on local tissue physico-chemical properties. The images reconstructed for the internal standards are shown in Figure 4 and show a rather uniform distribution of glutaric and adipic acids, indicating that the signals of the two acids are not highly dependent on the characteristics of the surface. These results contrast with those observed when the two acids were 'added' to the grapevine stem and tell us that differences in surface effects cannot be controlled by simply adding a "calibrant" to the spray solvent. This could be explained by the fact that desorption is not necessary in the ionization process when internal standards are sprayed in DESI solvent.

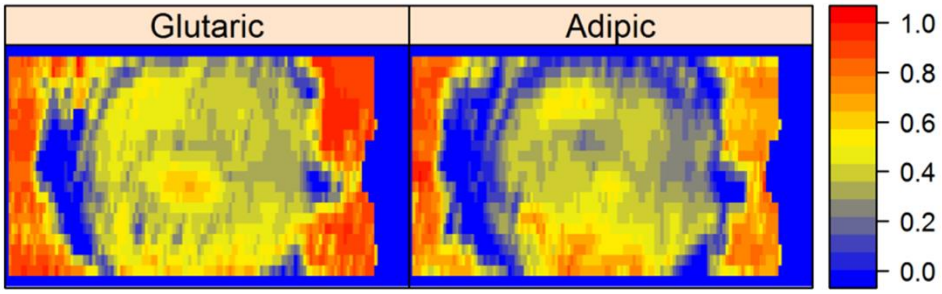

Fig 4 DESI imaging of glutaric and adipic acids added to the spray solvent. The color bar represents TIC normalized ion intensity from 0 (blue) to 1(red).

An attractive alternative, especially in untargeted DESI experiments, to minimize surface effects on the efficiency of metabolite desorption is to 'imprint' the tissues on a uniform surface while preserving the original distribution of the metabolites. This indirect DESI imaging has been applied in several contexts using porous Teflon [21-23], PTFE [15], print paper or TLC plate [24].

To verify the ability of imprinting in compensating the surface effects, the ideal way is to map the distribution of organic acids from the imprint of grapevine stem on PTFE surfaces, and then compare the results with the direct DESI imaging results. We have tried imprinting grapevine stem onto the PTFE surface but the results are not satisfying. The reasons are: 1). the grapevine stems used in our experiment were harvested at post-veraison stage and the water content in the grapevine stem at that time is too low to allow adequate organic acid transfer. 2). although increasing the pressure during imprinting improves the organic acid transfer efficiency but meanwhile the transfer efficiency difference between pith and outer pith region is also increased as their structures differ significantly (pith is spongeous and soft and outer pith region is hard and woody). 3). a recent study demonstrated that metabolite transfer efficiency can be improved with the assistance of solvent extraction and/or heating during imprinting, while ion intensity varies significantly under different solvent and/or heating conditions [26]. To avoid bias and exclude the possible effect brought by the organic acid transfer efficiency differences between pith and outer pith region on our DESI imaging results, we used grapevine leaf (Fig 5a) in our experiment as it is water-rich and the structural difference between leaf lamina and vein is minimum (the organic acid transfer efficiency difference is also minimum). As before, semi-quantitative distribution of malic, tartaric and citric acids in the grapevine leaf obtained from DESI images was compared with IC by separating the lamina and vein of leaves. DESI images revealed no differences between leaf lamina and leaf vein for the three organic acids (Fig 5b), consistent with the results obtained by IC (Fig 5c). Although we focused on a small number of compounds in only one tissue type, our results suggest that imprinting might be useful in minimizing desorption differences due to surface effects in structurally or biologically heterogeneous tissue. However, it is important to point out that this method is more suitable for water-rich samples and does not

yield good outputs for harder tissues like grapevine stem. A recent study demonstrated that metabolite transfer efficiency can be improved with the assistance of solvent extraction and/or heating during imprinting, while ion intensity varies significantly under different solvent and/or heating conditions [25]. Spatial resolution is another concern, as metabolites could be smeared during pressing [1]. Furthermore, we cannot exclude the possibility that homogeneous detection of the three organic acids over the grapevine leaf blade might be due to the fact that differences in their concentrations between leaf lamina and vein are averaged out during pressing. It is our opinion, therefore, that imprinting could be a promising technique to minimize surface effects, although it should be borne in mind that the overall approach needs further validation.

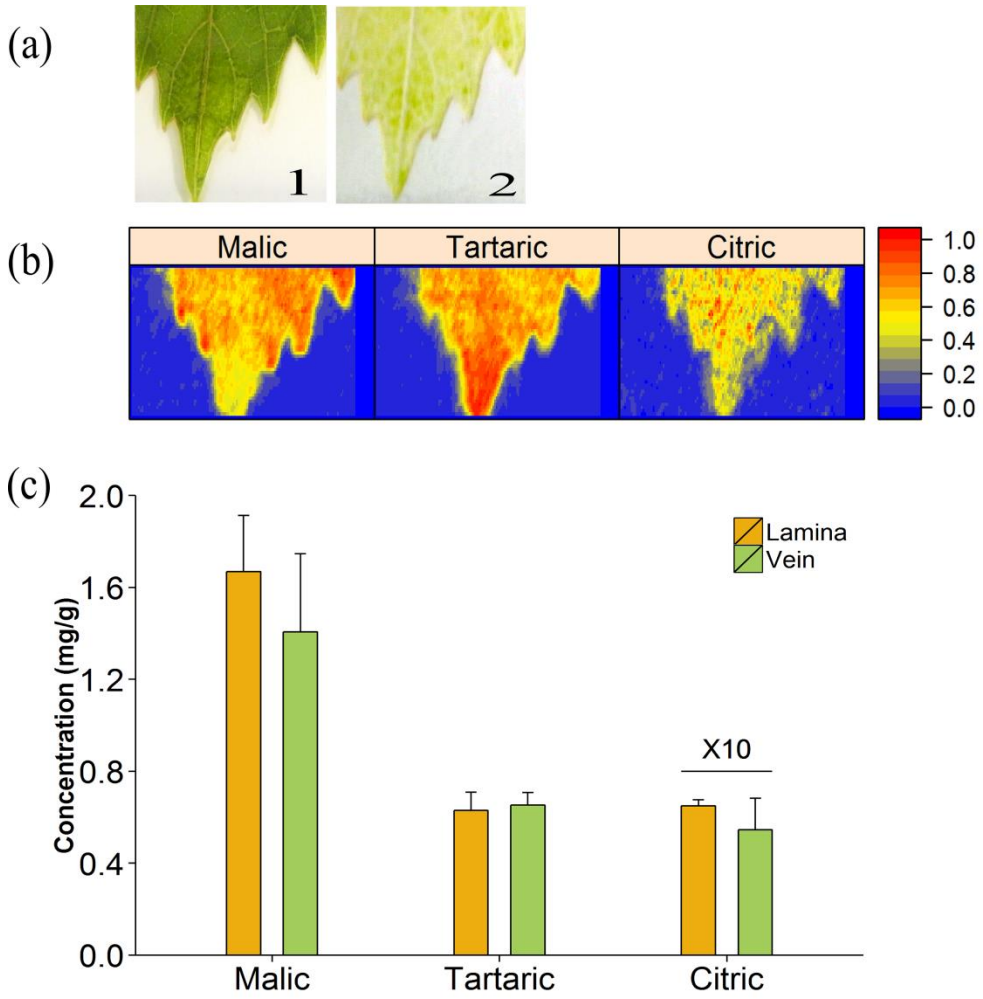

Fig 5 Quantitative mapping of three major organic acids (malic, tartaric and citric acids) in grapevine leaf blade. **(a)** Optical images of the grapevine leaf (1) and its imprint on a PTFE surface (2). **(b)** DESI imaging of the three organic acids at negative ion mode. The color bar represents TIC normalized ion intensity from 0 (blue) to 1(red). **(c)** IC quantification of the three organic acids in leaf lamina and leaf vein. Values represent mean+SD (n=3); values for citric acid are increased 10 times for better visualization. No statistical differences were found between leaf blade and leaf vein ($P<0.01$) for each organic acid according to a Wilcoxon signed-rank test.

4.3.2 DESI Profiling on PTFE

In the previous section, the role of surface effects on the output of DESI imaging experiments was investigated. These phenomena are likely due to differences in the local physico-chemical properties of the tissue surfaces. To understand how these properties affect the desorption process, we performed a series of DESI profiling experiments on PTFE surfaces with different porosities. Three surfaces, a) flat PTFE, b) PTFE with a pore size of 1-3 µm, 25-30% porosity (PTFE1), and c) PTFE with a pore size of 7-14 µm, 45-50% porosity (PTFE14), were used to mimic a heterogeneous sample tissue. A solution (2.5 mM) of five organic acids was spotted on the surfaces and analyzed by DESI.

Results of the DESI analysis are shown in Figure 6. The six plots in Figure 6a show how the absolute ion intensity of the 5 organic acids varies over time on the three different surfaces. Figure 6b, on the other hand, displays the absolute integrated signal over 1 minute (note that the relative abundances of the 5 organic acids vary with different integration times as they do not decay at the same rate (Fig S2)). Although deposited in equimolar amounts, ion intensities vary widely among the 5 organic acids. The integrated ion intensities for citric acid, for example, are at least 20 times higher than those for adipic acid on all three PTFE surfaces. This result is not

unexpected and is primarily due to their intrinsic pK_{a1} differences which largely determine their ionization efficiencies [26], the pK_{a1} values of citric acid being the lowest and adipic acid the highest [27, 28]. Figure 6b shows that, in terms of absolute response, PTFE14 gives optimum performance, followed by PTFE1 then flat PTFE. In terms of signal decay over time, figure 6a shows that the ion intensity of each organic acid is relatively stable on PTFE1, while flat PTFE has the poorest signal stability, the signals of glutaric and adipic acids disappearing after 1.5 min (data not shown). As expected, the compounds are more readily washed away from the flat surface, and this also affects the absolute intensity of the signal over 1 minute. On the other hand, PTFE1 porosity seems better able to 'cage' the metabolites on its surface and to therefore produce a more stable signal. More generally, it is known that surface roughness and porosity affect the degree of sample spreading upon spotting as well as the degree of washing away upon spay solvent splashing [6-9].

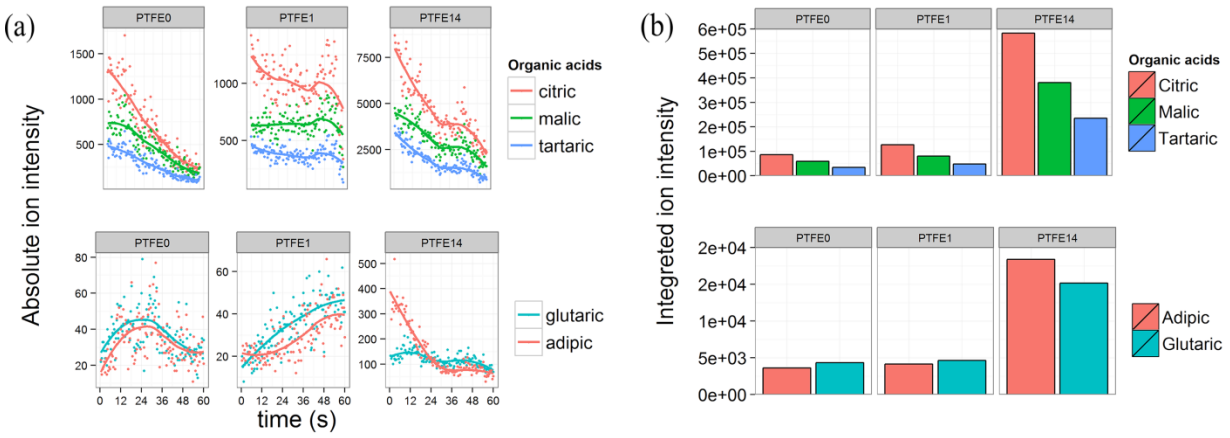

Fig 6 Absolute ion intensity of malic, tartaric, citric, glutaric and adipic acids detected on 3 different surfaces, PTFE0 (flat PTFE), PTFE1 (PTFE with pore size 1-3 µm) and PTFE14 (PTFE with pore size 7-14 µm), at negative mode. **(a)** Absolute ion intensity of each organic acid as a function of time. **(b)** Integrated ion intensity of each organic acid for 1 min.

As the model PTFE surfaces are chemically inert to the organic acids and DESI solvent, DESI profiling results on the PTFE surfaces suggest that the local physical properties of the tissue surfaces strongly affect the desorption process as well as their relative quantitative detection (in terms of integrated ion intensity).

Conclusions

It is known that sample surface properties affect the desorption processes in MSI, while it is often ignored that different surface properties within a structurally/biologically heterogeneous sample tissue can largely affect the quantitative detection of analytes, and may result in the MS images misrepresenting their true distribution. This phenomenon has also been reported in MALDI [29] and SIMS imaging [30]. Attention should be paid in interpreting biologically related questions when using this type of imaging information, as differences in the quantitative distribution of a metabolite in a sample tissue might simply reflect differences in specific physico-chemical interactions with the matrix and not differences in relative amounts.

Our investigation suggests that imprinting could be a solution for minimizing these surface effects, although the effectiveness of this strategy requires further investigation. As far as the addition of external standards is concerned, our results clearly indicate that the addition of a reference compound to the DESI spray has no significant effect, but enrichment of the samples with close analogues or stable isotope labeled compounds could be the way to go, similarly to what is normally done in MALDI [31, 32] and DESI [33]. It is important to point out, however, that this solution is expected to be optimal only in the case of targeted analysis because the ‘local environment’ can affect different metabolites in different ways. This observation *de facto* limits the value of untargeted imaging studies if their outcomes are not suitably validated.

The results of our imaging experiments, however, were highly reproducible, and showed consistent spatial distributions of organic acids in several stems of different plants collected in two growing seasons. Even where grapevine stems were dipped in an adipic and glutaric acid solution for 1 h, the distributions of malic, tartaric and citric acids did not alter significantly (Fig S3). Our results suggest that ion intensity in a DESI image is a function of metabolite concentration and tissue surface properties when instrumental and ion source parameters are constant. This ion intensity can be used as a characteristic descriptor of tissue type since both metabolite content and tissue surface are tissue specific. This information is potentially useful in distinguishing both intra- (as shown in grapevine stem) and inter-sample tissue differences, which are often impossible to resolve with a microscope. In this study, we successfully distinguished 6 different grapevine tissue types using Principal Component Analysis on ion intensities of 8 organic acids directly extracted from DESI images (Fig S4).

Reference

1. Lee, Y.J., et al., *Use of mass spectrometry for imaging metabolites in plants.* The Plant Journal, 2012. **70**(1): p. 81-95.
2. Svatos, A., *Mass spectrometric imaging of small molecules.* Trends Biotechnol, 2010. **28**(8): p. 425-434.
3. Takats, Z., et al., *Mass spectrometry sampling under ambient conditions with desorption electrospray ionization.* Science, 2004. **306**(5695): p. 471-473.
4. Wiseman, J.M., et al., *Desorption electrospray ionization mass spectrometry: Imaging drugs and metabolites in tissues.* Proc Natl Acad Sci U S A, 2008. **105**(47): p. 18120-18125.
5. Miura, D., Y. Fujimura, and H. Wariishi, *In situ metabolomic mass spectrometry imaging: recent advances and difficulties.* J Proteomics, 2012. **75**(16): p. 5052-5060.
6. Manicke, N.E., et al., *Desorption electrospray ionization (DESI) mass spectrometry and tandem mass spectrometry (MS/MS) of phospholipids and sphingolipids: ionization, adduct formation, and fragmentation.* J Am Soc Mass Spectrom, 2008. **19**(4): p. 531-543.
7. Ifa, D.R., et al., *Quantitative analysis of small molecules by desorption electrospray ionization mass spectrometry from polytetrafluoroethylene surfaces.* Rapid Communications in Mass Spectrometry, 2008. **22**(4): p. 503-510.
8. Douglass, K.A., et al., *Deconstructing Desorption Electrospray Ionization: Independent Optimization of Desorption and Ionization by Spray Desorption Collection.* J Am Soc Mass Spectrom, 2012. **23**(11): p. 1896-1902.

9. Takats, Z., J.M. Wiseman, and R.G. Cooks, *Ambient mass spectrometry using desorption electrospray ionization (DESI): instrumentation, mechanisms and applications in forensics, chemistry, and biology.* Journal of Mass Spectrometry, 2005. **40**(10): p. 1261-1275.
10. Abadia, J., et al., *Organic acids and Fe deficiency: a review.* Plant and Soil, 2002. **241**(1): p. 75-86.
11. Ma, J.F., P.R. Ryan, and E. Delhaize, *Aluminium tolerance in plants and the complexing role of organic acids.* Trends Plant Sci, 2001. **6**(6): p. 273-278.
12. Choi, Y.H., et al., *Are natural deep eutectic solvents the missing link in understanding cellular metabolism and physiology?* Plant Physiol, 2011. **156**(4): p. 1701-1705.
13. Kupina, S.A., C.A. Pohl, and J.L. Gannotti, *Determination of Tartaric, Malic, and Citric Acids in Grape Juice and Wine Using Gradient Ion Chromatography.* American Journal of Enology and Viticulture, 1991. **42**(1): p. 1-5.
14. D.R.E Possner , W.M.K., *The localization of acids, sugars, potassium and calcium in developing grape berries.* Vitis, 1985. **24**: p. 11.
15. Muller, T., et al., *Direct plant tissue analysis and imprint imaging by desorption electrospray ionization mass spectrometry.* Anal Chem, 2011. **83**(14): p. 5754-5761.
16. Scientific, T., *Higher Resolution Separation of Organic Acids and Common Inorganic Anions in Wine* 2011: p. 8.
17. Team, R.C., *R: A Language and Environment for Statistical Computin.* R Foundation for Statistical Computing, Vienna, Austria., 2013.
18. Wickham, H., *ggplot2: elegant graphics for data analysis.* Springer New York, 2009.
19. Sarkar, D., *Lattice: multivariate data visualization with R*. 2008: Springer.
20. Pratt, C., *Vegetative Anatomy of Cultivated Grapes--A Review.* American Journal of Enology and Viticulture, 1974. **25**(3): p. 19.
21. Li, B., et al., *Characterization of barley leaf tissue using direct and indirect desorption electrospray ionization imaging mass spectrometry.* Journal of Mass Spectrometry, 2011. **46**(12): p. 1241-1246.
22. Thunig, J., S.H. Hansen, and C. Janfelt, *Analysis of secondary plant metabolites by indirect desorption electrospray ionization imaging mass spectrometry.* Anal Chem, 2011. **83**(9): p. 3256-3259.
23. Li, B., et al., *Visualizing metabolite distribution and enzymatic conversion in plant tissues by desorption electrospray ionization mass spectrometry imaging.* Plant J, 2013.
24. Ifa, D.R., et al., *Tissue imprint imaging by desorption electrospray ionization mass spectrometry.* Analytical Methods, 2011. **3**(8): p. 1910-1912.
25. Cabral, E.C., et al., *Blotting Assisted by Heating and Solvent Extraction for DESI-MS Imaging.* J Am Soc Mass Spectrom, 2013.
26. Oss, M., et al., *Electrospray ionization efficiency scale of organic compounds.* Anal Chem, 2010. **82**(7): p. 2865-2872.
27. Kakola, J. and R. Alen, *A fast method for determining low-molecular-mass aliphatic carboxylic acids by high-performance liquid chromatography-atmospheric pressure chemical ionization mass spectrometry.* J Sep Sci, 2006. **29**(13): p. 1996-2003.
28. Hano, T., et al., *Extraction Equilibria of Organic-Acids with Tri-N-Octylphosphineoxide.* Journal of Chemical Engineering of Japan, 1990. **23**(6): p. 734-738.
29. Peukert, M., et al., *Spatially resolved analysis of small molecules by matrix-assisted laser desorption/ionization mass spectrometric imaging (MALDI-MSI).* New Phytol, 2012. **193**(3): p. 806-815.
30. Jones, E.A., N.P. Lockyer, and J.C. Vickerman, *Mass spectral analysis and imaging of tissue by ToF-SIMS—The role of buckminsterfullerene, C_{60}^{+}, primary ions.* International Journal of Mass Spectrometry, 2007. **260**(2): p. 146-157.

31. Reyzer, M.L., et al., *Direct analysis of drug candidates in tissue by matrix-assisted laser desorption/ionization mass spectrometry.* Journal of Mass Spectrometry, 2003. **38**(10): p. 1081-1092.
32. Landgraf, R.R., et al., *Considerations for quantification of lipids in nerve tissue using matrix-assisted laser desorption/ionization mass spectrometric imaging.* Rapid Commun Mass Spectrom, 2011. **25**(20): p. 3178-3184.
33. Lanekoff, I., et al., *Imaging nicotine in rat brain tissue by use of nanospray desorption electrospray ionization mass spectrometry.* Analytical chemistry, 2013. **85**(2): p. 882-889.

Chapter 5

High production of small organic dicarboxylate dianions by DESI and ESI

Yonghui Dong, Graziano Guella, Fulvio Mattivi, Pietro Franceschi

Notes:

This chapter has been prepared for submission. Dong Y. conducted the experiment, performed data analysis and wrote the draft; Guella G. designed the experiment, revised and approved the final manuscript; Mattivi F. approved the final manuscript; Franceschi P. conceived and design the experiment, revised and approved the final manuscript.

5.1 Introduction

Small organic dicarboxylic acids (SODAs) play an important role in many biological systems. In the specific case of plants they are key intermediates in carbon metabolism and can be present in high concentrations - often stored as K^+ salts - with important implications for the production of beverages like juices or wine.

Since dicarboxylic acids (H_2DCA) such as succinic, glutaric, adipic, malic and tartaric acid have pK_{a2} values in water lower than 6, in alkaline aqueous solutions they are expected to be present mostly as dicarboxylate anions (DCA^{2-}) followed by minor relative amount of the monoprotonated species $HDCA^-$. However, DCA^{2-} species are rarely (and scarcely) detected by mass spectrometric techniques no matter of the used ionization source used to carry these ions in the final gas phase [1]; in fact, due to their high gas phase proton affinity they easily tend a) to be protonated during solvent evaporation leading to $HDCA^-$ or b) to lose one electron leading to the corresponding radical anion or c) to dissociate into singly charged adduct ions and neutral fragments. For a given carbon backbone, the gas phase stability of DCA^{2-} can be increased by introducing additional functional groups which allow charge delocalization and/or favour intramolecular hydrogen bonding, as in the case of tartaric acid [2]. This complex behaviour coupled with a relatively simple structure has made SODAs an ideal system to study fundamental molecular phenomena like Coulomb repulsions [3] and solute-solvent interactions [4, 5]. From an experimental point of view, ESI should be the technique of election to produce gas phase DCA^{2-}, but it has been always quite difficult to produce these ionic species in significant amount, at least for H_2DCA with low molecular weight. In particular, a recent work by Tonner et al. demonstrates that the tartaric dianion (TA^{2-}) can be produced by ESI, albeit with low efficiency, only under restricted experimental conditions by hindering their spontaneous thermodynamic decomposition [2].

Since it is widely accepted that DESI follows an ESI-like dynamics [6, 7], the production of TA^{2-} specie in DESI-MS spectra was expected to be also highly inefficient. However, during Desorption Electrospray Ionization (DESI) imaging of SODAs in grape tissues (Figure 1), we have observed a relatively strong signal at m/z 72 attributable to this tartrate dianion, thus demonstrating that it can be produced in good yields also in standard MS conditions. As a consequence, this outcome seems to suggest the presence of significant and subtle differences between DESI and ESI ionization mechanisms.

In order to understand the mechanism of formation of DCA^{2-}, we designed a series of DESI and ESI experiments on SODAs differing for the length of the carbon backbone and the number of hydroxyl groups. In particular, we analyzed a) 3 H_2DCA acids of general structural formula HOOC-$(CH_2)_n$-COOH, i.e. succinic (n=2,H_2SA), glutaric (n=3,H_2GA) and adipic acid (n=4, H_2AA) and b) two hydroxylated dicarboxylic acids, malic (HOOC-CH_2-CHOH-COOH, H_2MA) and meso-tartaric acid (HOOC-CHOH-CHOH-COOH, H_2TA) (see Figure 1).

Since in grape tissue SODAs are often stored as potassium salts [8], different SODA potassium salts were used as starting point of all the MS experiments as prepared by titration of the corresponding acid with KOH (potassium hydroxide); in order to investigate any possible role played by counter-ions, we prepared (by titration with NaOH and LiOH) the corresponding sodium and lithium salts (for the details see the Experimental Section). DESI analysis was carried out on SODA aqueous solutions deposited and air dried on a chemically inert porous Teflon surface. For ESI measurements, the same SODA aqueous solutions were directly injected into the ion source by a syringe pump. To minimize possible differences due to different composition of needle-sprayers, the DESI sprayer was also used as ESI source by adjusting the source geometry (see Experimental Section).

Experimental section

Acetonitrile was purchased from Sigma-Aldrich (Italy), water was purified using a Mili-Q water purification system (Sartorius Stedim biotech Gmbh, Germany). Succinic (>99.5%), malic (>99.5%), glutaric (>99.0%) and adipic acids (>99.5%) were purchased from Fluka AG (Germany), L-tartaric acid (99.5%), lithium hydroxide monohydrate (99%), sodium hydroxide (>97%) and potassium hydroxide (>85%) were from Sigma Aldrich (Italy).

The dicarboxylate salts were produced by mixing equal volumes (20 mL, water/acetonitrile 1:4) of 0.5 mM aqueous solutions of each H_2DCA (succinic, malic, tartaric, glutaric and adipic acids) a) with a molar excess (1.5 mM) of alkali hydroxides (LiOH, NaOH, KOH) or b) with 2 mol equivalent (1.0 mM) of the same hydroxides. Three microliter of each solution was deposited on a porous PTFE sheet (pore size 1-3 μm, porosity 25-30%, Porex Corporation, Germany) and then was air dried before DESI analysis. Each solution was analysed 6 times with an acquisition time of 1 min.

All the MS experiments were performed using a Thermo-Fisher Scientific LTQ-Orbitrap XL mass spectrometer (Bremen, Germany) equipped with an OmniSpray™ ion source from Prosolia

Inc. (Indianapolis, IN). The typical instrumental parameters for standard DESI were: -100 V tube lens voltage, -10 V capillary voltage, 5 kV spray voltage, 200 ^{o}C capillary temperature, 2 micro scans, 200 ms MS injection time. Mass spectra were acquired in full scan negative mode over the m/z range of 50-200. The DESI source parameters used were: 55 degree spray angle, 1-1.5 mm tip-to-surface distance, ~ 4 mm tip-to-inlet distance, 10° collection angel, 8 bar nitrogen carrier gas pressure. A mixture of Milli-Q water and acetonitrile (1:4, vol/vol) was used as spray solvent and delivered at the flow rate of 3 μl min^{-1}.

ESI measurements were carried out by simply changing the DESY spray angle close to 45 degree, while keeping other instrumental and ion source parameters constant. Analyte solutions were injected directly into the inlet at the flow rate of 3 μl min^{-1}. Each solution was analyzed 6 times with an acquisition time of about 1 min.; ion source was washed by spraying Milli-Q water/acetonitrile 1:4 (v/v) for about 10 min at the flow-rate of 8 μl min^{-1}.

5.2 Results and Discussion

The outcomes of the complete set of our experiments is summarized in Figure 1 which shows the intensity of the DCA^{2-} ion with respect to the intensity of the corresponding base peak ($[M-H]^-$, always the most intense peak in the MS spectra). Only the results for K_2DCA salts are shown, but similar data were obtained for the corresponding sodium and lithium salts (see Figure 2S and Figure 3S in Appendix 3 for Na_2DCA and Li_2DCA salts, respectively).

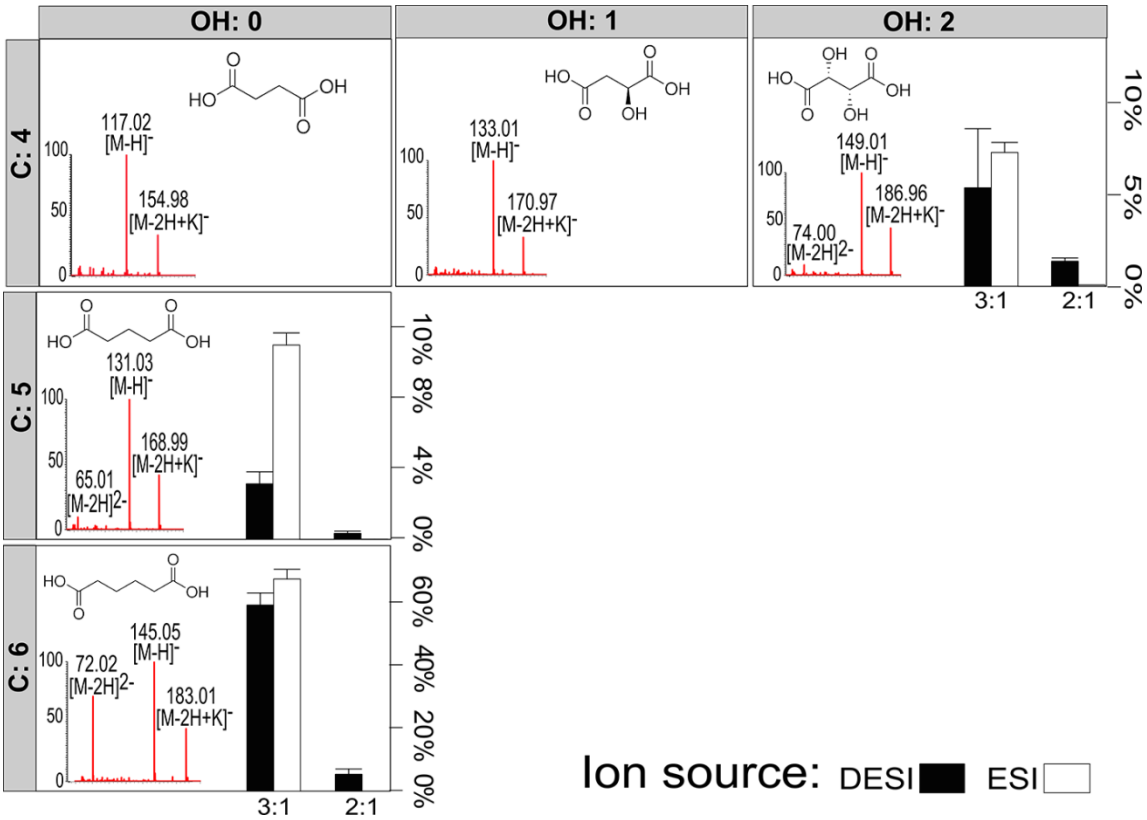

Figure 1. DCA^{2-} ion yields as observed in ESI and DESI ion-sources for K_2DCA aq. solutions. Dianion yields were calculated by the ratio of abundance of dianions to those of their respective deprotonated singly charged ions. Values represent mean ± SD (n=6). '3:1' represent salts obtained from DCA by using molar excess (3:1) of KOH whilst '2:1' represent salts obtained from DCA by using two molar equivalents (2:1) of KOH.

Each panel of the plot displays the results relative to SODAs with a different carbon backbone (first column) bearing a different number of hydroxyl groups (first row). The leftmost barplot illustrates the results obtained with aqueous solutions prepared by KOH/DCA in 3:1 ratio. In this condition for both sources, DCA^{2-} starts to be detectable for a carbon chain of at least five carbon atoms and the relative intensity, as expected, increases with the number of carbons. A longer chain, indeed, means a bigger separation between the two charges and the subsequent reduction of Coulomb repulsion stabilizes the doubly charged ion. Our findings are in keeping with previous investigations, which demonstrated that HOOC-$(CH_2)_2$-COOH is not stable in the gas phase [5, 9]. A simple calculation of the Coulomb repulsion energy $E_{rep}= e^2/4\pi\varepsilon_0 r$ between two electrons, at a distance r, suggests that the two negative charges in a molecule with a mutual

electron affinity of 3eV (electron affinity of carboxylate radical anions is about 3eV) can be stable when they are more than 5Å apart [2, 10]. The charge separation distance of 5.3Å for succinate estimated by Wang and co-workers [3] rationalizes why bare succinate dianion is not observable in the gas phase. In our conditions, the increase in the relative intensity with increased length of the chain is remarkable: for HOOC-$(CH_2)_4$-COOH the DCA^{2-} is as high as 60% of the deprotonated singly charged ion DCA^-. ESI and DESI seem to give qualitatively comparable results, even if the ESI relative yield was found a bit higher for HOOC-$(CH_2)_3$-COOH.

The role of the hydroxyl groups on the four carbon backbone is displayed in the first row of Figure 1. In our measurements, only H_2TA (bearing 2 hydroxyl groups) shows efficient production of DCA^{2-} ions in both DESI and ESI. Again, this result is in agreement with experiments and *ab-initio* calculations carried out by Tonner and co-workers [2], who demonstrated that TA^{2-} is the smallest dicarboxylate stable in the gas phase. Interestingly, however, in our experiments we have been able to produce a much stronger signal for the TA^{2-} at m/z 72 (around 8% of TA^-) than that reported in recent literature [2] where this species has been barely detected only under highly restricted ESI conditions. The observed strong DCA^{2-} ion yield is difficult to rationalize, we only have the experimental hint that ESI/DESI DCA^{2-} ion yield is higher on strongly alkaline solutions prepared by using a molar excess of metal hydroxides. From one side the expected higher pH of these solutions ensures higher molar fraction of TA^{2-} species even because the pK_{a2} of H_2TA in acetonitrile/water solution (4:1, v/v) should be much higher (at least of 5 magnitude order) than in aqueous solution. From the other side, however, higher concentration of the metal cations should lead, during ESI/DESI processes, to relevant formation of neutral (such as K^+--TA^{2-}--K^+) or singly charged (TA^{2-}--K^+) ion-pairs. The results seem to suggest that during ionization the metal ions can be selectively and efficiently "caged" by hydroxyl groups and they are not available to partially (or completely) neutralize the most abundant DCA^{2-} species in strong alkaline conditions.

To confirm the role of the free OH^- present in solution we reduced their amount, by using double metal salts to prepare the initial solution. The results of the experiments performed in these new conditions are summarized in the right barplot in Figure 1 (2:1). The effect of the reduction of free OH^- on the ESI spectra is striking: DCA^{2-} is practically undetectable in all cases. A minor signal is still visible (0.075% for TA, 0.006% for AA), but it is almost comparable with the

chemical noise and in line with that observed in literature [2]. This experiment highlights the role of OH^- in promoting the production of the dianions: obviously their presence is not affecting the molecular properties of the OAs, but it can reduce the extent of ion pairing K^+-- DCA^{2-} --K+ in ESI conditions.

The situation in DESI, however, is now different. The DCA^{2-} yield is indeed lowered, but the signals are still clearly present, indicating that in DESI, DCA^{2-} can be efficiently produced also when free from OH^- groups. A straightforward way to account for this observation is to suppose that in DESI there is another active "caging" mechanism which mimics the effects of the free OH^- excess. The particular nature of DESI suggests a possible solution. It is known that DESI involves the landing and releasing of charges on the surface [11], but when the surface is an insulator this will produce a local charge accumulation. In negative ion mode, the surface is expected to be negatively charged and it can attract and cage the K^+ ions thus favoring the formation of DCA^{2-} ions in the gas phase.

5.3 Conclusions

We have proposed a simple and efficient method to produce DCA^{2-} in DESI and ESI by introducing an excess amount of OH- in dicarboxylate solutions. Although the ionization dynamics is similar in DESI and ESI, our results indicate that the surface in DESI play a crucial role in determining the nature of the observed gas-phase ions. Our results have been obtained on a PTFE model surface, but the same phenomena are expected to happen if DESI is used to analyze plant tissue sections. There, the large amount of OH-rich polymers is expected to bind metal ions, favoring the formation of DCA^{2-} observed during our imaging experiments. From the analytical point of view, our study suggests that DCA^{2-} signal could be used in MS imaging experiments as a proxy to measure the distribution of SODA salts in plant tissues. The possible application of this idea will be the subject of further investigations.

Reference

1. Wang, G.D. and R.B. Cole, *Effects of solvent and counterion on ion pairing and observed charge states of diquaternary ammonium salts in electrospray ionization mass spectrometry.* J Am Soc Mass Spectrom, 1996. **7**(10): p. 1050-1058.
2. Tonner, R., et al., *Stability of gas-phase tartaric acid anions investigated by quantum chemistry, mass spectrometry, and infrared spectroscopy.* Journal of Physical Chemistry A, 2012. **116**(19): p. 4789-4800.

3. Wang, L.S., et al., *Probing the potential barriers and intramolecular electrostatic interactions in free doubly charged anions.* Physical Review Letters, 1998. **81**(13): p. 2667-2670.
4. Yang, X., et al., *Solvent-mediated folding of a doubly charged anion.* Journal of the American Chemical Society, 2004. **126**(3): p. 876-883.
5. Ding, C.F., X.B. Wang, and L.S. Wang, *Photoelectron spectroscopy of doubly charged anions: Intramolecular Coulomb repulsion and solvent stabilization.* Journal of Physical Chemistry A, 1998. **102**(45): p. 8633-8636.
6. Nefliu, M., et al., *Internal energy distributions in desorption electrospray ionization (DESI).* J Am Soc Mass Spectrom, 2008. **19**(3): p. 420-427.
7. Takats, Z., J.M. Wiseman, and R.G. Cooks, *Ambient mass spectrometry using desorption electrospray ionization (DESI): instrumentation, mechanisms and applications in forensics, chemistry, and biology.* Journal of Mass Spectrometry, 2005. **40**(10): p. 1261-1275.
8. W. Mark Kliewer, L.H.a.M.O., *Concentrations of Tartaric Acid and Malic Acids and Their Salts in Vitis Vinifera Grapes.* Am. J. Enol. Vitic, 1967. **18**(1): p. 13.
9. Herbert, J.M. and J. Ortiz, *Ab initio investigation of electron detachment in dicarboxylate dianions.* The Journal of Physical Chemistry A, 2000. **104**(50): p. 11786-11795.
10. Maas, W.P.M. and N.M.M. Nibbering, *Formation of Doubly Charged Negative-Ions in the Gas-Phase by Collisionally-Induced Ion-Pair Formation from Singly Charged Negative-Ions.* International Journal of Mass Spectrometry and Ion Processes, 1989. **88**(2-3): p. 257-266.
11. Basile, F., et al., *Analysis of lipids from crude lung tissue extracts by desorption electrospray ionization mass spectrometry and pattern recognition.* Analytical Biochemistry, 2011. **408**(2): p. 289-296.

Chapter 6

Conclusions and Future Work

6.1 Conclusions

In this thesis some of the central issues which have to be faced for the fruitful application of MSI to plant tissues have been addressed by using MALDI and DESI, for mapping the distribution of small metabolites in apple and grape, respectively.

High spatial resolution MALDI ion source coupled with high mass resolution Orbitrap was used to image the distribution of flavonols and dihydrochalcones in different parts of apple. To increase the chemical selectivity of this type of experiments, a novel data analysis approach based on Intensity Correlation Analysis has been also developed.

DESI imaging was used as a fast technique because it allows rapid analysis under ambient conditions without or with limited sample preparation. For this reason we have been using it to map the distribution of small organic acids in different grape tissues. Our investigation has demonstrated that the technique is reproducible and fast, but the sample surface properties largely affect the ionization process of organic acids. Furthermore, different surface properties in a structurally/biologically heterogeneous sample influence the ionization of target analytes at different degrees, resulting in the MS images misrepresenting their true distribution. The use Hyphenated mass spectrometry quantification methods such as GC-MS or LC-MS was necessary. Our experiments suggest that the impact of these phenomena could be reduced by tissue imprinting, but the potential of this approach will need further validation on different tissues and different analytes.

Our DESI experiments have been the occasion to investigate the mechanistic details of DESI ionization by studying the formation of small doubly charged anions in analytical conditions. It has been generally accept that ionization in DESI occurs by ESI mechanism, during our DESI imaging of tartrate in grape stem, we have observed a strong ion signal corresponding to the doubly charged anion of tartrate, while an ESI-based study failed to observe the bare tartrate dianion. This leads our interest to study the factors that can stabilize dianions in DESI. Our

results on several dicarboxylates using DESI and ESI suggest that the surface charging in DESI could trap the counterions, thus enhancing the doubly charged ion production.

6.2 Future directions

MSI is becoming an indispensable tool for molecular imaging of plants. It has been applied to study plant development, plant-environment interactions and functional genomics, but most of the studies are still focused on method development and technological application. Several factors are responsible for this situation. First of all experiments are time consuming so it is indeed difficult to analyze tissues in a real high throughput manner. Chemical sensitivity and low chemical specificity are another concern and this often requires the use of more standard validation analytical tools like GC-MS and LC-MS. The algorithms/software used for data analysis is another limiting factor: the use of MSI to foster biological interpretation requires being able to go beyond the sole production of nice pictures, making the analysis automatic and reproducible.

To make MSI an "off the shelf" tool which can be used to efficiently solve biological problems, advancements are then needed in several areas.

6.2.1 Sample preparation

Sample preparation is crucial to ensure the true distribution of analytes of interest. Small mistakes in sample preparation might significantly alter the quantitative detection of analyte molecules, resulting in misleading biological conclusions. Although many of the current standard MSI sample preparation methods have not changed significantly from those initially reported, plant sample preparation methods should be specifically investigated according to characteristics of the MSI instrument, nature of sample tissues and analytes of interest. In addition, sample preparation should be developed to be able to introduce the possibility of in vivo imaging with high temporal resolution (i.e. developing more 'soft' spray solvent system for DESI imaging).

6.2.2 Data analysis

Although a number of software packages are available for MSI image construction and/or MS imaging data analysis, there are many challenges to be overcome. For example, the large dataset

produced in MSI (i.e. a typical MALDI imaging dataset is comprised of 5,000-50,000 spectra, each having 10,000-100,000 intensity values) requires more time and memory efficient methods. Most of the current data processing methods are directly adopted from conventional mass spectrometry data analysis approaches. There are a lot to be done for MSI ion source and MSI dataset specific data analysis algorithm development. In addition, strategy regarding how to effectively co-register and MSI images and optical image is needed.

6.2.3 Quantitative imaging

There are many issues associated with semi-quantitation of MSI. Matrix effects, ion suppression (for MALDI), spray solvent system (for DESI), ionization efficiency and sample surface properties (for all MSI methods) are all factors that limit measured signal intensity truly representing target compound concentration. In particular, sample surface property differences over the sample tissue might mask the true distribution of analytes of interest as ionization efficiency is strongly affected by sample surface characteristics. Due to this reason, other quantification methods should be used to validate the MSI results. Isotopically labeled compound could be used for targeted MSI quantification by spraying it homogeneously over the sample surface prior MS imaging, while quantification for untargeted MSI is still challenging. One might subject the sample for LC-MS or GC-MS analysis to search for potential analytes of interest, and then use targeted MSI quantification strategy to acquire their exact quantitative distribution. However there are several limitations for this approach; it requires more samples, and the biomarkers are difficult to found if they are only highly localized in a small sample region. More versatile quantification methods for untargeted MSI are required.

6.2.4 High spatial resolution MSI

SIMS imaging is superior for high spatial resolution imaging of elements and small molecules at organelle level. However, it lacks the sensitivity of the mass range over m/z 1000 due to in-source fragmentation and molecular identification ability due to MS/MS incapability. The spatial resolution of MALDI imaging is partially limited by the size of matrix crystal, and DESI by the plume of spray solvent. Besides the efforts toward novel ion sources development, future work need to focus on new matrix development (for MALDI), spray solvent system (for DESI), and sample method to improve both spatial resolution and chemical sensitivity.

Appendix 1:

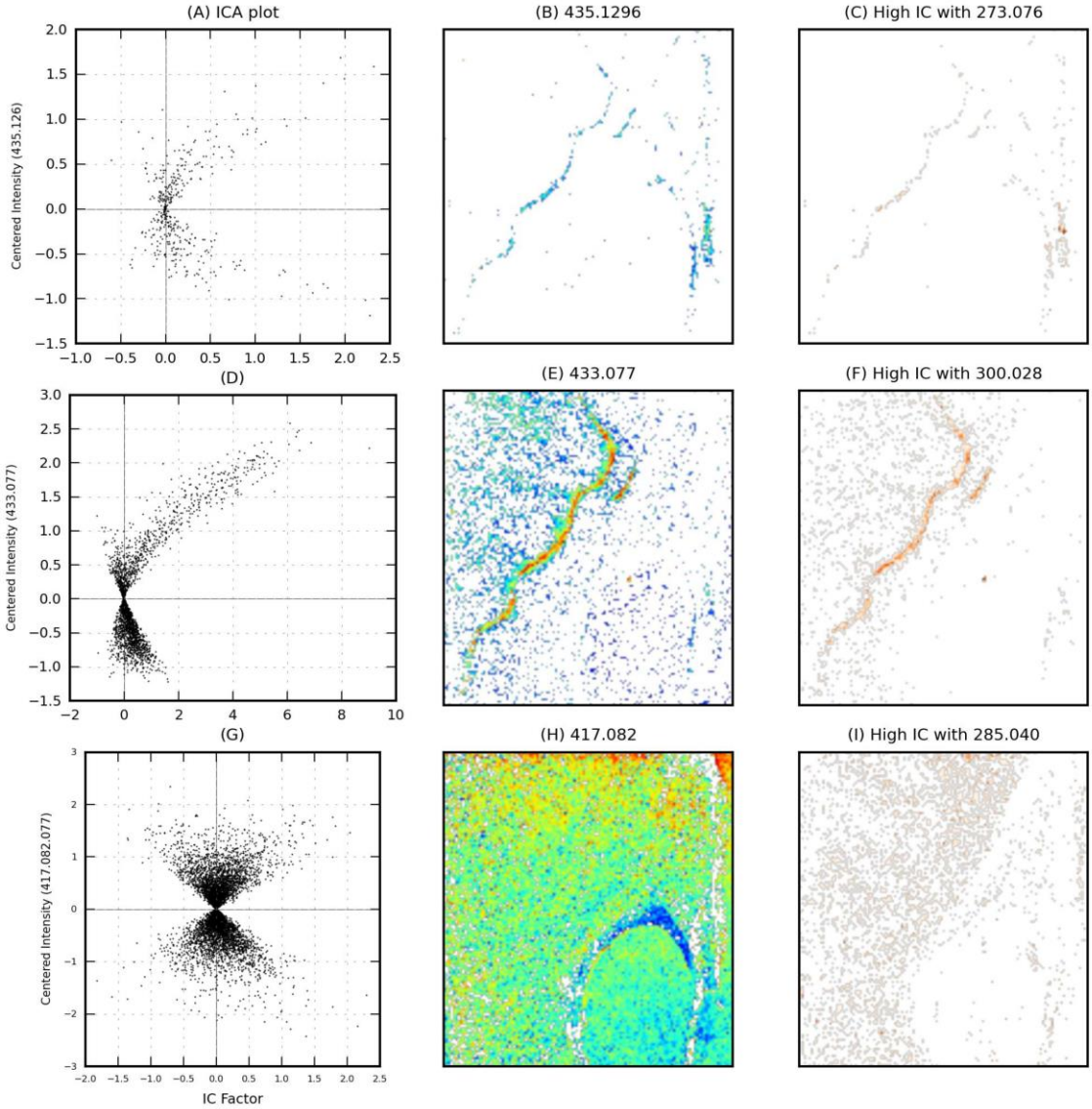

Figure S1: Pericarp region. MS images have been acquired with a raster step of 150 µm. (A,B,C) Intensity Correlation Analysis for masses at m/z 435.129 (assigned to phloretin-6S) and m/z 273.076 (assigned to phloretin). (A) ICA plot. (B) Image reconstructed from XIC at m/z 435.129 (logaritmic scaling, intensity from blue (low) to red (high)). (C) Image reconstructed from the pixels showing positive intensity correlation (scale from gray (low) to red (high). (D,E,F) ICA analysis for the ions at m/z 433.077 (assigned to quercetin-5S) and m/z 300.028 (assigned to quercetin). (G,H,I) ICA analysis for the ions at m/z 417.082 (assigned to kaempferol-5S) and m/z 285.040 (assigned to kaempferol).

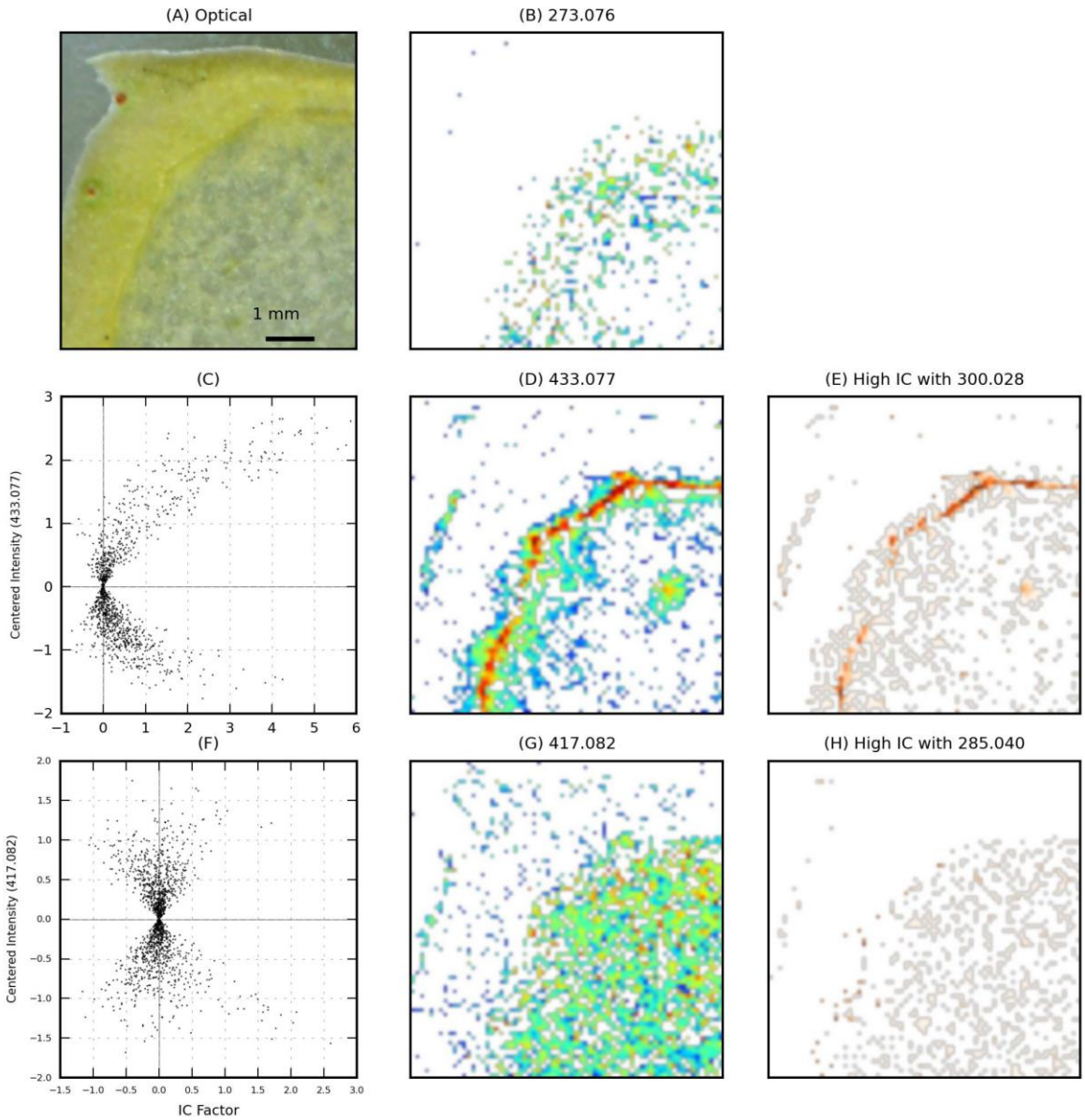

Figure S2: Skin region. MS images have been acquired with a raster step of 75 µm. (A) Optical Image. (B) Image reconstructed from XIC of m/z 273.076 (assigned to phloretin). (C,D,E) ICA analysis for the ions at m/z 433.077 (assigned to quercetin-5S) and m/z 300.028 (assigned to quercetin). (F,G,H) ICA analysis for the ions at m/z 417.082 (assigned to kaempferol-5S) and m/z 285.040 (assigned to kaempferol).

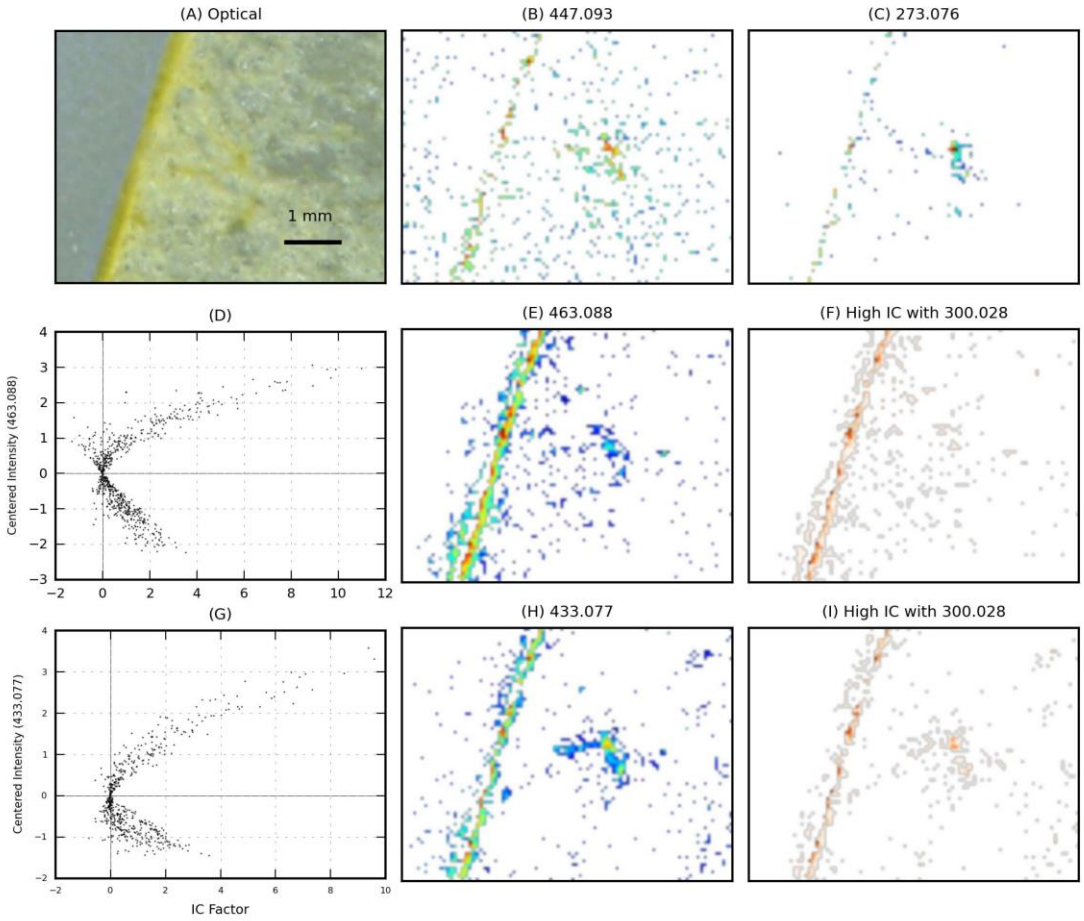

Figure S3: Skin region. MS images have been acquired with a raster step of 100 µm. (A) Optical Image. (B) Image reconstructed from XIC of m/z 447.093 (assigned to quercetin-rhamnoside). (C) Image reconstructed from the XIC of m/z 273.076 (assigned to phloretin). Note the higher intensity spot in correspondence of the cortical vascular system. (D,E,F) ICA analysis for the ions at m/z 463.088 (assigned to quercetin-6S) and m/z 300.028 (assigned to quercetin). (G,H,I) ICA analysis for the ions at m/z 433.077 (assigned to quercetin-5S) and m/z 300.028 (assigned to quercetin).

Table S1: Differences in ppm between the theoretical and the measured mass for the polyphenol glycosides detected in the three tissue sections (see Table 1). In the table only the metabolites with confirmed assignment are included. The value for the observed mass is obtained by combining all the spectra measured during the rastering of each tissue section.

Compound	Theoretical Mass	Observed Mass	Mass difference (ppm)
Endocarp Region			
Quercetin	300.0276	300.0270	2
kaempferol	285.0405	285.0397	2.7
Phloretin	273.0768	273.0759	3.3
phlor-6S	435.1297	435.1320	5.2
querc-rham	447.0933	447.0911	4.9
querc-5S	433.0776	433.0785	2.08
Skin Region: oblique section			
Quercetin	300.0276	300.0276	0
kaempferol	285.0405	285.0404	0.35
Phloretin	273.0768	273.0767	0.37
querc-5S	433.0776	433.0755	4.8
querc-6S	463.0882	463.0857	5.4
Skin Region: transverse section			
Quercetin	300.0276	300.0281	1.7
kaempferol	285.0405	285.0404	0.35

Phloretin	273.0768	273.0771	1.1
querc-5S	433.0776	433.0788	2.6
querc-6S	463.0882	463.0862	4.4

Appendix 2:

Quantification of malic, tartaric and citric acids in grape stem and grape leaf blade

Pith and out-pith-region (including xylem, phloem and periderms) were carefully separated, flash frozen in liquid nitrogen, and ground in a cryo-mill (Retsch, Haan, Germany) respectively. One gram of each was suspended in a fresh prepared extraction solution containing 1.2 ml methanol/water (2:1, vol/vol) and 0.8 ml chloroform. The extract was mixed by vortex for 10 s and sonicated for 10 min. The homogenate was centrifuged for 5 min at 5000 rpm at 4 ^{o}C. The supernatant was transferred through a 0.22 µm PVDF filter (Millipore Corporation, USA), leaving 1.5 ml total volume to a LCMS certified vials. Same method was used for extraction of the three organic acids in grape leaf lamina and leaf vein.

Organic acids were analyzed using high performance anion exchange chromatography (HPAEC) with suppressed conductivity detection (Dionex ICS-5000, Thermo Scientific). Briefly, An ion-exchange OmniPac Pax100 column (4 x 250 mm) and OmniPac Pax100 (4 x 50 mm) guard column were used to separate organic acids. A gradient mobile phase with a flow rate of 1.0 mL/min was applied using the following eluents: (A) a mixture of methanol (12%), ethanol (16%) in DI water, (B) 0.1 M NaOH in DI water and (C) 1 M NaOH in DI water. Prior to organic acids detection, eluents were suppressed by an anion suppressor (ASRS®300, 4 mm, Thermo Scientific). Pure organic acid standards were used to create the calibration curves for peak identification and quantification.

Direct infusion ESI-MS of glutaric and adipic acids in grape stem

Six calibrant solutions were prepared by a series of 10 time-fold dilution of a mother solution containing 2.5 µM/ml of glutaric and adipic acids. The 6 calibrant solutions were analyzed by a Thermo-Fisher Scientific LTQ-Orbitrap XL mass spectrometer (Bremen, Germany) coupled with an ESI source (Bremen, Germany). Typical instrumental parameters included: -120 V tube lens voltage, -10 V capillary voltage, 2 kV spray voltage, 275 ^{o}C capillary temperature, 6 sheath gas flow rate (arb), 2 micro scans, 200 ms MS injection time. Mass spectra for each calibrant were acquired in full scan at negative mode over the m/z range of 50-200 for 0.5 min, with an injection rate of 6 µl/s. Each calibrant was analyzed 6 times. Linear dynamic range for each

organic acid was determined by plotting its log-transformed concentration versus log-transformed average signal intensity at each concentration. These curves were fit to a least squares linear regression for each organic acid, the most linear R^2 >0.999 (Fig S1).

Glutaric and adipic acids enriched grape stems were prepared as described in DESI imaging experiment (b). Their extractions were performed as described for IC analysis. The extracts were diluted until their signal intensities fell within the defined linear range, their concentrations in pith and out pith were then estimated from the standard curves.

DESI imaging of organic acids in various grape tissues

Leaf blade, petiole, stem, node, rachis and receptacle were collected from the same shoot at post-veraison stage for DESI imaging, in which leaf blade was imaged by imprinting method and the other grape tissue types by direct DESI imaging. Sample preparation method for direct DESI imaging was similar as described for grape stem except that the vacuum dehydration time varied from 20 min to 1h depending on the tissue type. Totally 8 organic acids, including succinic, malic, theronic, tartaric, shikimic, ascorbic and citric acids were imaged. Those 8 organic acids have been confirmed both by their exact m/z by Orbitrap with the resolution set at 60,000 and by comparison of their MS/MS to those of their standards (table S1). Instrumental and DESI source settings were the same as described in DESI imaging of organic acids in grape stem.

Ion intensities of the 8 organic acids were extracted directly from DESI images of various grape tissue samples, and were normalized against the sum of their ion intensities. Principal Component Analysis was performed on normalized ion intensities of the 8 organic acids with ChemometricsWithR package [1] to distinguish different tissue types.

References

1. Ron W. P. Chemometrics With R: Multivariate Data Analysis in the Natural Sciences and Life Sciences. Springer press: Heidelberg, Germany.

Table S1. List of organic acids directly detected from grape tissue samples

Organic acids	Molecular formula	Measured m/z	Theoretical m/z	Mass accuracy (ppm)	MS/MS confirmed
Succinic	$[C_4H_6O_4\text{-}H]^-$	117.01919	117.01933	-1.213	Yes
Malic	$[C_4H_6O_5\text{-}H]^-$	133.01392	133.01425	-2.455	Yes
Threonic	$[C_4H_8O_5\text{-}H]^-$	135.02968	135.02990	-1.604	Yes*
Tartaric	$[C_4H_6O_6\text{-}H]^-$	149.00881	149.00916	-2.357	Yes
Shikimic	$[C_7H_{10}O_5\text{-}H]^-$	173.04537	173.04555	-1.021	Yes
Ascorbic	$[C_6H_8O_6\text{-}H]^-$	175.02480	175.02481	-0.034	Yes
Citric	$[C_6H_8O_7\text{-}H]^-$	191.01930	191.01973	-2.229	Yes
Gluconic	$[C_6H_{12}O_7\text{-}H]^-$	195.05059	195.05103	-2.235	Yes

*Due to the unavailability of threonic acid standard, the MS/MS data for this acid were compared with those in literature

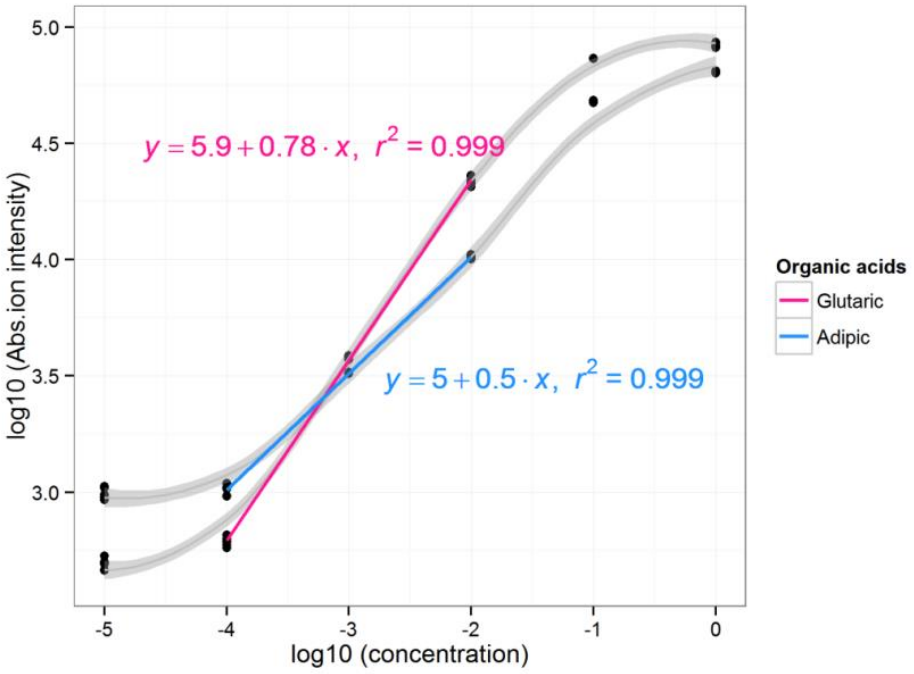

Figure S1. Dynamic ranges of glutaric and adipic acids obtained by direct infusion ESI-MS method. The signal intensity and concentration are both log-transformed. Linear dynamic ranges for both organic acids are between 10^{-4} and 10^{-1} dilution of 2.5 μM/ml mother solution.

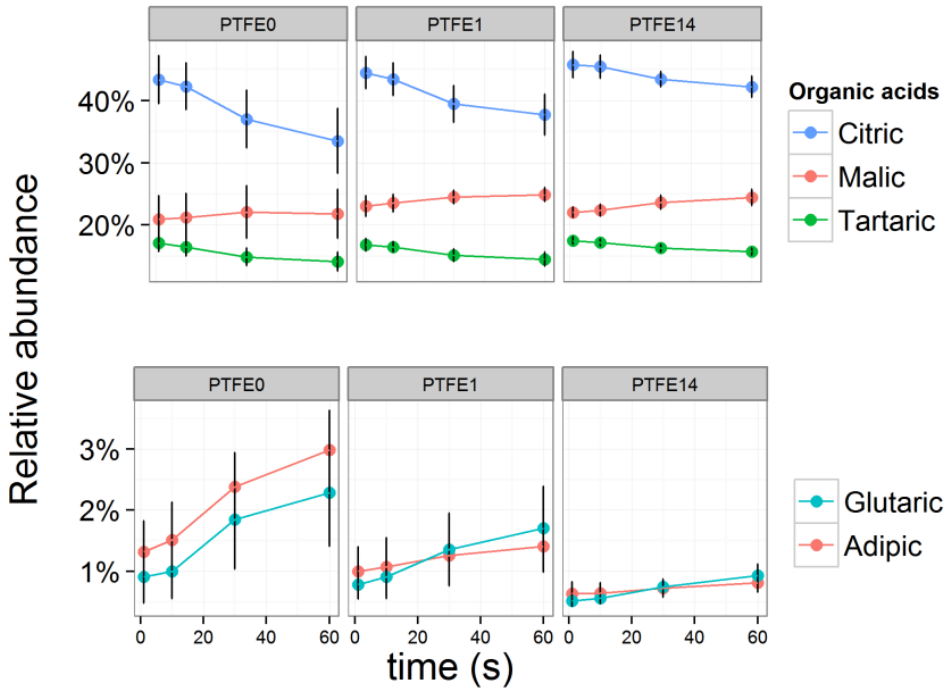

Figure S2. Relative abundance of malic, tartaric, citric, glutaric and adipic acids on 3 different PTFE surfaces, PTFE0 (flat PTFE), PTFE1 (PTFE with pore size of 1-3 µm) and PTFE14 (PTFE with pore size of 7-14 µm) calculated by integrating their respective ion intensities over 1, 10, 30, 60s. Values represent mean+SD (n=10).

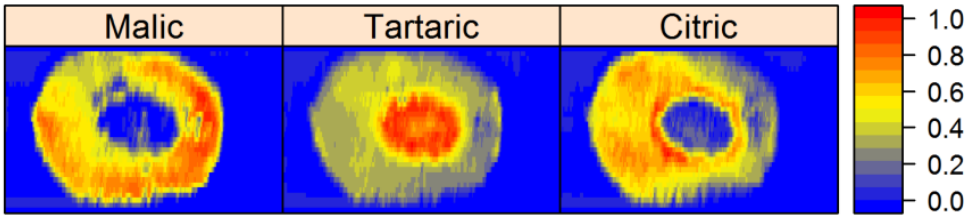

Figure S3. DESI imaging of malic, tartaric and citric acids at negative mode in a one-year-old grape stem which has been dipped into a glutaric and adipic acid solution for 1h. The color bar represents TIC normalized ion intensity from 0 (blue) to 1(red).

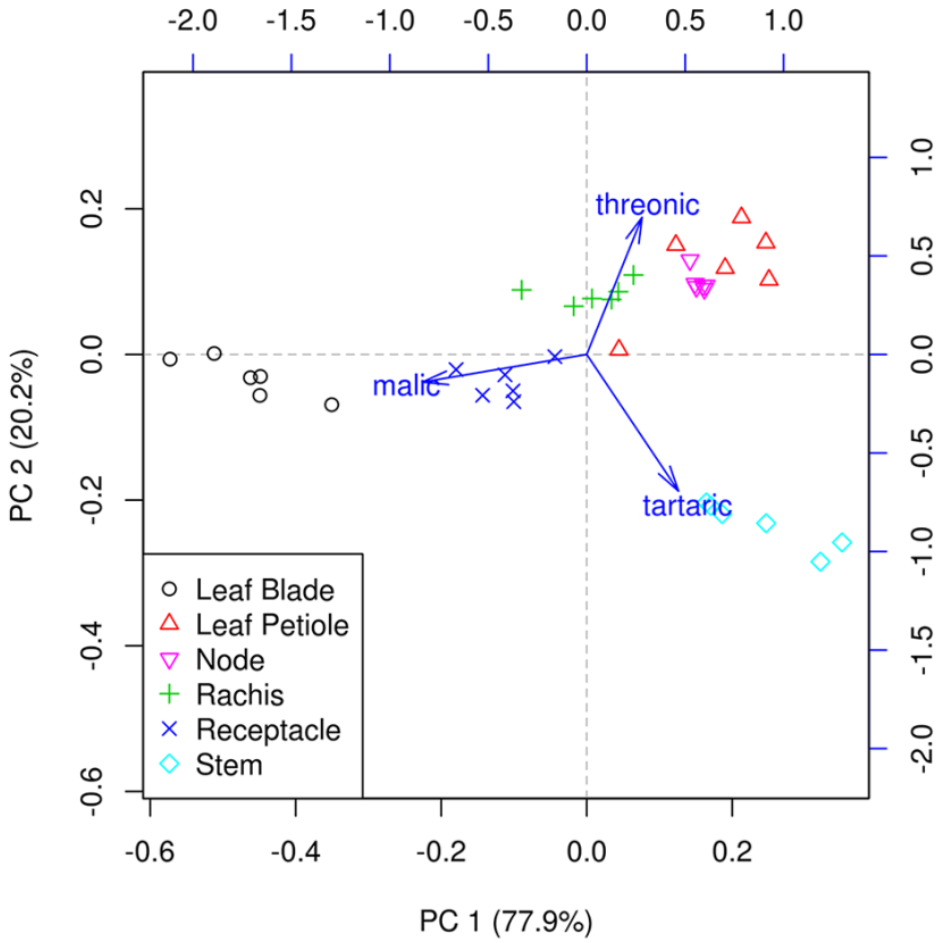

Figure S4. Principal Component Analysis of data from eight organic acids extracted from DESI images in 6 different grape tissue types (n=6). The first 2 PCs were selected for the best visualization of grape tissue separations; together they accounted for 98.1% of the total variance. Blue arrows show the projections of the three most important organic acids in defining the tissue separations into the 2 PCs.

Appendix 3:

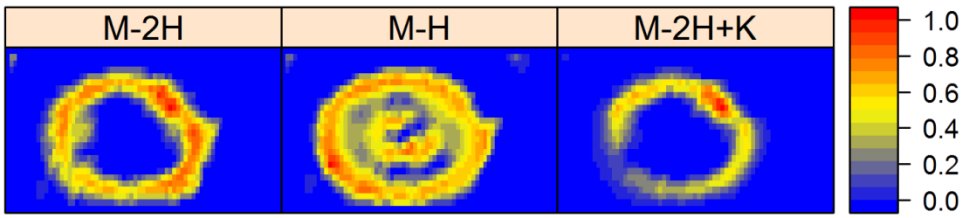

Figure S1. DESI images of tartrate in grape stem. M-2H denotes doubly charged tartrate dianions, M-H singly deprotonated ion and M-2H+K potassium adduct ions.

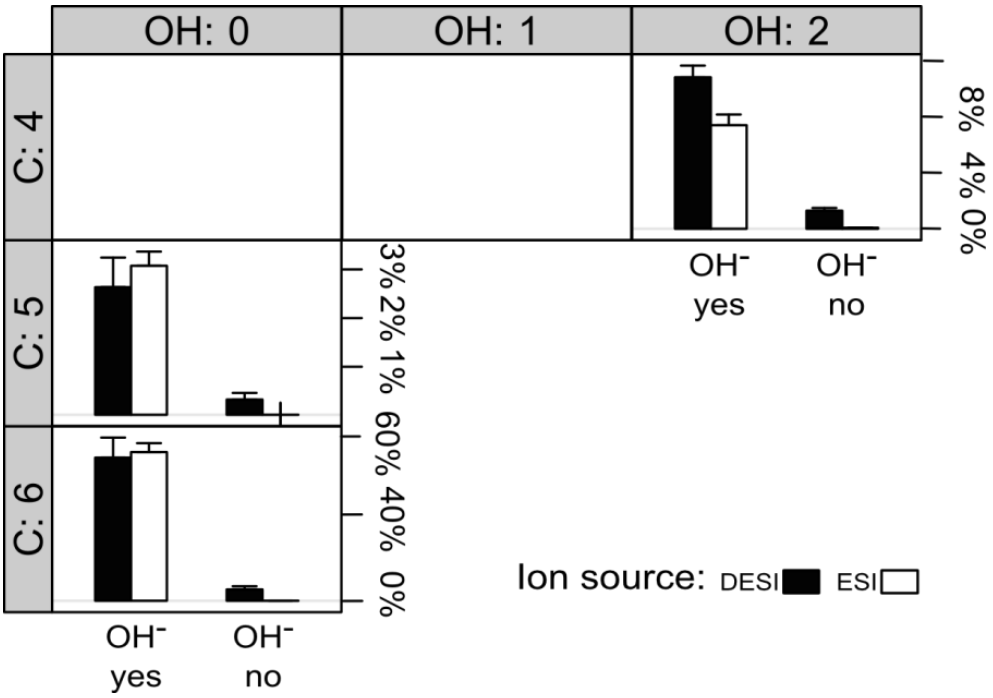

Figure S2. DCA^{2-} yields as observed in ESI and DESI ion-sources with Na^{+} being the counterion. Dianion yields were calculated by the ratio of abundance of dianions to those of their respective deprotonated singly charged ions. Values represent mean±SD (n=6). ‘OH^{-} yes’ is OH^{-} excess group (KOH:DCA, 3:1,mol/mol) and ‘OH^{-} no’ is no excess OH^{-} group (KOH:DCA, 2:1, mol/mol).

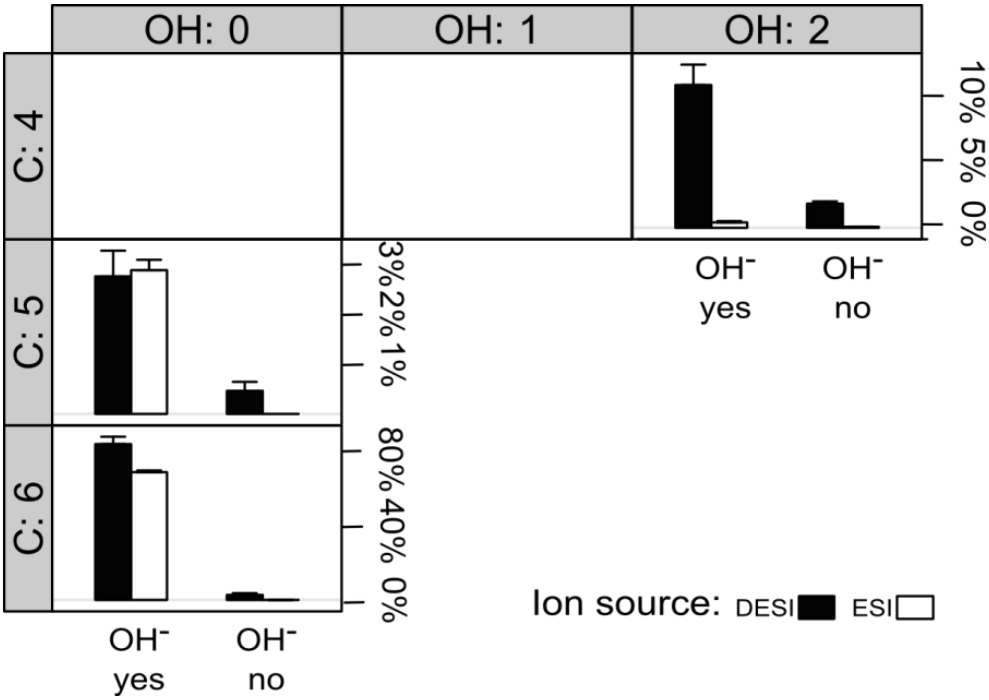

Figure S3. DCA^{2-} yields as observed in ESI and DESI ion-sources with Li^{+} being the counterion. Dianion yields were calculated by the ratio of abundance of dianions to those of their respective deprotonated singly charged ions. Values represent mean±SD (n=6). ‘OH^{-} yes’ is OH^{-} excess group (KOH:DCA, 3:1,mol/mol) and ‘OH^{-} no’ is no excess OH^{-} group (KOH:DCA, 2:1, mol/mol).

.